ONR

Design and Construction of a Mass-Spectrometer for the Study of Basic Processes in Plasma Physics

by

M. Mosharrafa and H. J. Oskam

July 1960 to July 1961

Technical Report No. 2

H. J. Oskam, Principal Investigator

Electrical Engineering Department

University of Minnesota

Contract No. Nonr-710(37)

Task No. 012-206

The research reported in this document has been sponsored by

Office of Naval Research

Department of the Navy

Washington 25, D. C.

This research is a part of Project DEFENDER, sponsored by the Advanced Research Projects Agency, Department of Defense.

Abstract

The measurement of the types of ions present in gaseous plasmas and their behavior as a function of time, gas pressure, method of plasma excitation, etc., is believed to be a necessity for obtaining conclusive interpretations of a large number of phenomena occurring in these plasmas. The theory of a mass-spectrometer of the quadrupole-field type is given. The reasons which led to the choice of this type of mass-spectrometer for the study of basic collision processes occurring in gaseous plasmas are discussed in detail. The mass-spectrometer can be outgassed at a temperature of 400°C in order to ensure ultra-high gas purity. Construction details of the mass-spectrometer, the associated electronic equipment and vacuum system are included in this manuscript.

TABLE OF CONTENTS

TABLE OF CONTENTS (CONTINUED)

TABLE OF CONTENTS (CONTINUED)

Chapter 1

Introduction

A renewed interest in the study of basic collision processes arose, during the last decade, in the field of Plasma Physics. This is mainly due to the realization that an understanding of the basic processes occurring in gaseous plasmas may be of use in fields relating to a) space-flight physics, b) rocket propulsion technology, c) conversion of thermal energy into electrical energy, d) blackout phenomena and e) production of energy by means of nuclear fusion.

As a consequence, a research group active in the study of basic phenomena in gaseous plasmas has been established at the Department of Electrical Engineering of the University of Minnesota. One of the main goals is to increase the understanding of the physics of disintegrating plasmas. The processes determining the rate of decrease of the charge density (electron density) are:

1. Recombination of electrons with positive charge carriers.

2. Diffusion (in most cases ambipolar) of charge carriers towards the boundaries of the plasma.

3. Attachment of electrons to neutral particles followed by negative ion-positive ion recombination.

4. Production of charge carriers during the disintegration period (afterglow period) of the plasma by metastable atom-metastable atom interactions.

5. Conversion of one type of ion into another type; for instance, the conversion of atomic ions into molecular ions is assumed to be an important process.

It is evident that, when confining the studies to the measurement of the electron density as a function of time during the afterglow period only, a conclusive interpretation of the measurements is risky if not without any value. It is, therefore, necessary to measure various quantities simultaneously and to combine the results obtained with the different measuring techniques.

In order to aid the interpretation of the complicated phenomena occurring in disintegrating plasmas, the identification of the type of ions present and their behaviour during the afterglow period becomes a necessity. Therefore, plans were made for the construction of a mass-spectrometer, which has a resolving power sufficient for distinguishing between the various types of ions, combined with a very high transmission and collection efficiency. This mass-spectrometer will make it possible to identify the types of ions present as well as their rate of change during the afterglow period.

This manuscript describes the development of a quadrupole type mass-spectrometer which meets these particular requirements. In addition, the other advantages this type has over the more conventional mass-spectrometers, will be discussed.

Since 1913, when J. J. Thomson developed the parabolic mass-spectrometer employing parallel electrostatic and magnetic fields, numerous techniques have been developed for mass analysis as is apparent through examination of the literature. The most common types of mass-spectrometers are:

Magnetic mass-spectrometers: This type analyzes the mass of monoenergetic ion beams by using 60°, 90°, or 180° homogeneous sector magnetic fields.

Time-of-flight mass-spectrometers: This type utilises the principle that the time needed for an ion with specific energy to traverse a drift space is mass dependent.

A rather new type of mass-spectrometer was developed by W. Paul and others at the University of Bonn, Germany, since 1953. This spectrometer employs the "mass filtering" principle, produced when injecting ions through a quadrupole rf field and dc field applied simultaneously. The quadrupole type spectrometer was chosen for our particular applications as it offers the following advantages over the other types:

1. The resolution of the instrument is variable and can be changed very easily by simply changing the ratio of the applied dc voltage to the rf voltage amplitudes. This makes it possible to ensure maximum efficiency and hence higher sensitivity throughout the entire mass range. This point will be discussed in greater detail in a subsequent chapter.

2. Contrary to the previously mentioned types of spectrometers, the quadrupole spectrometer offers no velocity discrimination; only an upper limit exists.

3. In contrast to the magnetic mass-spectrometer, the "mass filter" permits operation at higher residual gas pressures, because the stability characteristics of an ion are not changed (at least to a first approximation) by collisions with molecules of the residual gas (disregarding charge exchange). It is, therefore, expected that the line broadening caused by residual gases, as is known from magnetic mass-spectrometers,[1] will be substantially less in the case of the quadrupole spectrometer.[2]

4. No magnetic field requirements: It is well known that stray magnetic fields greatly disturb the conditions of an active as well as a passive plasma. The quadrupole spectrometer does not employ a magnetic field thus eliminating the shielding problem which becomes very difficult at high mass analysis with magnetic spectrometers.

5. It will be shown later that the injection conditions on the quadrupole spectrometer, and especially the allowable radial energies are quite tolerable thus eliminating the need for slits and other complicated focusing requirements. Moreover, this increases the efficiency of the mass-spectrometer.

6. The quadrupole mass-spectrometer described here has the extra feature of being bakeable thus insuring operation with a clean high-vacuum system.

The above considerations governed the decision as to the type of spectrometer to be used. The instrument is now being constructed at the Department of Electrical Engineering of the University of Minnesota.

References

1. Ehrenberg, H. Fr., "Isotopenanalysen an Blei aus Mineralen", Z. Physik 134, 317 (1953).

2. Paul, W., H. P. Reinhard and U. von Zahn, "Das elektrische Massenfilter als Massenspektrometer Und Isotopentrenner", Z. Physik 152 (2), 143 (1958).

Chapter 2

Theory of the Quadrupole Mass-Spectrometer

2.1 Introduction

The mass filtering action of the quadrupole mass-spectrometer is based on the behaviour of the solutions of the equations of motion of the injected charged particles. In this chapter, we will first obtain the differential equations of motion of the injected particles and then proceed to solve it under specific conditions of periodicity. We will then discuss the general theory of the solutions in order to be able to understand the behaviour of the solutions under various applied conditions and thus determine the stability regions essential for the operation of the spectrometer.

2.2 Equations of motion

The application of a voltage $(U + V \cos \omega t)$ on a hyperbola-shaped quadrupole shown in Fig. 2.1 results in the establishment of a potential distribution within the quadrupole region which can be written[1] as*

$$\phi = (U + V \cos \omega t) \frac{x^2 - y^2}{r_o^2} ,$$

where r_o is the distance from the origin to the point of intersection of the two rectangular hyperbolae with the x and y axes. Hence, the electric field distribution in the region is

$$E_x = - \frac{\delta \phi}{\delta x} = - 2 (U + V \cos \omega t) \frac{x}{r_o^2}$$

$$E_y = - \frac{\delta \phi}{\delta y} = 2 (U + V \cos \omega t) \frac{y}{r_o^2}$$

---

*We neglect end effects.

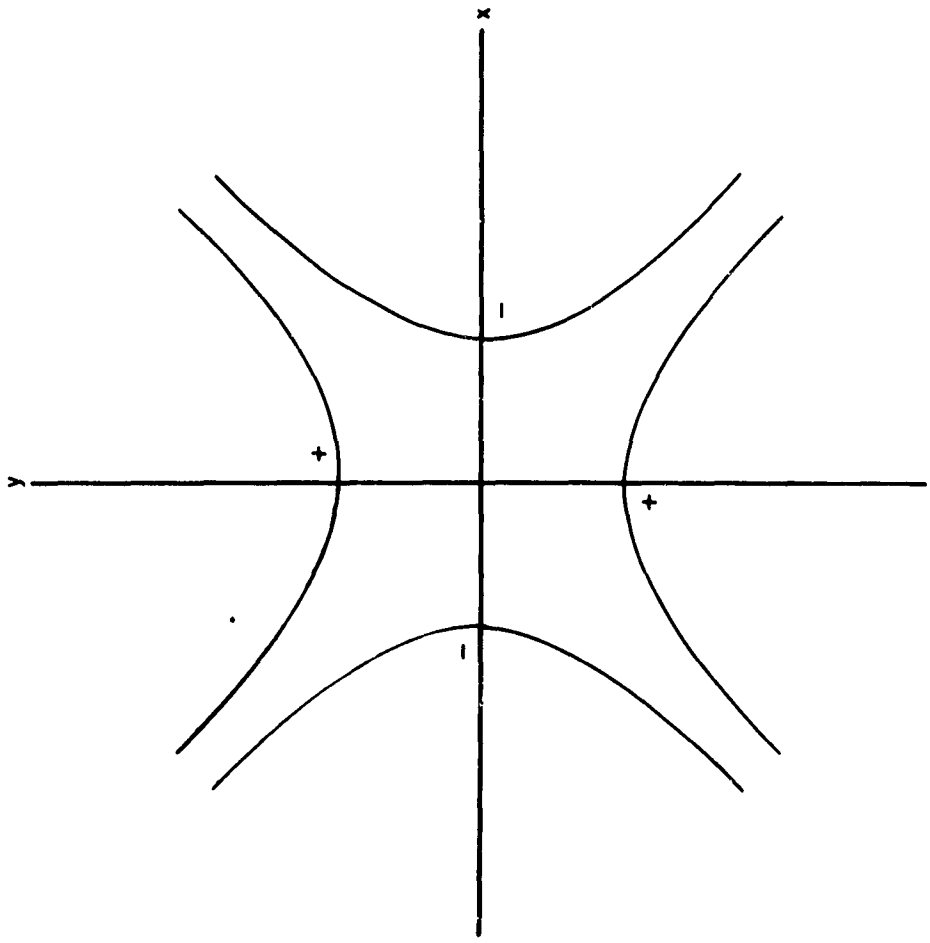

FIG 2.1

$$E_z = 0 \quad .$$

We will now proceed to analyze the motion of a positively charged particle injected in the z-direction into the electric field region. The equations of motion of a charged particle in the x, y and z directions are

$$m\ddot{x} = e E_x = -2 e (U + V \cos \omega t) \frac{x}{r_o^2}$$

or

$$m\ddot{x} + 2 e (U + V \cos \omega t) \frac{x}{r_o^2} = 0$$

$$m\ddot{y} - 2 e (U + V \cos \omega t) \frac{y}{r_o^2} = 0$$

and

$$m\ddot{z} = 0$$

or

$$m\dot{z} = \text{constant}.$$

Since the sign of the dc. component of the field in the y-direction is negative, the force due to this constant field exerts a defocusing influence on the ions (tends to increase y). In the x-direction, however, the particles are focused by the constant component of the field.

It is to be noted, however, that the ac component of the field dominates the motion of the ions since the amplitude V is larger than U as will be illustrated later.

Consider the motion in the x-direction:

$$m\ddot{x} + \frac{2 e}{r_o^2} (U + V \cos \omega t) x = 0 \quad . \qquad (2.1)$$

Let $\omega t = 2\gamma$, so that

$$\frac{dx}{dt} = \frac{\omega}{2}\frac{dx}{d\gamma}$$

and

$$\frac{d^2x}{dt^2} = \frac{\omega}{2}\frac{d}{d\gamma}\left(\frac{\omega}{2}\frac{dx}{d\gamma}\right) = \frac{\omega^2}{4}\frac{d^2x}{d\gamma^2} .$$

Substitution in equation 2.1 gives

$$\frac{\omega^2}{4}\frac{d^2x}{d\gamma^2} + \left(\frac{2eU}{m r_o^2} + \frac{2eV}{m r_o^2}\cos 2\gamma\right) x = 0$$

or

$$\frac{d^2x}{d\gamma^2} + \left(\frac{8eU}{m\omega^2 r_o^2} + \frac{8eV}{m\omega^2 r_o^2}\cos 2\gamma\right) x = 0 .$$

Denoting

$$a = \frac{8eU}{m\omega^2 r_o^2} \quad \text{and} \quad q = \frac{4eV}{m\omega^2 r_o^2}$$

gives

$$\frac{d^2x}{d\gamma^2} + (a + 2q\cos 2\gamma)\, x = 0 . \tag{2.2}$$

Following the same procedure, one can easily find the equation of motion in the y-direction to be

$$\frac{d^2y}{d\gamma^2} - (a + 2q\cos 2\gamma)\, y = 0 . \tag{2.3}$$

Equations (2.2) and (2.3) describing the motion of the charged particles in the field are "Mathieu type equations". The behaviour of the particles is thus determined by the properties of the solutions of those equations.

The Mathieu equation is a linear, second order differential equation with constant periodic coefficients. Mathieu, in 1868,[2] while determining the vibrational modes of a stretched membrane having an elliptical boundary, obtained an equation of the form

$$\frac{d^2v}{dz^2} + (a-2q\cos 2z)\ v = 0 .$$

This equation is considered to be the normal form of a Mathieu equation. We will apply, in our case, the normal form and proceed to solve the equation

$$\frac{d^2x}{d\gamma^2} + (a-2q\cos 2\gamma)\ x = 0 . \qquad (2.4)$$

Negative values of q, or a phase shift of $\pm \frac{\pi}{2}$ applied to equation (2.4) yields the equation describing the motion of the charged particles in the x-direction. Negative values of "a" yield the equation for the motion in the y-direction.

2.3 Periodic solutions

The solution of equation (2.4) takes different forms according to the values of "a" and q. For the present, we shall confine our attention to appropriate solutions, periodic in γ, with period π or 2π. One should note that the solutions to be obtained are by no means general solutions, but will serve as a guiding line towards understanding the general behaviour of the solutions which will follow later. As a consequence of the periodicity, "a" has definite values called Characteristic Numbers.

When q = 0, the solution of equation (2.4) becomes quite simple and will include terms in sin mx or cos mx, where

$$a = m^2 \quad , \quad m = 1 \ , \ 2 \ , \ 3 \ , \text{ etc.}$$

We shall adopt the convention that the coefficient of cos mx and sin mx is unity for all q,[2] without any loss of generality, since we will discuss each type of solution separately.

When $q \neq 0$, for the solution of equation (2.4) to have period π or 2π, "a" is to be a function of q.[3]

Let

$$a = m^2 + \alpha_1 q + \alpha_2 q^2 + - - - - - \quad .$$

To illustrate a method of finding a particular solution we take $a = m^2 = 1$

For $q \gtrless 0$

$$a = 1 + \alpha_1 q + \alpha_2 q^2 + - - - - - \quad .$$

2.3.1 Cosine-series solutions

Let

$$x = \cos \gamma + q\, c_1(\gamma) + q^2 c_2(\gamma) + - - - \quad , \qquad (2.5)$$

since the solution reduces to $x = \cos \gamma$ when $q = 0$.

Thus

$$x'' = d^2x/d\gamma^2 = - \cos \gamma + q\, c_1'' + q^2 c_2'' + - - - - \quad ,$$

where

$$c_1'' = \frac{d^2 c_1}{d\gamma^2} \quad .$$

Hence

$$ax = \cos \gamma + q(c_1 + \alpha_1 \cos \gamma) + q^2(c_2 + \alpha_1 c_1 + \alpha_2 \cos \gamma) + - - - .$$

Substituting into equation (2.4) and equating coefficients of like powers of q, we get

$$q^0: \quad \cos \gamma - \cos \gamma = 0$$

$$q^0: \quad c_1'' + c_1 - \cos 3\gamma + (\alpha_1 - 1) \cos \gamma = 0.$$

Hence

$$(D^2 + 1)\, c_1 = \cos 3\gamma - (\alpha_1 - 1) \cos \gamma \quad ,$$

where

$$D = \frac{d}{d\gamma} \quad \text{and} \quad D^2 = \frac{d^2}{d\gamma^2} \quad .$$

The particular integral for the second term on the right hand side, viz.

$(\alpha_1 - 1) \cos \gamma$ gives

$$\frac{1}{2} (\alpha_1 - 1)\, \gamma \cos \gamma \quad ,$$

which is nonperiodic.

Thus

$$\alpha_1 = 1 \quad \text{and} \quad c_1'' + c_1 = \cos 3\gamma$$

so that

$$c_1 = \frac{-\cos 3\gamma}{9 - 1} = -\frac{1}{8} \cos 3\gamma \quad ,$$

similarly, equating the coefficients of q^2 we get

$$c'' + c_2 + \alpha_1 c_1 - 2c_1 \cos 2\gamma + \alpha_2 \cos \gamma = 0 \quad .$$

Hence

$$c_2'' + c_2 - \frac{1}{8} \cos 3\gamma + \frac{1}{8} \cos 5\gamma + (\frac{1}{8} + \alpha_2) \cos \gamma = 0 \, .$$

Following the same reasoning, we obtain

$$\alpha_2 = -\frac{1}{8}$$

so that

$$c_2'' + c_2 = \frac{1}{8} \cos 3\gamma - \frac{1}{8} \cos 5\gamma$$

or

$$c_2 = -\frac{1}{64} \cos 3\gamma + \frac{1}{192} \cos 5\gamma \quad .$$

Proceeding in the same manner for higher orders of q we obtain the coefficients α and c and upon substitution in equation (2.5) we get a solution of Mathieu's equation, periodic in γ with period 2π. It is denoted by $ce_1(\gamma,q)$ and represented by the series

$$ce_1(\gamma,q) = \cos\gamma - \frac{1}{8} q \cos 3\gamma + \frac{1}{64} q^2 (-\cos\gamma + \frac{1}{3}\cos 5\gamma)$$

$$- \frac{1}{512} q^3 (\frac{1}{3}\cos 3\gamma - \frac{4}{9}\cos 5\gamma + \frac{1}{18}\cos 7\gamma)$$

$$+ \frac{1}{4096} q^4 (\frac{11}{9}\cos 3\gamma + \frac{1}{6}\cos 5\gamma - \frac{1}{12}\cos 7\gamma$$

$$+ \frac{1}{180}\cos 9\gamma) + O(q^5) \quad .$$

The value of "a" necessary to yield this solution, i.e., the Characteristic Number is

$$a = 1 + q - \frac{1}{8} q^2 - \frac{1}{64} q^3 - \frac{1}{1536} q^4 + \frac{11}{36864} q^5 + O(q^6) \quad .$$

The notation $ce_m(\gamma,q)$ signifies a cosine type Mathieu function of order m, which reduces to a multiple of $\cos m\gamma$ when $q = 0$. It is clearly seen that there is an infinite number of solutions of this form which are even periodic functions in γ.

2.3.2 Sine-series solutions

Considering the case that $m^2 = 1$, but now assume a solution of the type

$$x = \sin\gamma + q\, s_1(\gamma) + q^2 s_2(\gamma) + - - - - - -$$

and proceeding in a manner similar to that adopted in section 2.3.1 we obtain a sine type of Mathieu function designated $se_1(\gamma,q)$ as

$$se_1(\gamma,q) = \sin\gamma - \frac{1}{8}q\sin 3\gamma + \frac{1}{64}q^2(\sin 3\gamma + \frac{1}{3}\sin 5\gamma)$$

$$- \frac{1}{512}q^3(\frac{1}{3}\sin 3\gamma + \frac{4}{9}\sin 5\gamma + \frac{1}{18}\sin 7\gamma)$$

$$+ \frac{1}{4096}q^4(-\frac{11}{9}\sin 3\gamma + \frac{1}{6}\sin 5\gamma + \frac{1}{12}\sin 7\gamma + \frac{1}{180}\sin 9\gamma)$$

$$+ O(q^5) \quad ,$$

provided

$$a = 1 - q - \frac{1}{8}q^2 + \frac{1}{64}q^3 - \frac{1}{1536}q^4 - \frac{11}{36864}q^5 + O(q^6) \quad .$$

2.3.3 Solutions of higher order

One can proceed in a similar manner to evaluate the solutions of Mathieu's differential equation for $m > 1$ and also compute the Characteristic Numbers a_m , b_m corresponding to solutions $ce_m(\gamma,q)$, $se_m(\gamma,q)$ respectively.

One obtains the following values

$$a_o = -\frac{1}{2}q^2 + \frac{7}{128}q^4 - \frac{29}{2304}q^6 + \frac{68687}{18874368}q^8 + O(q^{10})$$

$$b_1 = 1 - q - \frac{1}{8}q^2 + \frac{1}{64}q^3 - \frac{1}{1536}q^4 - \frac{1}{36864}q^5$$

$$+ \frac{49}{589824}q^6 - \frac{55}{9437184}q^7 - \frac{265}{113246208}q^8 + O(q^9)$$

a_1 : replace q by $-q$ in the expression for b_1

$$b_2 = 4 - \frac{1}{12}q^2 - \frac{5}{13824}q^4 - \frac{289}{79626240}q^6 + \frac{21391}{458647142400}q^8 + O(q^{10})$$

$$a_2 = 4 - \frac{5}{12}q^2 - \frac{763}{13824}q^4 - \frac{1002401}{79626240}q^6 - \frac{1669068401}{458647142400}q^8 + O(q^{10})$$

$$b_3 = 9 + \frac{1}{16}q^2 - \frac{1}{64}q^3 - \frac{13}{20480}q^4 + \frac{5}{16384}q^5 - \frac{1961}{23592960}q^6$$

$$+ \frac{609}{104857600}q^7 - O(q^8)$$

a_3 : replace q by -q in the expression for b_3

$$b_4 = 16 + \frac{1}{30} q^2 - \frac{317}{864000} q^4 + \frac{10049}{2721600000} q^6 + O(q^8)$$

$$a_4 = 16 + \frac{1}{30} q^2 + \frac{433}{864000} q^4 - \frac{5701}{2721600000} q^6 + O(q^8)$$

$$b_5 = 25 + \frac{1}{48} q^2 + \frac{11}{774144} q^4 - \frac{1}{147456} q^5 + \frac{37}{891813888} q^6 + O(q^7)$$

a_5 : replace q by -q in the expression for b_5

$$b_6 = 36 + \frac{1}{70} q^2 + \frac{187}{43904000} q^4 - \frac{5861633}{92935987200000} q^6 + O(q^8)$$

$$a_6 = 36 + \frac{1}{70} q^2 + \frac{187}{43904000} q^4 + \frac{6743617}{92935987200000} q^6 + O(q^8)$$

When $m \geqslant 7$, the following formula[3] is correct up to (and including) the term in q^6

$$a_m , b_m = m^2 + \frac{1}{2(m^2-1)} q^2 + \frac{5m^2+7}{32(m^2-1)^3(m^2-4)} q^4$$

$$+ \frac{9m^4 + 58m^2 + 29}{64(m^2-1)^5(m^2-4)(m^2-9)} q^6 + - - - - -$$

These formulae are used to calculate "a" when q is adequately small and of either sign.

It should also be noted that

1. The functions: ce_{2n} , se_{2n+2} (n=0,1,2, - - - -) are periodic with period π.
2. The functions: ce_{2n+1} , se_{2n+1} (n=0,1,2, - - - -) are periodic with period 2π.
3. All the above functions have n real zeros in the region $0 < \gamma < \pi/2$.

Ince[4] has tabulated the values of a_o , a_1 - a_5 and b_1 , b_2-b_6 in the range q = 0 - 40 to 10 significant figures. Plotting these results in Cartesian coordinates yields the chart shown in Fig. 2.2.

Upon examining the chart, one arrives at the following conclusions:

a. The chart is symmetrical about the a-axis and so are the characteristic curves a_{2n} and b_{2n+2} .

b. Characteristic curves a_{2n+1} and b_{2n+1} are asymmetrical.

c. Except for the a_o curve, each characteristic curve intersects the q-axis twice, i.e., each curve has two zeros.

d. Two characteristic curves do not intersect.

2.4 General theory

We will now proceed to analyse the solutions existing in the different regions of the chart of Fig. 2.2. In order to be able to arrive at a complete understanding of the different types of existing solutions, we must first discuss the general theory of Mathieu-type solutions (functions), deducing the regions of stability and instability and thereby arriving at the basic understanding of the mass filtering action upon which the mass-spectrometer operates.

2.4.1 Solutions with period π

The following discussion applies to any linear differential equation of the second order with single-valued periodic coefficients, an example of which is the Mathieu equation in question.

If $y_1(\gamma)$ and $y_2(\gamma)$ be any two periodic solutions which constitute a fundamental system, the complete solution is

$$y = Ay_1(\gamma) + By_2(\gamma) .$$

If the period of each of the solutions is π, then

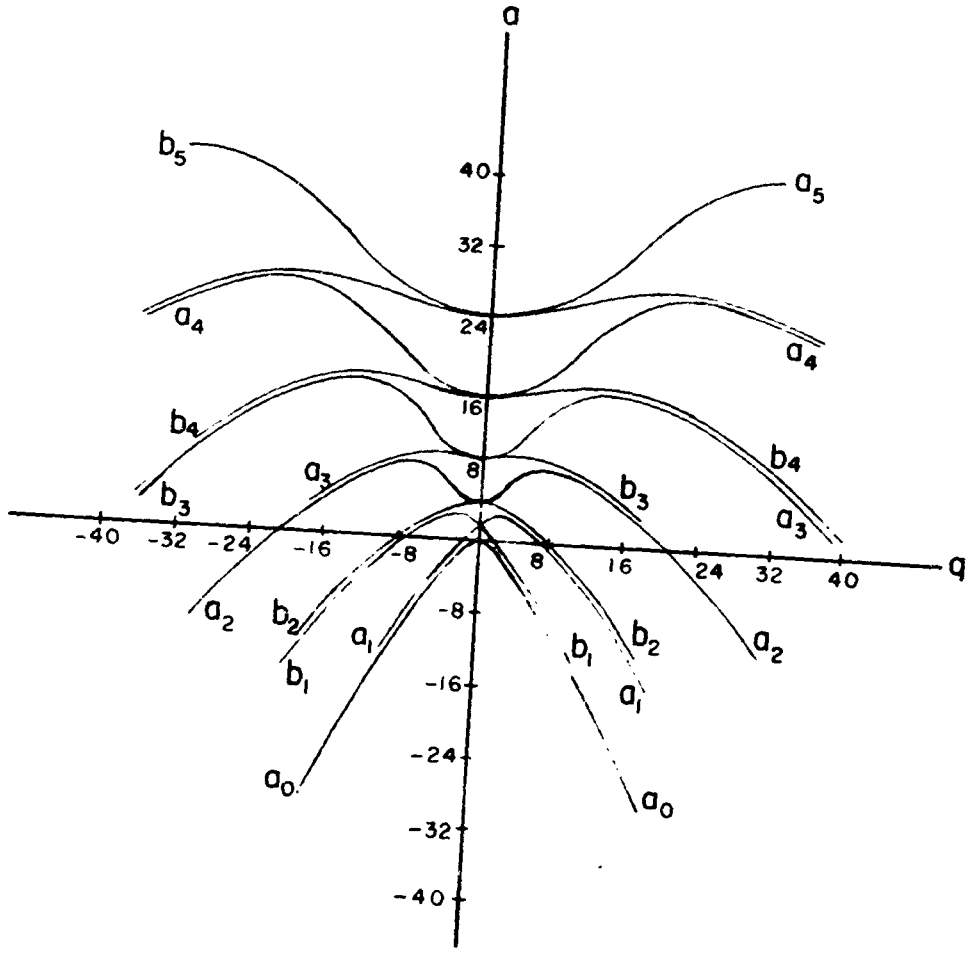
a
q
40
32
24
16
8
-8
-16
-24
-32
-40
-40
-32
-24
-16
-8
8
16
24
32
40
b_5
a_5
a_4
a_4
b_4
b_4
a_3
b_3
b_3
a_3
a_2
b_2
a_1
b_1
a_0
b_1
b_2
a_2
a_1
a_0

FIG 2.2

$$y_1(\gamma+\pi) \quad \text{and} \quad y_2(\gamma+\pi)$$

are also solutions. In accordance with the theory[5]

$$y_1(\gamma+\pi) = \alpha_1 y_1(\gamma) + \alpha_2 y_2(\gamma)$$

$$y_2(\gamma+\pi) = \beta_1 y_1(\gamma) + \beta_2 y_2(\gamma) \quad ,$$

where α_1 , α_2 , β_1 , β_2 , are constants determinable from the conditions at $\gamma = 0$ say.

Thus

$$y(\gamma+\pi) = Ay_1(\gamma+\pi) + By_2(\gamma+\pi)$$

$$= A\left[\alpha_1 y_1(\gamma) + \alpha_2 y_2(\gamma)\right] + B\left[\beta_1 y_1(\gamma) + \beta_2 y_2(\gamma)\right]$$

$$= (A\alpha_1 + B\beta_1)\, y_1(\gamma) + (A\alpha_2 + B\beta_2)\, y_2(\gamma) \quad .$$

If a <u>constant</u> ϕ could be found such that

$$(A\alpha_1 + B\beta_1) = \phi A \quad \text{and} \quad (A\alpha_2 + B\beta_2) = \phi B$$

then we can write

$$y(\gamma+\pi) = \phi y(\gamma)$$

or

$$A(\alpha_1 - \phi) + B\beta_1 = 0$$

giving

$$-A/B = \beta_1/(\alpha_1 - \phi)$$

and

$$A\alpha_2 + B\beta_2 = \phi B$$

giving

$$-A/B = \frac{\beta 2 - \phi}{\alpha_2} \quad .$$

Thus

$$\frac{(\beta_2-\phi)}{\alpha_2} = \frac{\beta_1}{(\alpha_1-\phi)}$$

or

$$\phi^2 - (\alpha_1 + \beta_2)\,\phi + (\alpha_1\beta_2 - \alpha_2\beta_1) = 0 \ .$$

α_1 , α_2 , β_1 , β_2 , could be easily determined from initial conditions, hence obtaining the required values for ϕ.

Considering Mathieu's equation, let the constant

$$\phi = e^{\mu\pi} \ ,$$

where μ is a number dependent upon the initial conditions and the parameters "a" and q.

Define also in general*

$$\phi(\gamma) = e^{-\mu\gamma} y(\gamma) \ ,$$

which incorporates the time dependence of ϕ through γ.

Thus

$$\phi(\gamma+\pi) = e^{-\mu(\gamma+\pi)}\, y(\gamma+\pi)$$

$$= e^{-\mu(\gamma+\pi)}\, \phi y(\gamma) = e^{-\mu\gamma}\, y(\gamma) = \phi(\gamma) \ ,$$

so that

$\phi(\gamma)$ is periodic in γ with period π.

Since $y(\gamma)$ is a solution of the type of differential equation under consideration, it follows that $e^{\mu\gamma}\,\phi(\gamma)$ is also a solution.

Complete solution of the equation

By virtue of periodicity π, taking

$$\phi(\gamma) = \sum_r c_{2r} e^{2r\gamma i}$$

---

*The solution is defined in this form for easier manipulations since Fourier expansion will be applied later.

and

$$\phi(-\gamma) = \sum_r c_{2r} e^{-2r\gamma i} .$$

In general, $\mu = \alpha + i\beta$, α, β real and $e^{\mu\gamma}\,\phi(\gamma)$ is a formal solution of Mathieu's equation. Since the equation is unchanged when replacing γ by $-\gamma$, $e^{-\mu\gamma}\,\phi(-\gamma)$ is an independent solution, provided $\alpha \neq 0$ or when $\alpha = 0$, β is nonintegral.

The complete solution of Mathieu's equation

$$\frac{d^2y}{d\gamma^2} + (a - 2q\cos 2\gamma)\, y = 0$$

is therefore

$$y(\gamma) = Ae^{\mu\gamma} \sum_r c_{2r} e^{2r\gamma i} + Be^{-\mu\gamma} \sum_r c_{2r} e^{-2r\gamma i} \qquad (2.6)$$

A and B are arbitrary constants evaluated from initial conditions.

Upon examining the solution obtained, one can readily see that, since the summation terms are both periodic, the stability of the solution will depend on the value of μ. Three cases arise

1. μ real: $y(\gamma) \longrightarrow \infty$ as $\phi \longrightarrow \infty$.

   The first part of solution is, therefore, unstable and the second part is stable. The complete solution is thus unstable.

2. μ complex: i.e., $\mu = \alpha + i\beta$ and $\alpha \neq 0$,

   so that

   $$y(\gamma) \longrightarrow \infty \qquad \text{as} \qquad \gamma \longrightarrow \infty \quad \text{(solution unstable).}$$

3. $\mu = i\beta$: we obtain the stable solution

   $$y(\gamma) = A\sum_r c_{2r} e^{(2r+\beta)\gamma i} + B\sum_r c_{2r} e^{-(2r+\beta)\gamma i} .$$

   If β is a rational fraction p/s, the summation terms are both periodic, with period $2s\pi$.

When β is irrational, the solution is oscillatory, but bounded and non-periodic, i.e., the solution never repeats itself at any time interval.

In actual applications, it is possible to arrange that μ be either real or imaginary, but not complex and that $0 < \beta < 1$ for convenience.

2.4.2 Solutions with period 2π

Take 2π to be the period of $\phi(\gamma)$, then

$$\mu(-\pi) = \mu(\pi)$$

$$y(-\pi) = e^{-\mu\pi}\,\phi(-\pi) \quad \text{and} \quad y(\pi) = e^{\mu\pi}\,\phi(\pi)$$

so that

$$y(\pi) - e^{-2\mu\pi}\,y(-\pi) = 0 \ .$$

Similarly

$$y'(\pi) - e^{-2\mu\pi}\,y'(-\pi) = 0 \ ,$$

Substituting $y = Ay_1(\gamma) + By_2(\gamma)$

gives

$$A(y_1(\pi) - e^{-2\mu\pi}\,y_1(-\pi)) + B\,(y_2(\pi) - e^{-2\mu\pi}\,y_2(-\pi)) = 0$$

and

$$A(y_1'(\pi) - e^{-2\mu\pi}y_1'(-\pi)) + B\,(y_2'(\pi) - e^{-2\mu\pi}\,y_2'(-\pi)) = 0 \ ,$$

For A and B nonzero, we get

$$e^{4\mu\pi} - \frac{D}{C^2}\,e^{2\mu\pi} + 1 = 0 \ ,$$

where

$$D = y_1(-\pi)\,y_2'(\pi) + y_1(\pi)\,y_2'(-\pi) - y_2(-\pi)\,y_1'(\pi) - y_2(\pi)y_1'(-\pi)$$

and

$$C^2 = y_1(\pi)\,y_2'(\pi) - y_2(\pi)\,y_1'(\pi) = y_1(-\pi)\,y_2'(-\pi) - y_2(-\pi)\,y_1'(-\pi)$$

Thus

$$\cosh 2\mu\pi = \frac{D}{2C^2} \quad .$$

This equation is also valid for period $n\pi$ ($n \geqslant 2$). This equation determines the value of μ once the initial conditions are known.

To make μ either pure real or pure imaginary ($\mu = i\beta$; $0 < \beta < 1$), when the parametric point (a,q) lies in certain regions of the (a,q) plane, it is essential that:

In the solution $y = e^{\mu\gamma}\,\phi(\gamma)$, $\phi(\gamma)$ should have a period of 2π instead of π. This follows from a close inspection of equation (2.6). The results previously obtained are applicable if for π we write 2π, take

$$\phi(\gamma) = \sum_r c_{2r+1} e^{(2r+1)\gamma i}$$

and also change 2r to (2r+1) in all the infinite series.

The form of solution when $\mu = i\beta$; $0 \quad \beta \quad 1$ is, therefore, given by

$$y_1(\gamma) = A \sum_r c_{2r} \cos (2r+\beta)\gamma \qquad (2.7)$$

and

$$y_2(\gamma) = B \sum_r c_{2r} \sin (2r+\beta)\gamma \ , \qquad (2.8)$$

so that

$$y(\gamma) = A \sum_r c_{2r} \cos (2r+\beta)\gamma + B \sum_r c_{2r} \sin (2r+\beta)\gamma \quad .$$

The initial conditions are substituted to determine the arbitrary constants A and B.

2.5 Practical form of solution*

---

*This method is introduced at this stage since it was found to be the best method by which we could fully determine and understand the stable and unstable region of the a-q plane.

As previously illustrated, from the theory of linear differential equations, one knows that the solution is of the type

$$y = Ae^{\mu\gamma}\,\phi(\gamma) + Be^{-\mu\gamma}\,\psi(\gamma) \quad , \tag{2.9}$$

where A and B are arbitrary constants, μ is a constant depending on the parameters "a" and q of the differential equation. The functions $\phi(\gamma)$, $\psi(\gamma)$ are periodic in γ. For certain values of "a" and q, the constant μ vanishes, and the solution y is then a purely periodic function of γ, but in general, μ is different from zero.

While the general character of the solution from the function theory point of view is known, its actual analytical determination presents great difficulties. The chief impediment is that the constant μ cannot readily be found in terms of "a" and q.

Whittaker[6] has solved this difficulty by introducing a new parameter in place of "a" which is denoted by* α. The parameter μ whose value is required, and the parameter "a" itself will be expressed in terms of α and the parameter q, so that when "a" and q are given, α could first be found and then find μ from α and q and ultimately obtain the solution y of the equation.

As previously illustrated, the periodic solution of the equations is a form of Fourier infinite series expansion. This form of series suggests that they may be degenerate cases of a general solution of Mathieu's equation, having the form

$$y_1 = e^{\mu\gamma}\,u(\gamma,\alpha)$$

---

*Note that α is a parameter here and not the constant previously employed.

where

$$u = \sin(\gamma-\alpha) + s_3 \sin(3\gamma-\alpha) + s_5 \sin(5\gamma-\alpha) + - - - -$$

$$+ c_3 \cos(3\gamma-\alpha) + c_5 \cos(5\gamma-\alpha) + - - - - \quad ,$$

where α is a new parameter.

Under this definition, the two solutions y_1 and y_2 will correspond to putting $\alpha = 0$, and $\alpha = \pi/2$ respectively in the above general solution.

It is also observed that there is no term in $\cos(\gamma-\alpha)$, this really constitutes the definition of α. The possibility of obtaining series which remain convergent for all real values of α depends on our choosing α in this manner. The coefficient of $\sin(\gamma-\alpha)$ is taken to be unity, which amounts to fixing the arbitrary constant by which the solution is multiplied.

Since a, q and α are interrelated, we assume

$$a = 1 + q f_1(\alpha) + q^2 f_2(\alpha) + q^3 f_3(\alpha) + - - - - -$$

and

$$\mu = q g_1(\alpha) + q^2 g_2(\alpha) + q^3 g_3(\alpha) + - - - - -$$

and take

$$u(\gamma,\alpha) = \sin(\gamma-\alpha) + q h_1(\gamma,\alpha) + q^2 h_2(\gamma,\alpha) + - - -$$

where

f, g are functions of α.

h are periodic functions of γ, α (periodic in γ).

Substituting these expressions in Mathieu's differential equation, equating coefficients of q^0, q^1, q^2, - - - - to zero and applying the periodicity requirement we obtain the values for the f, g and h functions and we find that*

*It is noted that the generality of the solution is not affected by assuming the sine series expansion, since the cosine series is incorporated in the value obtained for "a" as shown.

$$a = 1-q\cos 2\alpha + \frac{1}{4}q^2(-1 + \frac{1}{2}\cos 4\alpha) + \frac{1}{64}q^3\cos 2\alpha$$

$$+ \frac{1}{16}q^4(\frac{1}{3} - \frac{11}{32}\cos 4\alpha) - \frac{1}{32}q^5(\frac{1}{9}\cos 2\alpha - \frac{13}{128}\cos 6\alpha)$$

$$+ \frac{1}{8192}q^6(-\frac{893}{27} + \frac{9181}{216}\cos 4\alpha - \frac{35}{4}\cos 8\alpha) - - - - \qquad (2.10)$$

$$= 1-q\cos 2\alpha - \mu^2 + qs_3$$

$$\mu = -\frac{1}{2}q\sin 2\alpha + \frac{3}{128}q^3\sin 2\alpha - \frac{3}{1024}q^4\sin 4\alpha$$

$$- \frac{1}{4096}q^5(\frac{137}{9}\sin 2\alpha - \frac{9}{2}\sin 6\alpha)$$

$$+ \frac{1}{16384}q^6(\frac{337}{27}\sin 4\alpha - \frac{15}{4}\sin 8\alpha) + - - - - \qquad (2.11)$$

$$= \frac{1}{2}q(-\sin 2\alpha + c_3)$$

Also

$$s_3 = -\frac{1}{8}q + \frac{1}{64}q^2\cos 2\alpha - \frac{1}{512}q^3(-\frac{14}{3} + 5\cos 4\alpha)$$

$$+ \frac{1}{4096}q^4(\frac{-74}{9}\cos 2\alpha + 7\cos 6\alpha) + - - - -$$

$$c_3 = \frac{3}{64}q^2\sin 2\alpha - \frac{3}{512}q^3\sin 4\alpha + \frac{1}{4096}q^4(-\frac{274}{9}\sin 2\alpha$$

$$+ 9\sin 6\alpha) + - - - -$$

$$s_5 = \frac{1}{192}q^2 - \frac{1}{1152}q^3\cos 2\alpha + \frac{1}{4096}q^4(-\frac{155}{54} + \frac{82}{27}\cos 4\alpha) + - - - -$$

$$c_5 = -\frac{1}{2304}q^3 + \frac{1}{49152}q^4\cos 2\alpha + - - - -$$

$$s_7 = -\frac{1}{9216}q^3 + \frac{1}{49152}q^4\cos 2\alpha + - - - -$$

$$c_7 = \frac{35}{442368}q^4\sin 2\alpha + - - - -$$

$$s_9 = \frac{1}{737280} q^4 - - - -$$

Note that "a" is an even function of α while μ is an odd function of α. Thus the second independent solution of Mathieu's equation takes the form

$$y_2 = e^{-\mu\gamma}\, u(\gamma,-\alpha)$$

y_1 and y_2 constitute a fundamental system and the complete solution, with two arbitrary constants, is

$$y = Ae^{\mu\gamma}\, u(\gamma,\alpha) + Be^{-\mu\gamma}\, u(\gamma,-\alpha) \qquad (2.12)$$

It is clearly seen, now, that when $\alpha = -\pi/2$ then $\mu = 0$, $c_3 = c_5 = - - - - - = 0$, and the series for "a" becomes that previously obtained for "a_1" and

$$s_3 = -\frac{1}{8} q - \frac{1}{64} q^2 - \frac{1}{1536} q^3 + \frac{11}{36864} q^4 + - - - - \quad ,$$

Substituting, we obtain the series for $ce_1(\gamma,q)$. Similarly, when $\alpha = 0$ we obtain the series for $se_1(\gamma,q)$.

It can be shown that this form of solution will differ from that previously obtained through a constant multiplier. This is to be expected, since the solution of Mathieu's equations must be unique.

2.6 Division of the (a,q)-plane into stable and unstable regions

Referring to Fig. 2.2 which shows the portion of the plane for which the characteristic curves a_m, b_m for the Mathieu functions of integral order have been computed, we will consider the region in Fig. 2.2 lying between a_1 and b_2.

The curve a_1 is obtained by substituting $\alpha = -\pi/2$ in equation (2.10). Now, if $\alpha = -\pi/2 + i\theta$ then $\cos 2\alpha = -\cosh 2\alpha$ whatever the sign of θ and so if $q > 0$ is fixed, equation (2.10) shows that "a" increases with increasing θ until b_2 is reached. Now considering the curve b_2,

it has been shown[7] that this curve is obtained by substituting $\alpha = 0$ in the expression

$$a = 4 + \frac{1}{2} q^2 \left(\frac{1}{3} - \frac{1}{2} \cos 2\alpha\right) + - - - - - \quad . \tag{2.13}$$

If we let $\alpha = 0+i\theta$ in this equation, it is seen that "a" decreases with increasing θ until a_1 is regained. Thus, between a_1 and b_2, with $q > 0$, α is complex or imaginary depending on whether equation (2.10) or (2.13) is employed.

Taking $\alpha = \frac{1}{2}\pi+i\theta$ and substituting in equation (2.11) for μ in terms of α shows μ to be imaginary. ($\sin 2\alpha = -i\sinh 2\theta$).

In the region between a_1 and b_2, therefore, the solution of Mathieu's equation is stable. In other words, for imaginary or complex quantities for α, starting from b_2 and a_1, respectively, the solution is confined to the region between these two curves irrespective of the value of θ, thereby producing a stable solution.

We will now discuss the third possibility of values α could have, viz., real values.

Starting from b_2, where $\alpha = 0$ in equation (2.10), taking α to be real, for $q > 0$, "a" increases as α decreases until a_2 is reached where $\alpha = -\pi/2$. Since α is real in the intervening region, the series for μ will show to yield μ real and hence the solution is unstable for any point (a,q) in this region. Starting from a_1 with real values for α will also show that between a_1 and b_1, an unstable region exists. Following along the lines of the above argument, it can be shown that the region between a_2 ($\alpha = -\pi/2$) and b_3 ($\alpha = 0$) is a stable region.

It is thus possible to divide the (a,q) plane, for $q > 0$, into zones in which the solution of Mathieu's equation corresponding to a

point (a,q) is either stable or unstable.

One can also follow a similar argument for $q < 0$, by writing -q for q in the previous series and hence divide the entire (a,q) plane into stable and unstable regions. The result is shown in Fig. 2.3.

Conclusions

1. When the point (a,q) with $q > 0$ lies between a_m , b_{m+1} then μ is imaginary and the two solutions of Mathieu's equation are stable.

2. When the point (a,q) with $q > 0$ lies between b_m , a_m then μ is real provided the appropriate form of solution is taken and the complete solution of Mathieu's equation is unstable.

2.7 Form of solution for different regions of the (a,q) plane

1. Stable solution:

a. q small and positive*

When (a,q) lies between a_{2n} , b_{2n+1} , for the first solution, we take

$$y_1(\gamma) = e^{i\beta\gamma} \sum_r c_{2r} e^{2r\gamma i} = e^{i\beta\gamma} \phi_{2r}(\gamma) \qquad (2.14)$$

or

$$y_1(\gamma) = \sum_r c_{2r} \cos (2r+\beta)\gamma \qquad (2.15)$$

or

$$y_1(\gamma) = e^{i\beta\gamma} \sin (2n\gamma - \alpha) + s_2 \sin (2\gamma-\alpha) + s_4 \sin (4\gamma-\alpha) + - - - -$$
$$+ c_2 \cos (2\gamma-\alpha) + c_4 \cos (4\gamma-\alpha) + - - - - , \qquad (2.16)$$

---

*This solution is practically suitable for the case when q is small, i.e., the series converges rapidly.

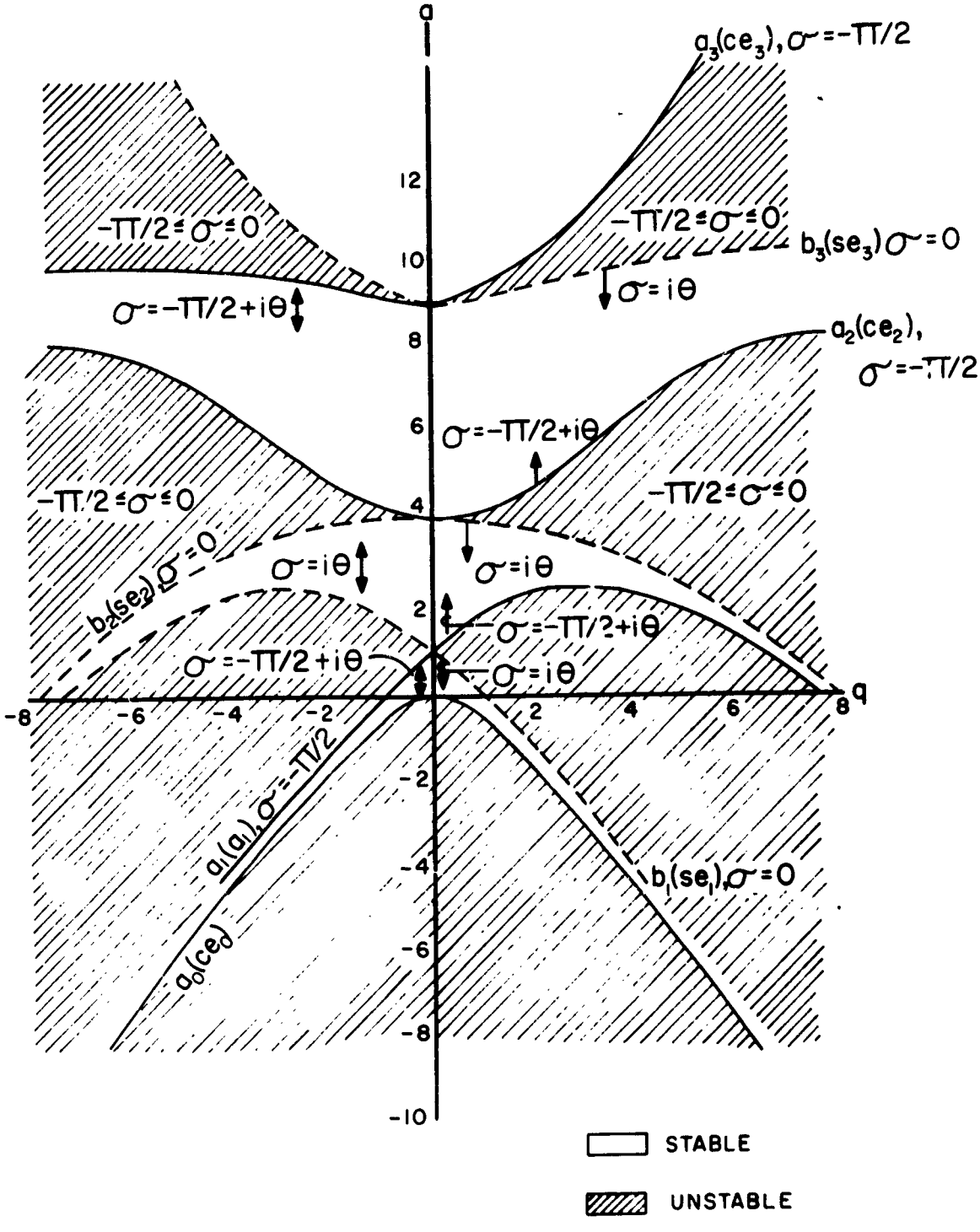

FIG 2.3

STABLE AND UNSTABLE REGIONS IN THE a-q PLANE

there being no term in cos $(2n\gamma-\alpha)$, e.g., if n=1, $c_2=0$.

In these series, β is real and $0 < \beta < 1$. The coefficients c_{2r} , s_{2r} are obtained as shown previously.

When (a,q) lies between a_{2n+1} , b_{2n+2} , the first solution is taken as

$$y_1(\gamma) = e^{i\beta\gamma} \sum_r c_{2r+1}\, e^{(2r+1)\gamma i} = e^{i\beta\gamma}\phi_{2r+1}(\gamma) \qquad (2.17)$$

or

$$y_1(\gamma) = \sum_r c_{2r+1} \cos\,(2r+1+\beta)\gamma \qquad (2.18)$$

or

$$y_1(\gamma) = e^{i\beta\gamma} \left[\sin\left((2n+1)\gamma-\alpha\right) + s_1 \sin\,(\gamma-\alpha)\right.$$

$$+ s_3 \sin\,(3\gamma-\alpha) + - - - - -$$

$$\left. + c_1 \cos\,(\gamma-\alpha) + c_3 \cos\,(3\gamma-\alpha) + - - -\right] \quad , \qquad (2.19)$$

there being no term in cos $\left[\,(2n+1)\gamma-\alpha\right]$, e.g., if n=1, $c_3=0$.

The second solution is obtained by writing $-\gamma$ for γ in (2.14) and (2.17), sin for cos in (2.15) and (2.18) and $-\beta$ for β, $-\alpha$ for α in (2.16) and (2.19).

When the initial conditions are specified, all forms of solution yield, naturally, an identical result since the solution is unique.

b. q moderate and positive

Same as (a) except that the form represented by equation (2.16) and (2.19) is usually unsuitable for computation when $q > 0.4$ approximately.

2. Unstable solution:

a. q small and positive

When (a,q) lies between a_{2n+2} , b_{2n+2} the first solution is taken as

$$y_1(\gamma) = e^{\mu\gamma} \sum_r e_{2r} e^{2r\gamma i} = e^{\mu\gamma} \phi_{2r}(\gamma)$$

or

$$y_1(\gamma) = e^{\mu\gamma} \Big[\sin(2n\gamma-\alpha) + s_2 \sin(2\gamma-\alpha) + s_4 \sin(4\gamma-\alpha) + - - -$$

$$+ c_2 \cos(2\gamma-\alpha) + c_4 \cos(4\gamma-\alpha) + - - - - - \Big] ,$$

where $\mu(\text{real}) > 0$ and remarks in 1.(a) apply.

When (a,q) lies between b_{2n+1} , a_{2n+1} , the first solution is taken as

$$y_1(\gamma) = e^{\mu\gamma} \sum_r c_{2r+1} e^{(2r+1)\gamma i} = e^{\mu\gamma} \phi_{2r+1}(\gamma)$$

or

$$y_1(\gamma) = e^{\mu\gamma} \Big[\sin\Big((2r+1)\gamma-\alpha\Big) + s_1 \sin(\gamma-\alpha)$$

$$+ s_3 \sin(3\gamma-\alpha) + - - - - -$$

$$+ c_1 \cos(\gamma-\alpha) + c_3 \cos(3\gamma-\alpha) + - - - \Big] .$$

Note that the period of $\phi_{2r}(\gamma)$ is π, while that of $\phi_{2r+1}(\gamma)$ is 2π.

b. q moderate and positive: as 1.(b).

3. Any solution for $q < 0$:

Replace γ by $(\pi/2 - \gamma)$ in the solution for $q > 0$. In other words, the obtained stability regions are applicable to negative ions also in the mass-spectrometer.

2.8 Mathieu functions of fractional order

In general the operating point for a defined ion mass will lie within the regions of stability (or unstability). Also, the solutions corresponding to operating points lying exactly on the (a) and (b) lines are quite critical and are therefore not quite adequate for mass-spectrometric purposes. Therefore, we will discuss in this section the solutions of fractional order.

A Mathieu function of fractional order ρ is that which satisfies Mathieu's equation and reduces to $\cos \rho\gamma$ or $\sin \rho\gamma$ when $q = 0$, i.e., $m^2 = \rho^2$.

In this case ρ is real, positive and either rational or irrational. Assuming

$$ce_\rho(\gamma,q) = \cos \rho\gamma + \sum_r q^r C_r(\gamma) \tag{2.20}$$

$$se_\rho(\gamma,q) = \sin \rho\gamma + \sum_r q^r s_r(\gamma) \tag{2.21}$$

$$a = \rho^2 + \sum_r A_r q^r$$

and proceeding analytically in the same manner as in section 2.3 we obtain the following results

$$\begin{aligned} ce_\rho(\gamma,q) = \cos \rho\gamma &- \frac{1}{4} q \left[\frac{\cos (\rho + 2)\gamma}{(\rho + 1)} - \frac{\cos (\rho - 2)\gamma}{(\rho - 1)} \right] \\ &+ \frac{1}{32} q^2 \left[\frac{\cos (\rho + 4)\gamma}{(\rho + 1)(\rho + 2)} + \frac{\cos (\rho - 4)\gamma}{(\rho - 1)(\rho - 2)} \right] \\ &- \frac{1}{128} q^3 \left[\frac{(\rho^2 + 4\rho + 7) \cos (\rho + 2)\gamma}{(\rho - 1)(\rho + 1)^3 (\rho + 2)} \right. \\ &\left. - \frac{(\rho^2 - 4\rho + 7) \cos (\rho - 2)\gamma}{(\rho + 1)(\rho + 1)(\rho - 1)^3 (\rho - 2)} \right] \\ &+ \left[\frac{\cos (\rho + 6)\gamma}{3(\rho + 1)(\rho + 2)(\rho + 3)} - \frac{\cos (\rho - 6)\gamma}{3(\rho-1)(\rho-2)(\rho-3)} \right] + \cdots \end{aligned} \tag{2.22}$$

$$se_\rho(\gamma,q) = \sin \rho\gamma - \frac{1}{4} q \left[\frac{\sin (\rho + 2)\gamma}{(\rho + 1)} - \frac{\sin (\rho - 2)\gamma}{(\rho - 1)} \right]$$

$$+ \frac{1}{32} q^2 \left[\frac{\sin (\rho + 4)\gamma}{(\rho + 1)(\rho + 2)} + \frac{\sin (\rho - 4)\gamma}{(\rho - 1)(\rho - 2)} \right] + - - \qquad (2.23)$$

$$a = \rho^2 + \frac{1}{2(\rho^2 - 1)} q^2 + \frac{(5\rho^2 + 7)}{32(\rho^2 - 1)^3 (\rho^2 - 4)} q^4$$

$$+ \frac{9\rho^4 + 53\rho^2 + 29}{64(\rho^2 - 1)^5 (\rho^2 - 4)(\rho^2 - 9)} q^6 + - - - - - - \qquad (2.24)$$

These formulae are suitable for computation when $q^2/2(\rho^2 - 1) \ll \rho^2$, $\rho > 0$, i.e., the series converges rapidly. Since "a" has the same value for both solutions, the complete solution becomes

$$y = A\ ce_\rho(\gamma,q) + B\ se_\rho(\gamma,q) \quad , \qquad (2.25)$$

where A and B are two arbitrary constants and ρ is non-integral. Also note that in this case: $\rho = m+\beta$.

2.9 Application of the previously outlined theory to the mass-spectrometer

In the mass-spectrometer case, we are dealing with two Mathieu differential equations simultaneously, describing the motion of the charged particles in the x and y directions as previously shown. The requirement is thus, that both solutions (in the x and y directions) be stable simultaneously.

Let us now proceed to analyze the equations simultaneously.

$$\frac{d^2x}{d\gamma^2} + (a + 2q \cos 2\gamma)\, x = 0 \qquad (2.26)$$

and

$$\frac{d^2y}{d\gamma^2} - (a + 2q \cos 2\gamma)\, y = 0 \quad , \qquad (2.27)$$

Apart from the phase shift, the difference between the two equations and the normal form is the fact that "a" in equation (2.24) is negative, i.e., the equation of motion in the y-direction results from substituting (-a) in equation (2.27) (and the phase shift which has no influence on the stable or unstable properties of the solution). Referring to the (a,q) chart of Fig. 2.3, which shows the regions of stability for the solution of Mathieu's equation, we observe

1. Equation (2.26) for the x-direction motion has "a" $>$ 0 and hence the stable solutions of this equation are confined to the upper half of the chart.

2. Equation (2.27) for the y-direction motion, has "a" $<$ 0 and hence the stable solutions of this equation are those of the lower half of the plane.

One can now easily determine the regions where both solutions are stable by simply folding the plane about the q-axis. Several regions of stability are obtained, the largest of which is that bounded by the q-axis, the a_o curve and the b_1 curve. This region is that which determines the operation of the mass-spectrometer and is hence of greatest interest to us.

The first step will be to plot this region more accurately using the formulae for a_o and b_1 obtained previously.

$$a_o = -\frac{1}{2}q^2 + \frac{7}{128}q^4 - \frac{29}{2304}q^6 + \frac{68687}{18874368}q^8 + O(q^{10})$$

and

$$b_1 = 1 - q - \frac{1}{8}q^2 + \frac{1}{64}q^3 - \frac{1}{1536}q^5 + O(q^6)$$

Since, in this region $0 < q < 1$, one can neglect terms in powers of

$q > 4$ in b_1 and power of $q > 6$ in a_o.

Thus

$$a_o = -\frac{1}{2} q^2 + \frac{7}{128} q^4 - \frac{29}{2304} q^6 \qquad (2.28)$$

and

$$b_1 = 1 - q - \frac{1}{8} q^2 + \frac{1}{64} q^3 - \frac{1}{1536} q^4 . \qquad (2.29)$$

A plot of equations (2.28) and (2.29) is shown in Fig. 2.4 in which we distinguish four different regions.

Region 1: Solution for x stable, solution for y unstable; thus a region of unstable particle motion.

Region 2: Both x and y solutions stable. Hence, when the operating point lies in this region, the particle motion is stable.

Region 3: Solution for x and y unstable; thus motion unstable.

Region 4: Solution for x unstable, solution for y stable; thus motion unstable.

We conclude that, if the parameters (U, V, m, ω, r_o) for a specific particle of mass m are such that the operating point lies within region 2 of the stability diagram of Fig. 2.4, the motion of the particle is stable and hence it will pass through the quadrupole field attaining a finite amplitude of vibration and could thus be detected at the output of the mass-spectrometer. If the operating point lies outside region 2, the particle will oscillate with exponentially increasing amplitude and will eventually be lost at the electrodes. This is the principle of "mass filtering" upon which the mass-spectrometer operates.

Referring to the original equations of motion of the ions, developed in section 2.1, we defined "a" and q as follows:

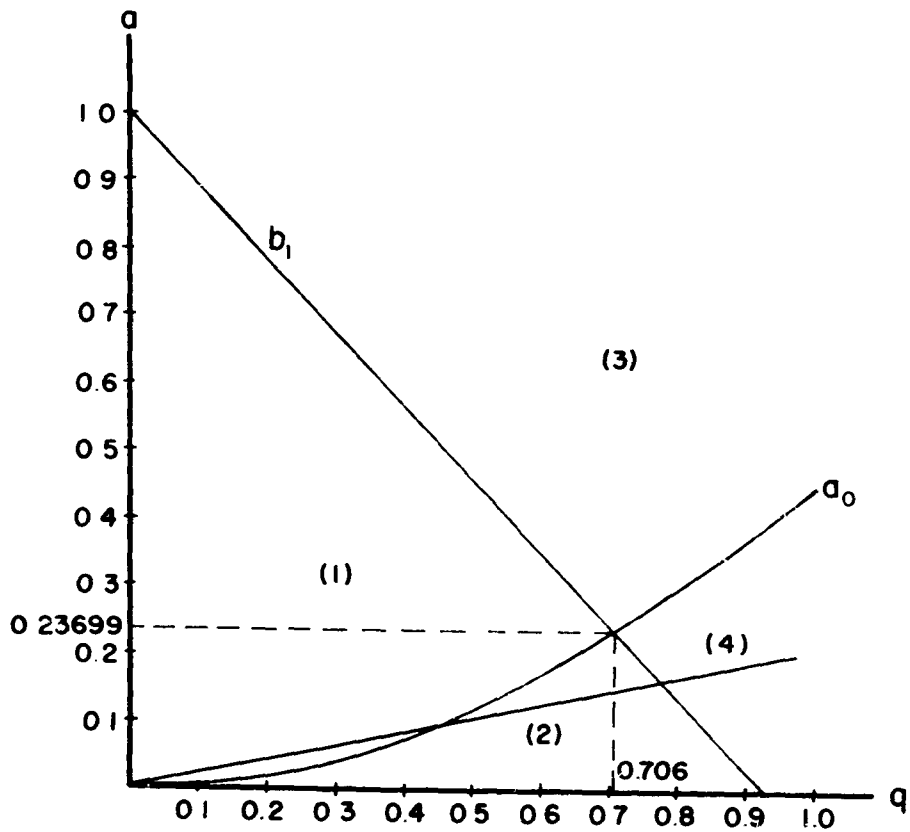
a
1 0
0 9
0 8
0 7
0.6
0 5
0 4
0 3
0 23699
0.2
0 1
b_1
(3)
a_0
(1)
(4)
(2)
0.706
q
0 1
0.2
0 3
0.4
0 5
0 6
0 7
0.8
0.9
1.0

FIG 3.4

$$a = \frac{8 \cdot e \cdot U}{m r_o^2 \omega^2} \tag{2.30}$$

and

$$q = \frac{4 \cdot e \cdot V}{m r_o^2 \omega^2} \tag{2.31}$$

where

U = amplitude of applied dc voltage

V = amplitude of applied rf voltage

e = electron charge

ω = rf frequency

r_o = field radius

m = mass of charged particles

It is observed that the ratio a/q = 2U/V represents a straight line in the (a,q) plane in Fig. 2.4, and passing through the origin with slope 2U/V, therefore, independent of the mass of the particle. In other words, for a set ratio of U/V, the operating points for all masses from 0 - ∞ will lie on a straight line through the origin. It is thus evident that only these mass values which lie in region 2 of Fig. 2.4 will have stable solutions and hence, could be detected at the output of the spectrometer. As the line approaches the vertex of region 2 (slope increased) the number of masses related to ions having stable orbits is decreased.

The slope of the line, i.e., 2U/V, thus determines the resolution of the mass-spectrometer.

We will now consider region 2, the stability region, in more detail and discuss various important parameters pertaining to the motion of the stable ion orbits.

We have shown that $\mu = i\beta$ in the stable region and referring to section 2.4.2, the general solution of the equation of motion for the charged particles in this region is*

$$x(\gamma) = A \sum_r c_{2r} \cos (2r + \beta)\gamma + B \sum_r c_{2r} \sin (2r + \beta)\gamma \qquad (2.32)$$

or $(0 < \beta < 1)$

$$x(\omega t) = A \sum_r c_{2r} \cos (r+\beta/2)\, \omega t + B \sum_r c_{2r} \sin (r+\beta/2)\, \omega t. \qquad (2.33)$$

It is to be noted that A and B contain the initial conditions, i.e., the injection conditions of the ions, whereas the coefficients c_{2r} and β depend only on "a" and q. Thus the paths of all ions of the same mass differ only, in their motion, in the constants A and B corresponding to the difference in their initial conditions of injection, viz., x_o, $\dot{x}_o$, t_o, where $\dot{x}_o$ is the initial velocity. They all have the same frequency spectrum of vibration $\omega_o = \beta\omega/2$, $\omega_1 = (1-\beta/2)\omega$, $\omega_2 = (1+\beta/2)\omega$ etc.

Ions of different mass have, on the other hand, different values for the coefficients c_{2r} and β due to their different operating points in the stability region. The frequency spectra of their motion, and especially the fundamental frequency $\omega_o = \beta\omega/2$ are, therefore, different.

2.9.1 Iso-β-chart

Referring to Fig. 2.2, it is noted that when the parametric point lies in a stable region, equation (2.24) of section 2.8 may be adapted to calculate β. When $q > 0$, as

---

*We are only going to consider from now on the solution of one of the two equations of motion since the stability is not affected by the phase of injection.

is the case and if the curves bounding the region are a_m(lower), b_{m+1}(upper), $m \geqslant 0$, we take $\rho = m+\beta$ and from (2.24) follows

$$\rho^2 = a - \frac{1}{2(\rho^2 - 1)} q^2 - \frac{(5\rho^2 + 7)}{32(\rho^2 - 1)^3 (\rho^2 - 4)} q^4$$

$$- \frac{9\rho^4 + 58\rho^2 + 29}{64(\rho^2 - 1)^5 (\rho^2 - 4) (\rho^2 - 9)} q^6 + O(q^8) . \qquad (2.34)$$

As mentioned previously, this formula is usable under the condition that $|a| \gg |q^2/2 (\rho^2 - 1)|$ and that the ratio of each of the terms in q^{2r} to its predecessor is small. For a first approximation we have $\rho^2 = a$. Inserting this in the term in q^2 and omitting the others, the second approximation is

$$q^2 = a - \frac{q^2}{2(a - 1)} . \qquad (2.35)$$

Substituting from (2.35) into the second term on the right hand side of (2.34) and $\rho^2 = a$ in the third and fourth, yields the third approximation

$$\rho^2 = a - \frac{(a-1)}{2(a - 1)^2 - q^2} q^2 - \frac{(5a+7)}{32(a - 1)^3 (a - 4)} q^4$$

$$- \frac{9a^2 + 58a + 29}{64(a - 1)^5 (a - 4) (a - 9)} q^6 + O(q^8) .$$

Since $\rho^2 = (m + \beta)^2$, we obtain

$$\beta \simeq a - \frac{(a - 1)}{2(a - 1)^2 - q^2} q^2 - \frac{(5a + 7)}{32(a - 1)^3 (a - 4)} q^4$$

$$- \frac{9a^2 + 58a + 29}{65(a - 1)^5 (a - 4) (a - 9)} q^6 - m ,$$

provided no denominator vanishes.

When the above conditions do not apply, β may be calculated using the continued fractions method as described by McLachlan.[3]

In our case, the region of interest for the operation of the mass spectrometer lies between a_o (folded) and b_1 of Fig. 2.4.

Consider region 2, the region of stability of the solution to Mathieu's equation, i.e., the region between a_o (folded) and b_1. In this region $0 < \beta < 1$ ($\rho = m+\beta$), we proceed to calculate for any assigned β, say 0.6, the "a" for q increasing from zero in small steps, and the points plotted give the characteristic curve $\beta = 0.6$. By computing a series of curves at intervals of, say, $\beta = 0.1$, we can plot an iso-β-chart of the type depicted in Fig. 2.5.

These iso-β lines will prove very useful in analysing the line form of mass peaks as will be shown later. It should be noted that one could proceed in a similar manner to obtain the iso-μ lines in the unstable regions of the solutions of Mathieu's equation.

2.9.2 Injection conditions and maximum amplitude of vibration

It was previously mentioned that the stability of the path of an ion in the spectrometer depends solely on the operating point (a,q) and not on the ion's injection conditions. But for a stable ion to reach the collector, it is evident that the amplitude of its vibration must remain smaller than the distance r_o of the electrodes from the field axis, i.e., x_{max} , $y_{max} < r_o$. Since the maximum amplitude of vibration depends on the operating point as well as on the initial conditions of the ion motion, the influence of the injection conditions must be investigated.

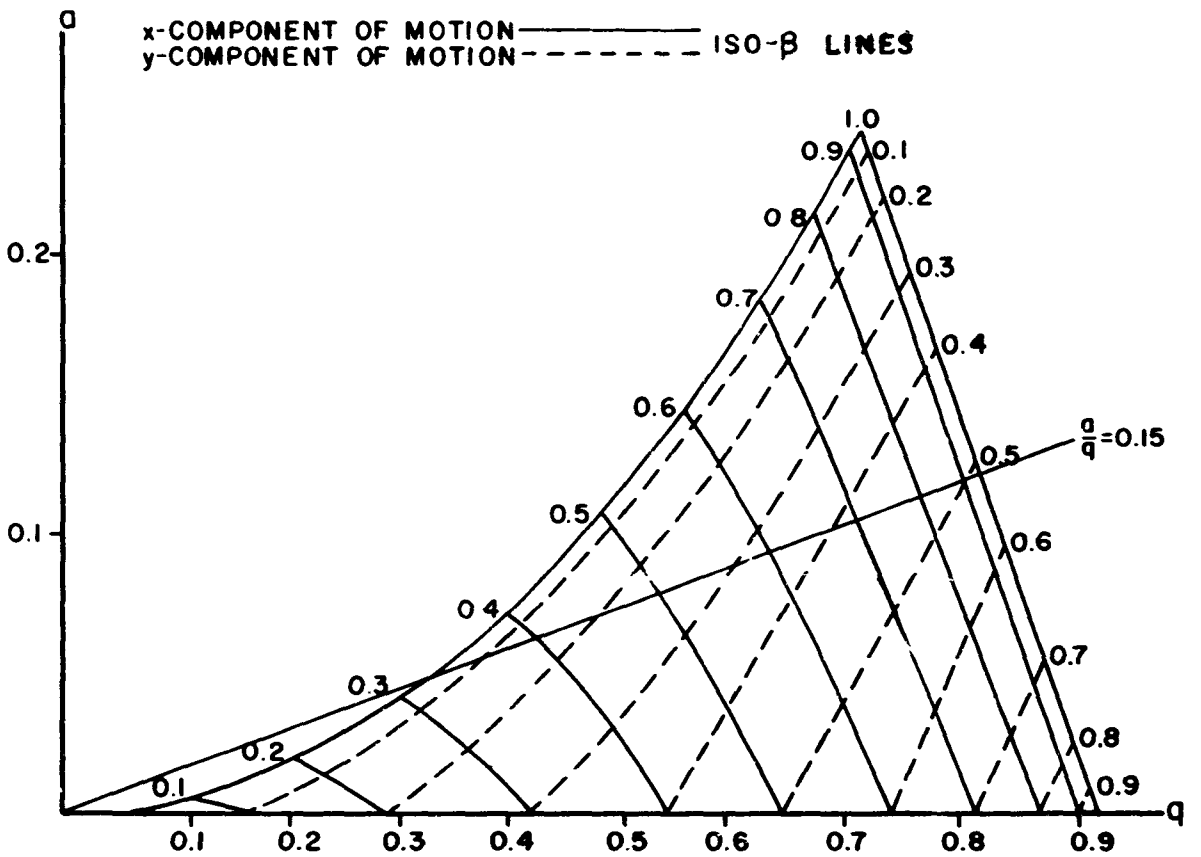

FIG 2.5
ISO-β CHART $0 \leq \beta \leq 1.0$

The maximum amplitude, obtained from equation (2.33) in the previous section is found to be

$$|x_{max.}| = \sqrt{A^2 + B^2} \cdot \sum_r |c_{2r}| \quad . \tag{2.36}$$

One should note that, in spite of the fact that the solution $x(\gamma)$ is not exactly periodic, after only a few vibrations, the actual vibration amplitude very closely approaches x_{max}.[8]

The calculation of $A(\gamma_o , x_o , \dot{x}_o)$ and $B(\gamma_o , x_o , \dot{x}_o)$ is based on using the basic systems of solutions $x_1(\gamma)$, and $x_2(\gamma)$, i.e.,

$$x(\gamma) = Ax_1(\gamma) + Bx_2(\gamma) \quad . \tag{2.37}$$

Differentiating (2.37) with respect to γ, and inserting the initial conditions $(x_o , (\frac{dx}{d\gamma})_{x_o} , \gamma_o)$ in the equation and substituting in equation (2.36), we get

$$|x_{max}| = \frac{1}{W} \sum_r |c_{2r}| \cdot \Big[(x_o \cdot x_2'(\gamma_o) - x_o' \cdot x_2(\gamma_o))^2 + (x_o' \cdot x_1(\gamma_o) - x_o \cdot x_1'(\gamma_o))^2 \Big]^{1/2} \tag{2.38}$$

where W is the Wronski determinant, and $x' = \frac{dx}{d\gamma}$.

For any given phase of injection γ_o , $x_1(\gamma_o)$, $x_2(\gamma_o)$, $x_1'(\gamma_o)$, $x_2'(\gamma_o)$ are constants and the quantity under the radical in equation (2.38) is a fourth order expression in x_o and x_o'. Equation (2.38) represents an ellipse in a (x_o, x_o') plane. Setting $x_m = r_o$, this ellipse connects all points (x_o, x_o') which, for fixed γ_o , have the same maximum amplitude of vibration r_o. For different phases of injection, a family of ellipses, with the parameter γ_o , is obtained.

Calculations for $a = 0$ and $\beta = 0.2, 0.5, 0.8$ were carried out by Fischer.[8] The results are presented in Fig. 2.6.

It can be seen that the maximum amplitude r_o is larger than the initial coordinate for all phases of injection except $\gamma_o = \pi/2$, where they could be equal. Thus, even in the center of the stable region, i.e., with best focusing, only a certain portion of the total field cross section can be utilized for the injection of ions.

Injection parallel to the axis

It is observed that the maximum amplitude $\frac{x_m}{x_o}$, $\frac{y_m}{y_o}$ are single valued functions of β. This makes it possible to construct lines of equal $\frac{x_m}{x_o}$, $\frac{y_m}{y_o}$, instead of iso-β lines, in the stability diagram as shown in Fig. 2.7. Setting $x_m = r_o$, then x_o, y_o represent the greatest distance off the field axis at the point of injection of the ion of stable trajectory, at which this ion, with the specific position of the operating point in the stability region, can still traverse the quadrupole field, whatever the ion's phase of injection may be.

As the operating point is moved along the mass line into the stability region, an increase in intensity will result, beginning at the limit of stability, since as the distance from this limit increases, even the ions entering the field farther away from the axis will be focused (allowable x_o , y_o increase towards the inner part of the stability diagram).

It is thus possible to attain 100% transmission provided the injection diaphragm is not too large. When the second limit of stability is approached on the mass line, a decrease of intensity will occur. The resulting observed mass peak, in this ideal case will be a trapezoid with sides of unequal slopes and a flat top representing the region of

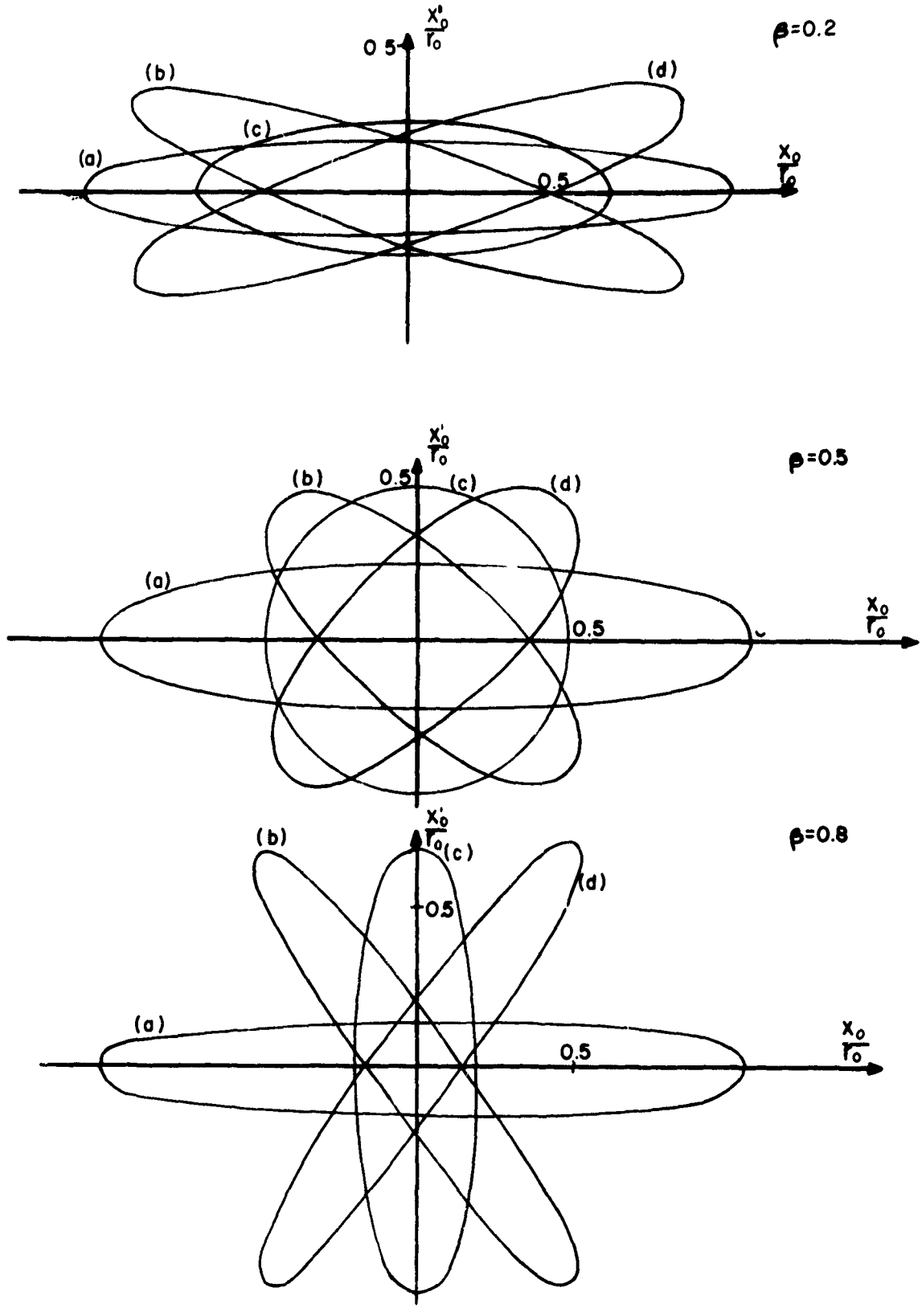

FIG 2.6

ADMISSIBLE INJECTION CONDITIONS FOR DIFFERENT OPERATING POINTS & PHASES OF INJECTION (a) $\xi_0 = \pi/2$ (b) $\xi_0 = 3\pi/4$ (c) $\xi_0 = 0$ (d) $\xi_0 = \pi/4$

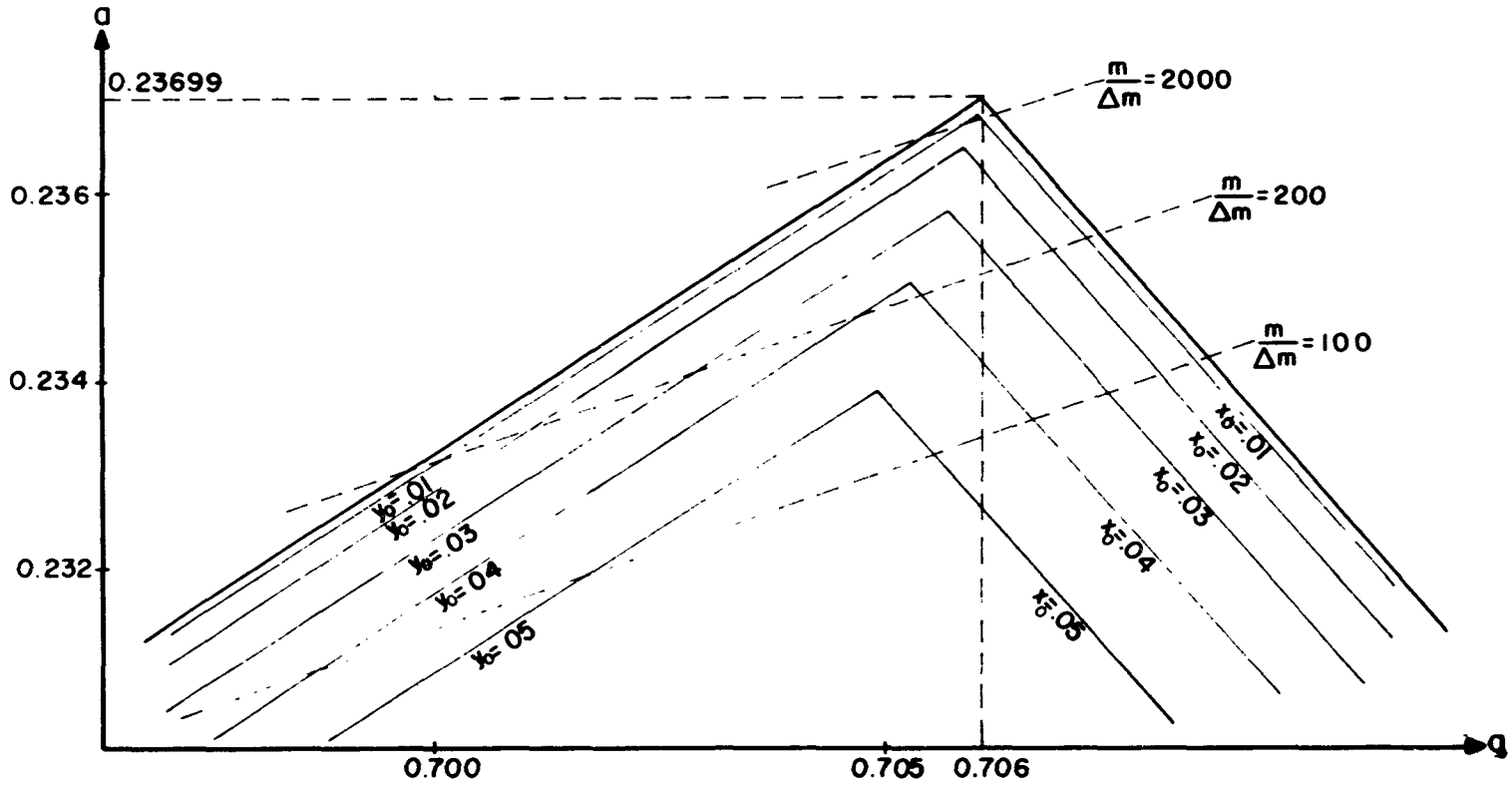

FIG 2.7
ADMISSIBLE INITIAL CONDITIONS (X_0, Y_0) WITH $r_0 = 1$ & $\dot{x}_0 = \dot{y}_0 = 0$

100% transmission. It is seen that this case could only be achieved at low resolving powers and/or small diaphragms. At high resolving powers, the line form changes to triangular, the intensity thus decreases and is inversely proportional to the resolution.

It has been shown that for a specified $\beta_{x,y}$ and setting $x_m = r_o$, there is an upper limit for $x_o, y_o = f(\omega t_o)$ for which the ions can still traverse the quadrupole field. By averaging over all phases of injection, one obtains the probability that a "stable" ion having initial conditions x_o, y_o ($\dot{x}_o = \dot{y}_o = 0$) can traverse the field. It is found that this probability decreases very rapidly above a certain value x_o, y_o which are a function of β and r_o.

2.9.3 Resolving power

It was previously mentioned that the resolving power of the instrument is mainly determined by the slope of the line of operation. The resolving power can thus be increased through increasing the slope of this mass line in the stability diagram by appropriately choosing the ratio U/V; this displaces the operating point higher into the upper corner of the stability "triangle". This means, however, that the operating point will approach very closely the limit of stability, with a resulting unavoidable increase in the maximum amplitude of vibration of the stable ions.

In order to gain a quantitative appreciation of this effect, the maximum amplitudes of vibration of ions, having defined initial conditions, were calculated numerically by Paul, et al.,[8] with specific reference to the position of the operating point. They found that for a resolving power above 70, only the region $0.69 < q < 0.71$ and $0.23 < a < 0.24$ is of interest. They assumed that, in this region, the

stability boundaries and the iso-β lines in the stability diagram could be approximated to straight lines (Fig. 2.7). The vertex of the stability triangle lies at

$$q_{limit} = 0.70600 \quad \text{and} \quad a_{limit} = 0.23699 \text{ .}$$

Paul, et al., have also calculated the relation between a and β_x , β_y for a value of q = 0.70600, where

β_x = β corresponding to the x-direction vibrational motion

and

β_y = β corresponding to the y-direction vibrational motion.

The relations obtained are:

$$(1-\beta_x)^2 = (0.23699 - a)/1.93750 \qquad (2.39)$$

and

$$\beta_y^2 = (0.23699 - a)/0.79375 \text{ .} \qquad (2.40)$$

Equations (2.39) and (2.40) establish a relationship between the position of the operating point (a,q) and the respective characteristic exponents β_x and β_y. Paul, et al.,[8] have also calculated the values for the coefficients c_{2r} , using the continued fraction expansion[3,9]

$$\frac{c_{2r}}{c_{2r-2}} = \frac{-q/(2r+\beta)^2}{1-a/(2r+\beta)^2} - \frac{q^2/(2r+\beta)^2\,(2r+2+\beta)^2}{1-a/(2r+2+\beta)^2}$$

$$- \frac{q^2/(2r+2+\beta)^2\,(2r+4+\beta)^2}{1-a/(2r+4+\beta)^2} + - - - -$$

with the normalisation $c_o = 1$.

Equations (2.36), (2.37), (2.38) enable us to obtain the maximum amplitudes of ions having stable trajectories in the x and y directions

for different positions of the operating point β, as a function of the two sets of initial conditions (ωt_o , x_o , $\dot{x}_o$) and (ωt_o , y_o , $\dot{y}_o$). Paul, et al, have carried out the calculations and the results are represented in fig. 2.8.

Fig. 2.8a shows the results obtained for injection parallel to the field axis, i.e.,

$$\dot{x}_o = \dot{y}_o = 0 \quad \text{and} \quad x_o \, , \, y_o \neq 0 \, ,$$

Fig. 2.8b shows the case of injection at the field axis of ions having radial velocities, i.e.,

$$x_o = y_o = 0 \quad \text{and} \quad \dot{x}_o \, , \, \dot{y}_o \neq 0 \, ,$$

One can conclude from the curves that x_m and y_m increase in inverse proportion to $1-\beta_x$ and β_y respectively.

We will adopt the convention of using the half width Δm of a mass peak at m as a measure of the resolving power as shown in Fig. 2.9. Paul and Raether[10] have obtained an expression for the resolving power in terms of the parameter "a" when q = 0.706. Their results could be numerized as follows:

a) For low resolving powers, where Δm is practically equal to the total line width

$$\frac{m}{\Delta m} = \frac{0.178}{0.23699 - a_{0.706}} \quad , \qquad (q = 0.706) \tag{2.41}$$

where $a_{0.706}$ is the value of "a" at q = 0.706.

b) For high resolving powers, where the peaks become triangular in shape

$$\frac{m}{\Delta m} = \frac{0.357}{0.23699 - a_{0.706}} \tag{2.42}$$

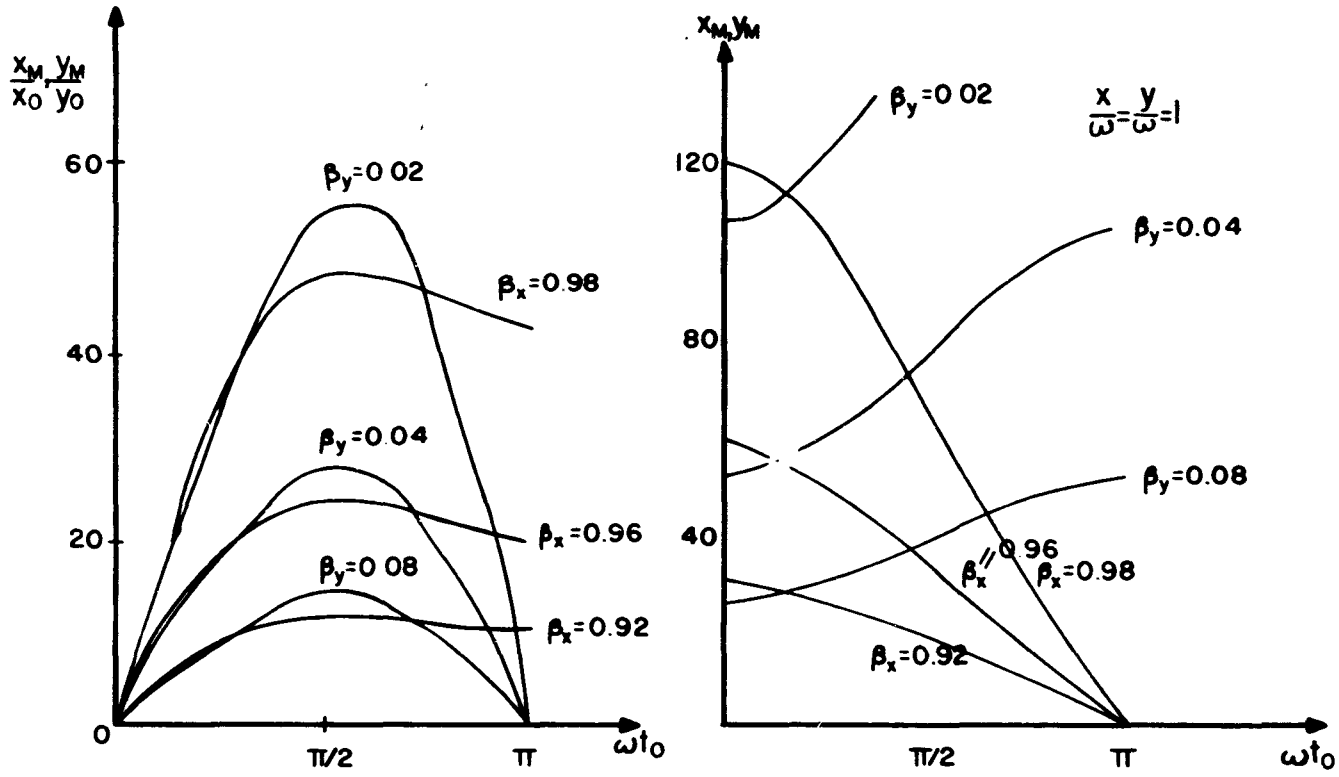

FIG 2.8

MAXIMUM AMPLITUDE OF VIBRATION

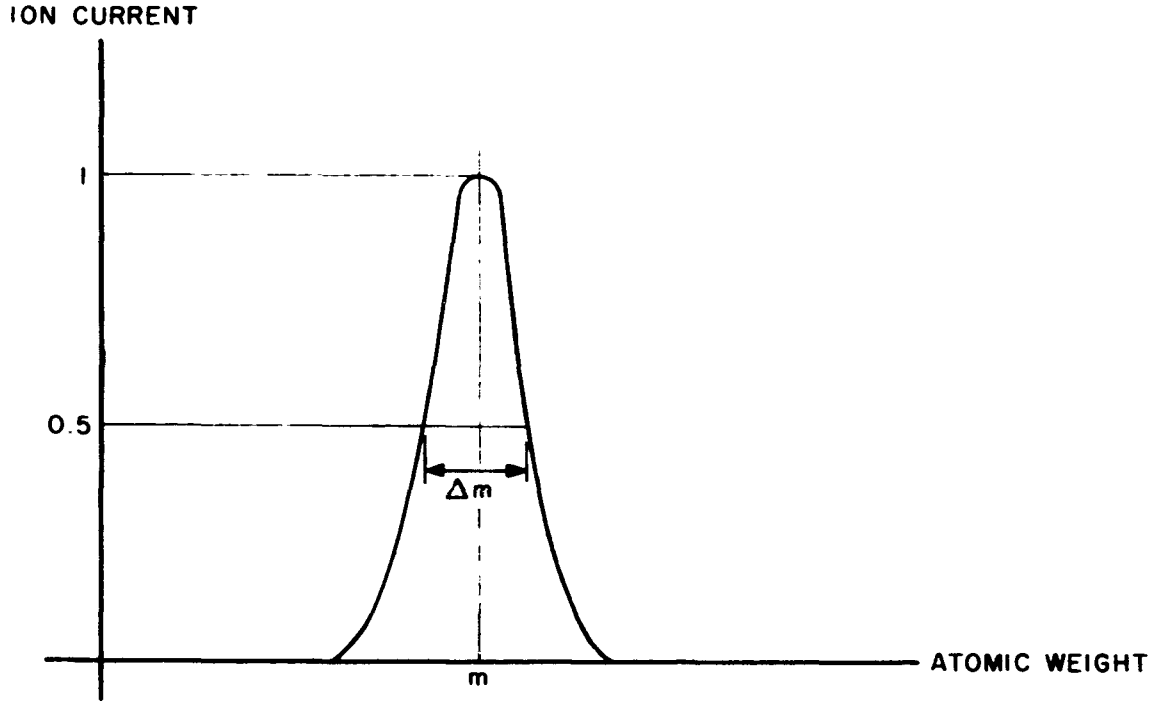

FIG 2.9

(Δm is equal to half the base width approx.). Combining equations (2.39), (2.40), (2.41), (2.42) a relationship between β, x_m , y_m and the resolving power was derived for injection parallel to the axis for high resolving powers

$$\frac{x_m}{x_o} \, , \frac{y_m}{y_o} < 1.8 \quad (m/\Delta m)^{1/2} \quad , \tag{2.43}$$

It is, therefore, concluded that the maximum amplitude increases only as the square root of the resolution; this is of importance when one desires to increase the resolving power.

One also obtains from equations (2.39) through (2.42) and Fig. 2.4 the admissible radial velocities of "stable" ions for injection at the axis

$$\dot{x}_m \, , \dot{y}_m < 0.16 \, r_o \, \omega \, (\frac{\Delta m}{m})^{1/2} \quad , \tag{2.44}$$

The ions of different masses are required to remain a certain number "n" of high-frequency periods in the field in order to ensure that the amplitude of the "unstable" ions will attain a value larger than r_o , and hence be eliminated at the electrodes. This number "n" is a function of the desired resolving power and sets an upper limit to the admissible injection velocity of the ions. It was found experimentally[8] that, for resolving powers around 100

$$n \simeq 3.5 \, (m/\Delta m)^{1/2} \quad . \tag{2.45}$$

This requirement introduces the relationship between the length L of the mass-spectrometer tube and the accelerating potential. This was found by Raether[10] to be

$$L \gg r_o \, \pi \, (\frac{2 \, U_{acc}}{V})^{1/2} \qquad q$$

where U_{acc} is the accelerating potential. This sets a lower limit to the length of the tube for practical accelerating potentials.

2.9.4 Stability and accuracy criteria

The behaviour of the mass-spectrometer is determined largely by the position of the operating point in the stability diagram. It is thus required that the parameters "a" and q be stabilised to approximately $1/(2m/\Delta m)$ of their value.

It follows upon examining the expressions for "a" and q that U and V, the dc and rf frequency voltage amplitudes respectively, be stabilised to better than $1/2m/\Delta m$ of their value. Also, the limitations on the frequency ω and the field radius r_o are more severe since they appear in the expression for "a" and q raised to the 2nd power.

Short spatially limited inaccuracies of r_o, however, cannot essentially influence the stability behaviour of the ions, since a displacement of the operating point in the stability diagram can only be caused by field defects which are operative for many high-frequency periods.

References

1. Paul, W. and H. Steinwedel, "Ein neues Massenspektrometer ohne Magnetfeld", Z. Naturforschg. 8a, 448 (1953).

2. Mathieu, E', "Memoire sur le mouvement vibratoire d'une membrane de forme elliptique", Jour. de Math. Pures et Appliquees (Jour. de Liouville) 13, 137 (1868).

3. Mclachlan, N. W., "Theory and Application of Mathieu Functions", Oxford, (1951).

4. Ince, E. L., "Tables of the elliptic cylinder functions", Proceedings Roy. Soc. Edinburgh 52, 355 (1932).

5. Floquet, G., "Sur les equations differentielles lineaires", Ann. de l'Ecole normale Superieure, 12, 47 (1883).

6. Whittaker, E. T., "General solution of Mathieu's equations", Proc. Edinburgh Math. Soc. 32, 75 (1914).

7. Young, A. W. "Quasi-periodic solutions of Mathieu's equation", Proc. Edinburgh Math. Soc. 32, 81 (1914).

8. Paul, W., H. P. Reinhard and U. von Zahn, "Das elektrische Massenfilter als Massenspektrometer und Isotopentrenner", Z. Phys. 152(2), 143 (1958).

9. Ince, E. L., "Mathieu funct ons of stable type", Philos. Mag. 6, 547 (1928).

10. Paul, W., and M. Raether, "Das elektrische Massenfilter", Z. Phys. 140, 262 (1955).

General References

A. Blanch, G., "Computation of Mathieu functions", Jour. Math. and Phys. M.I.T. 25, 1 (1946).

B. Dougall, J., "Solution of Mathieu's equation", Proc. Edin. Math. Soc. 34, 4 (1916).

C. Goldstein, S., "Mathieu functions", Trans. Camb. Phil. Soc. 23, 303 (1927).

D. Ince, E. L., "Periodic solutions of linear differential equations with periodic coefficients", Proc. Camb. Phil. Soc. 23, 44 (1926).

E. Ince, E. L., "Tables of elliptic cylinder functions", Proc. Roy. Soc. Edin. 52, 355 (1932).

F. Ince, E. L., "Relations between the elliptic cylinder functions", Proc. Roy. Soc. Edin. 59, 176 (1939).

G. Ince, E. L., "Characteristic numbers of Mathieu's equation", (1) Proc. Roy. Soc. Edin. 46, 20 (1925).

M. Mclachlan, N. W., "Mathieu functions and their classification", Jour. Math. and Phys. M.I.T. 25, 209 (1946).

N. Mclachlan, N. W., "Computation of solution of Mathieu's equation", Phil. Mag. 36, 403 (1945).

Chapter 3

Design Calculations

In this chapter the calculations of the various parameters inherent to the mass-spectrometer will be presented. The choice of the parameters will be discussed in terms of the requirements set by the planned experiments.

3.1 Resolving power considerations

One of the great advantages of the quadrupole-type mass-spectrometer is, as mentioned previously, the ease by which the resolving power can be changed if necessary. A constant resolving power, on the other hand, is possible irrespective of the mass of the ion to be analyzed.

In the study of basic collision processes in plasmas, besides identifying the ions through mass analysis, the efficiency of the mass analysing instrument is of prime importance since it is desired to detect ion currents of very small value (of the order of 10^{-18} amps). The design of the mass-spectrometer was, therefore, based on maximum efficiency and not on constant resolving power; the only "resolving" requirement being that the peak at a certain mass is not affected by the presence of neighboring masses. Theoretically, this means that the condition

$$\frac{m}{\Delta m} \geqslant 2m ,$$

as illustrated, in Fig. 3.1, has to be satisfied.

Here

m = mass to be analyzed

Δm = curve width at 1/2 the height.

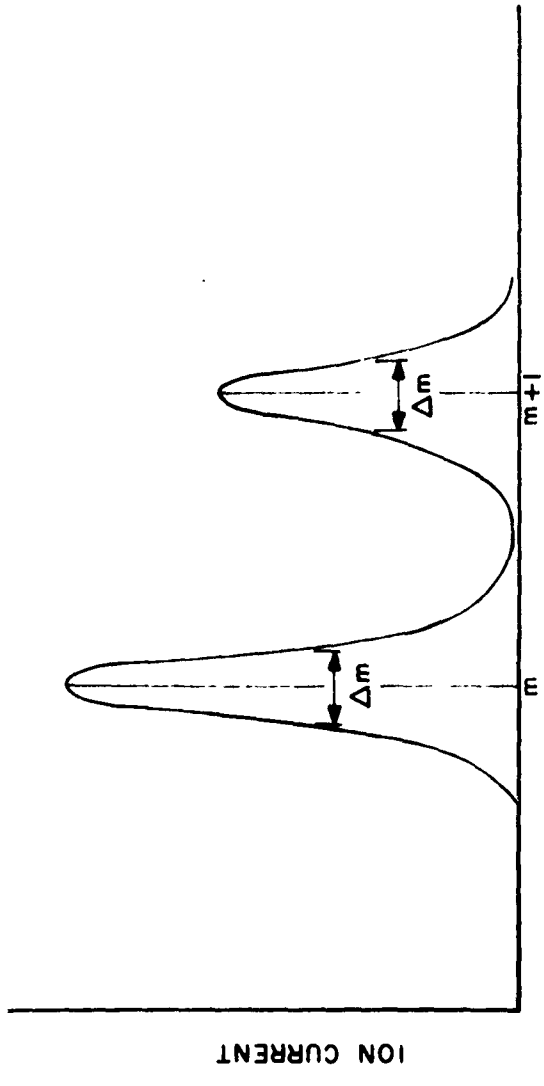

FIG 3.1

In conclusion, to obtain maximum collecting efficiency, the resolving power will have to be decreased at low masses for the following reasons:

1. At high resolving power, the intensity of the ion beam current is inversely proportional to the resolution.

2. Accelerating potential considerations.

The mass spectrometer is planned to operate in a mass range of 1 to 125. The field radius r_o was chosen to be 2 cm. This choice was based on obtaining a compromise between the power requirements (increases with r_o^4) and the increase of tolerances in initial conditions with larger r_o.

3.2 Quadrupole voltage and frequency calculations

Expressions for the required ac and dc voltages could be obtained from the parameters "a" and q as follows:

The expression for the rf voltage amplitude V follows from

$$q = \frac{4eV}{mr_o^2\omega^2}$$

or

$$V = \frac{m}{4e} r_o^2\omega^2 q \quad .$$

Substituting

$$e = 1.601 \times 10^{-19} \text{ coulomb}$$

$$m = 9.107 \times 10^{-31} \times 1836 \times A \text{ kilogram}$$

$$q = 0.706^* \quad ,$$

*The calculations are performed assuming the operating point of the mass spectrometer to be at the vertex of the stability triangle (a = 0.23699; q = 0.706), i.e., the resolution is assumed to be infinity (ideal).

we find

$$V = 7.287\ r_o^2\ f^2\ A \text{ volts} \qquad (3.1)$$

where

r_o is in cm

f is in Mc/s

A is the atomic weight of the ion.

The expression for the dc voltage U is determined by

$$\frac{a}{q} = \frac{2U}{V} = \frac{0.23699}{0.706} ,$$

or

$$U = 0.16784\ V ,$$

so that

$$U = 1.223\ r_o^2\ f^2\ A \text{ volts} , \qquad (3.2)$$

Choice of Frequency

The mass selection is obtained through varying either the frequency or the voltages or both. In this spectrometer, both the frequency and voltages will be varied in order to stabilise an ion with specific mass. The frequency will be changed in steps, thus determining the mass range and the voltages will select the masses within the set range.

It is to be noted that the rf and dc voltages should be varied such that the ratio between them remains constant (U/V = const.) for maintaining a constant resolution of the instrument. The reason for the simultaneous monitoring of frequency and voltage is based upon the high-frequency power requirements and the desired mass range.

The high-frequency power requirement for the quadrupole system was calculated by Paul et al.[1] The following expression was obtained:

$$N = 6.5 \times 10^{-4} \times \frac{C \quad A^2 \quad f^5 \quad r_o^4}{Q} \quad \text{watts,} \qquad (3.3)$$

where

N = power required in watts

C = capacity of the system in μμf

A = atomic weight of the ion

f = rf frequency in Mc/s

r_o = field radius in cm

Q = quality factor of the output circuit.

It is observed, at first glance, that the required power is a function of the fifth power of the frequency*. Since the aim is to achieve a wide mass range with reasonable power and voltage requirements, as well as resolution, a detailed investigation of the behaviour of power and voltage with atomic mass and frequency is necessary. With

r_o = 2 cm., substitution in equation (3.1) gives

$$V = 7.287 \times 4 \times f^2 \times A$$

$$= 29.148\ f^2\ A \text{ volts}. \qquad (3.4)$$

The capacity of the system is found experimentally to be approximately 100 μμf and when choosing a reasonable value for Q

---

*This is only a first order approximation since the dielectric constant of the system changes with the introduction of the charged particles and thus with frequency. The equivalent dielectric constant $k_{eq} = 1 - \frac{ne^2}{m_o \omega^2}$; the actual expression for power will be:

$N = C_1 A^2 f^5 - c_2 A f^3$, where c_1 and c_2 are constants.

(100 say), we get

$$W = 6.5 \times 10^{-4} \times 1.0 \times 16\, A^2 f^5 \quad \text{watts}$$

$$= 1.04 \times 10^{-2}\, A^2 f^5 \quad . \qquad (3.5)$$

A plot of required voltages and power versus atomic weight A for different frequencies is shown in Fig. 3.2. It follows immediately that in order to attain a wide mass selection range with reasonable ranges of rf voltage and power, one should use as low a frequency as possible. It is not possible, however, to use very low frequencies, since, in this case one has to increase the length of the spectrometer tube and/or decrease the accelerating potential for the ions in order to fulfill the condition that the "vibrating" ions should remain a definite number of high frequency periods in the field to obtain satisfactory resolution. This point will be discussed in detail in section 3.3. A compromise was made and the length of the tube was taken to be 100 cm. The required frequencies are thus

0.5 Mc/s to cover the mass range 125-50

1.0 Mc/s to cover the mass range 50-12

2.0 Mc/s to cover the mass range 12-1,

Under these conditions, using equation (3.4) and (3.5), we find that the required rf power will vary between the approximate limits of 50 watts for A = 12 and a few tenths of a watt for hydrogen.

The required rf voltage V will hence vary between 1450 and 116 volts. The plot of V versus atomic weight A, shown in Fig. 3.3 will serve to calibrate the instrument.

3.3 Determination of maximum ion accelerating potentials

The accelerating potential applied to the ions entering the spectrometer determines, for a fixed tube length, the number of high

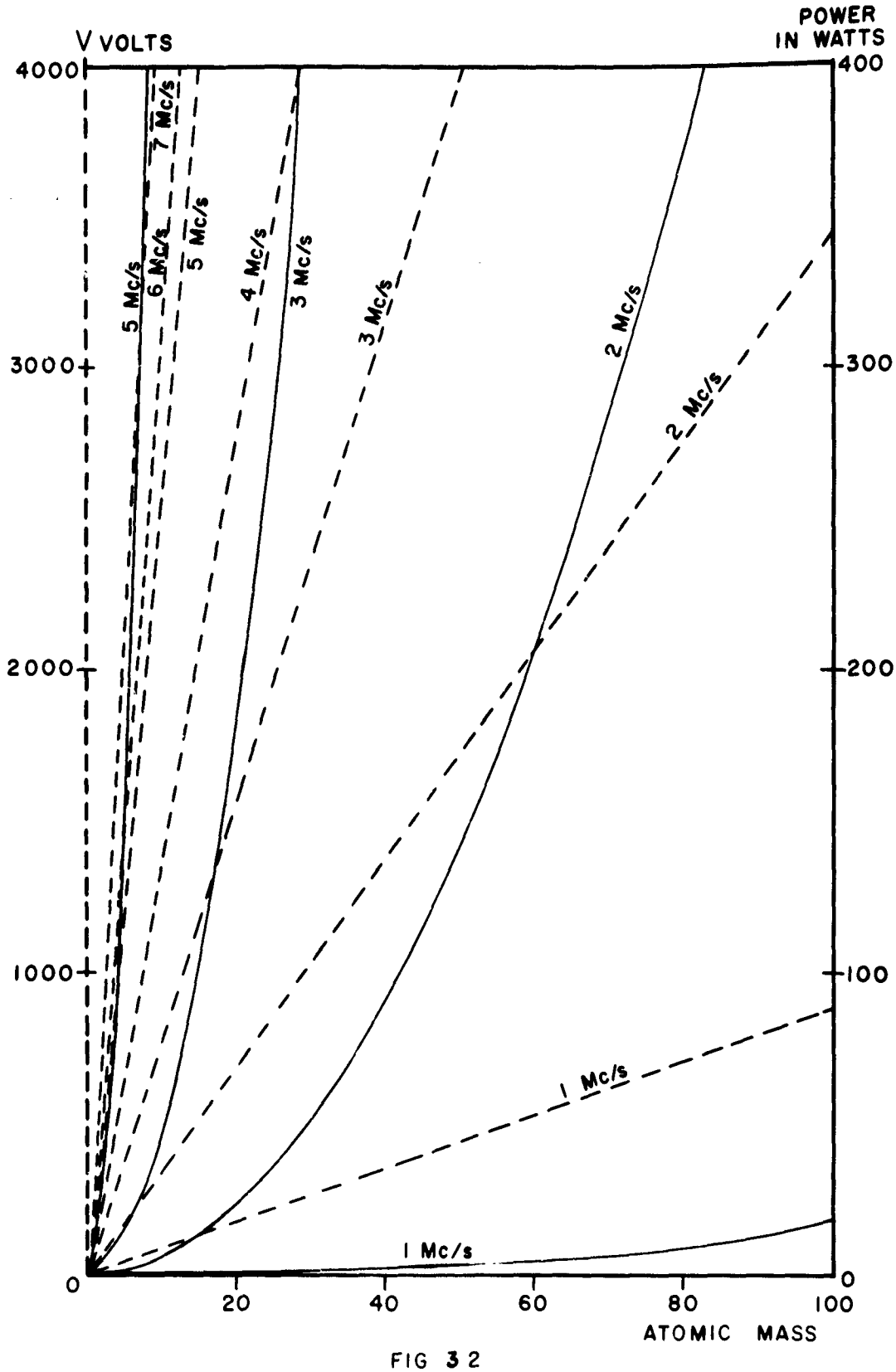

FIG 32

EFFECT OF FREQUENCY ON REQUIRED r f POWER & VOLTAGE

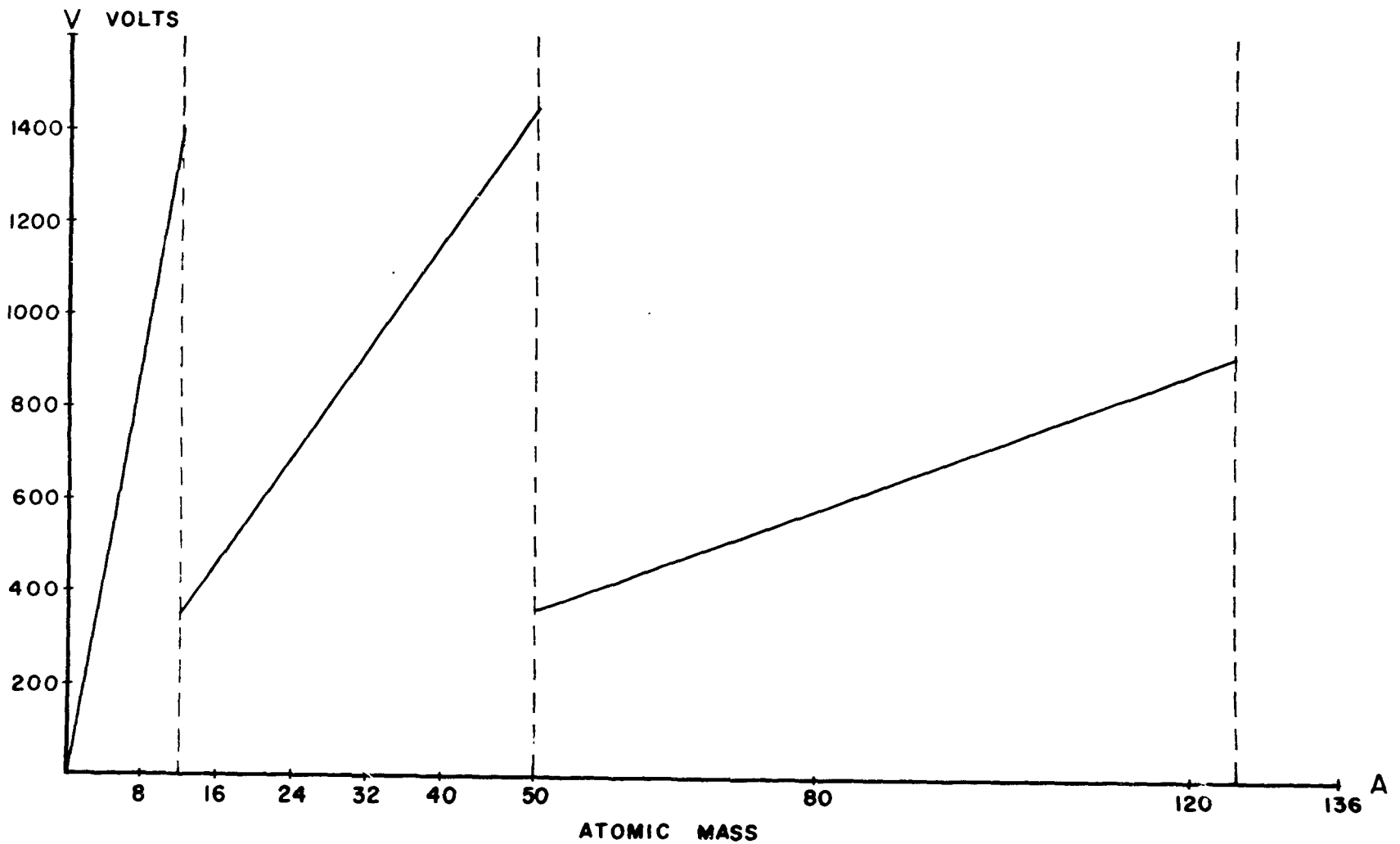
V VOLTS
1400
1200
1000
800
600
400
200
8
16
24
32
40
50
80
120
136
A
ATOMIC MASS

FIG 3.3

frequency periods the ions remain in the quadrupole field since there is no field force directed along the axis of the tube. With reference to chapter 2, the minimum number of high frequency periods necessary to ensure complete loss of unstable ions at the electrodes and hence good resolution was found experimentally to be[1]

$$n \simeq 3.5 \left(\frac{m}{\Delta m}\right)^{1/2},$$

Hence, the drift time of the ion through the field must be larger or equal to n high frequency periods. We will now proceed to obtain an expression for the maximum allowable accelerating potential from the above relation.

The velocity of a singly charged particle in terms of its energy in electron volts is given by[2]

$$V_z = \frac{5.93 \times 10^7}{\left(A \frac{m_H}{m_e}\right)^{1/2}} u^{1/2} \text{ cm/sec},$$

where

u is the energy in electron volts

m_H is the mass of the hydrogen atom

m_e is the mass of the electron

A is the atomic weight of the particle

$m_H = 1836\, m_e$.

Total time needed for n high frequency periods is

$$T = \frac{10^{-6}}{f_{Mc}} n .$$

Minimum time of ionic flight through the quadrupole field

$$T_{total} = \frac{10^{-6}}{f_{Mc}} 3.5 \left(\frac{m}{\Delta m}\right)^{1/2} \text{ sec.}$$

so that the maximum allowable velocity of ions is

$$V_s = \frac{10^2 L}{T_{total}} = \frac{10^8 Lf}{3.5} \left(\frac{\Delta m}{m}\right)^{1/2} \quad \text{cm/sec.} \quad ,$$

where

L is the length of the field in meters

f = frequency of applied voltage in Mc/s.

Hence

$$10^8 L \frac{f}{3.5} \left(\frac{\Delta m}{m}\right)^{1/2} = \frac{5.93 \times 10^7}{(1836\ A)^{1/2}} u^{1/2}$$

so that the maximum accelerating potential ϕ_{max} is given by

$$\phi_{max} = \left(\frac{10\ Lf}{3.5 \times 5.93}\right)^2 \times 1836\ A \frac{\Delta m}{m}$$

or

$$\phi_{max} = 4.26 \times 10^2\ L^2\ f2\ A \frac{\Delta m}{m} \quad \text{volts} \quad .$$

The advantage of lowering the resolution when analysing low mass values is again evident. It enables the use of a shorter tube length, while maintaining an appropriate value of accelerating potential. Moreover, it avoids, the bulkiness of a larger tube, hence, cutting down the pumping and bakeout requirements. For L equal to 1 meter, we have

$$\phi_{max} = 4.26 \times 10^2 f^2 A \frac{\Delta m}{m} \quad .$$

The resolutions chosen, and hence the resulting required accelerating potentials for the three different mass ranges are as follows:

mass range:	1-12	12-50	50-125
resolution:	1:100	1:250	1:250
maximum accelerating potential in volts:	18-216	20.5-85	21-53 ,

A plot of accelerating potential versus atomic weight A is shown in Fig. 3.4.

When we take the minimum condition for the resolving power, i.e.,

$$\frac{\Delta m}{m} = \frac{1}{2m} ,$$

we obtain

$$\phi_{max} = 213\ L^2 f^2 \quad \text{volts} .$$

The smallest frequency used is 1/2 Mc/s, so that for this frequency

$$\phi_{max} = 53\ L^2 \quad \text{volts} .$$

It is seen that the choice of a length L smaller than 1 meter would give rather low and impractical values for the maximum allowable acceleration potential.

3.4 Calculation of dc voltage requirements

It was shown previously that the ratio $\frac{\text{dc applied voltage}}{\text{rf applied voltage}}$ determines the resolution of the mass-spectrometer. In this case, the resolution is variable in two steps 1:100 for mass values 1 to 12 and 1:250 for mass values 12 to 125.

At q = 0.706, the relation between the resolution and the values of "a", for high resolving power, as is the case, was given in chapter 2 as

$$\frac{m}{\Delta m} = \frac{0.357}{0.23699 - a_{0.706}}$$

Step I

$$\frac{m}{\Delta m} = 100 = \frac{0.357}{.23699 - a^{(1)}_{0.706}}$$

so that

$$a^{(1)}_{0.706} = 0.23699 - 0.00357 = 0.23342 ,$$

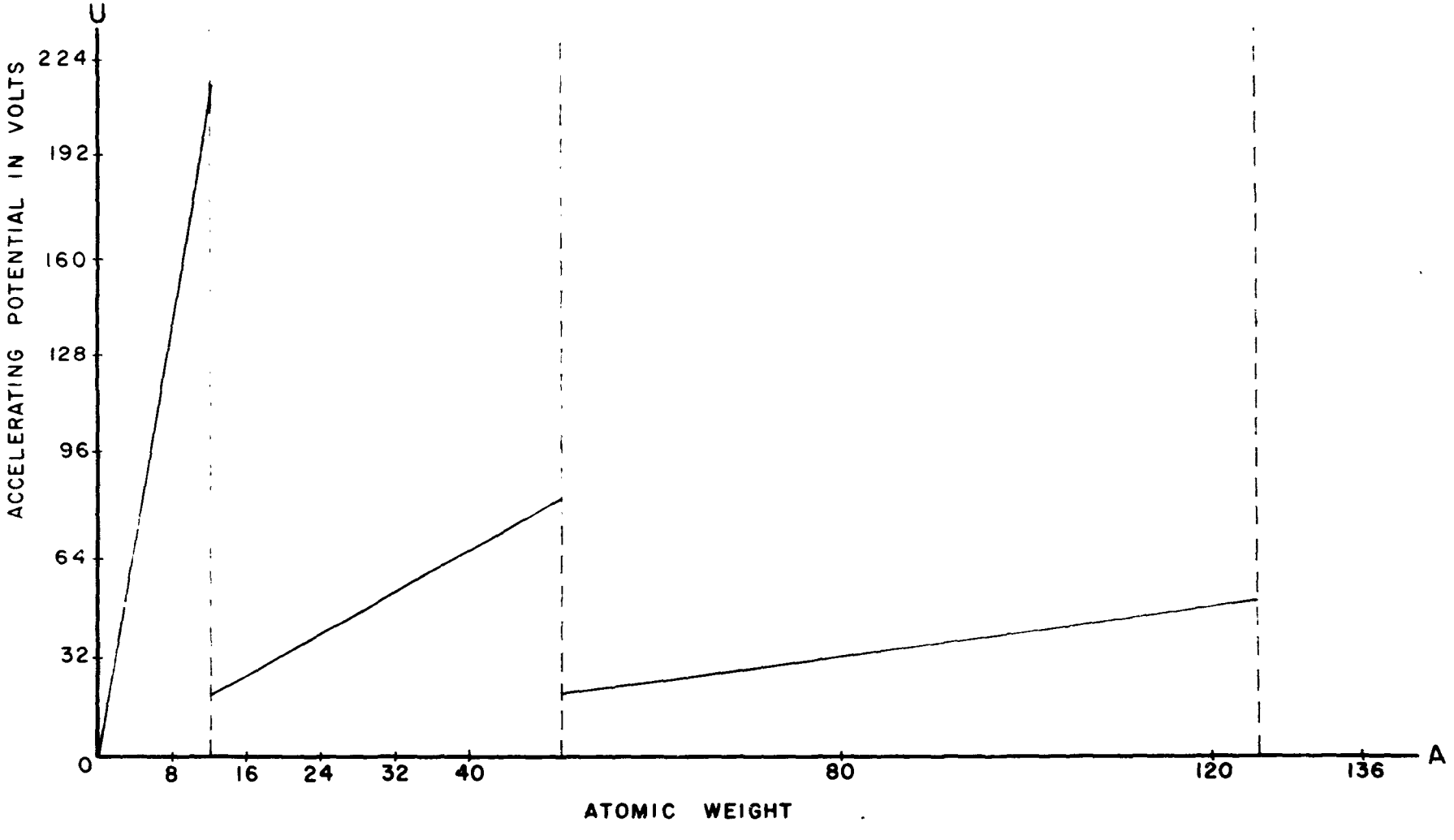
U
ACCELERATING POTENTIAL IN VOLTS
224
192
160
128
96
64
32
0
8
16
24
32
40
80
120
136
A
ATOMIC WEIGHT

FIG 3 4

Thus

$$\frac{U^{(1)}}{V} = \frac{a^{(1)}}{2q} = \frac{0.23342}{2 \times 0.706} = 0.16531 .$$

Substituting the range of variation obtained for V, we find that $U^{(1)}$ will vary from 20 volts for hydrogen to 240 volts for A = 12.

Step II

$$\frac{\Delta m}{\Delta m} = 250 = \frac{0.357}{0.23699 - a^{(2)}_{0.706}}$$

$$a^{(2)}_{0.706} = 0.23699 - 0.001428 = 0.23556$$

Thus

$$\frac{U^{(2)}}{V} = \frac{a^{(2)}}{2q} = \frac{0.23556}{1.412} = 0.16683$$

$U^{(2)}$ will thus range from 63 volts for A = 13 to 243 volts for A = 50 and from 60 volts for A = 50 to 152 volts for A = 125.

3.5 Maximum allowable radial energy of the injected ions

The variation of the allowable radial energy with the "off symmetry" of the injected ions was discussed in detail in chapter 2. The relation was illustrated to be of an elliptic nature and was summarised in Fig. 2.6. From the practical point of view, however, we will limit ourselves to the case of injection at the field axis and use the expression obtained by Paul, et al[1] for determining the maximum allowable radial energy of the ions, namely

$$u_{r_{max}} \simeq \frac{V}{15(m/\Delta m)} \quad \text{electron volts,}$$

where V is the rf voltage amplitude.

This quantity represents the largest amount of radial energy a "stable" ion is allowed to possess while still being focused by the quadrupole field. This point is very important in designing the ion source for the attainment of the high degree of sensitivity and collection efficiency required in the present instrument. Since this condition is proportional to the applied rf voltage, it becomes most severe in the case of hydrogen as in this case

$$V = 116 \quad \text{volts}$$

so that

$$u_{r_{max}} \simeq \frac{116}{15 \times 100} \simeq 0.075 \text{ electron volts.}$$

It is seen that this value is rather small, approximately twice the thermal energy of the ions at room temperature. This value, however, is by no means obstructive since the ion source to be utilized with the spectrometer is a diffusion type in which the ions diffusing out of the gaseous plasma are essentially thermal. The ion source will be discussed in detail in chapter 5.

The excellent feature of the quadrupole mass-spectrometer, namely, the variable resolving power facility, again proves to be very advantageous. The maximum allowable radial energy could be greatly increased by lowering the resolution. It was shown that a practical resolving power of $\frac{m}{\Delta m} \geqslant 2m$ is sufficient for the studies planned.

Inserting this in the expression for $u_{r_{max}}$, we get

$$u_{r_{max}} = \frac{V}{15 \times 2m}$$

and from equation (2.4)

$$V = 29.148 f^2 A \quad \text{volts,}$$

so that

$$u_{r_{max}} = \frac{29.148}{30} f^2 \simeq f^2 \quad \text{electron volts,}$$

where f is in Mc/s.

It can readily be seen that, in the case of low masses, where a frequency of 2 Mc/s is employed, the ion is allowed to have a radial energy of 4 ev and will still remain stable in orbit and thus efficiently detected.

3.6 Summary

Mass-Spectrometer Specifications

r_o: 2 cm

length: 100 cm

mass range:	1-12	12-50	50-125
frequency:	2.0Mc/s	1.0Mc/s	0.5Mc/s
resolving power:	1:100	1:250	1:250
rf voltage:	116-1400	380-1457	364-910

power consumption: 0.6 - 50 watts

References

1. Paul, W., H. P. Reinhard and U. von Zahn, "Das elektrische Massenfilter als Massenspektrometer und Isotopentrenner", Z. Physik 152(2), 143 (1958).

2. Oskam, H. J. "Plasma Physics", Lecture series given at the Department of Electrical Engineering of the University of Minnesota.

Chapter 4

General Description and Outline of the Mass-Spectrometer

In the following chapters, an attempt will be made to illustrate the different problems that were encountered in the construction of the mass-spectrometer and the efforts to solve them.

A block diagram of the complete mass-spectrometer is shown in Fig. 4.1. The ions produced in a gas discharge tube are allowed to diffuse out of the plasma through the glass wall via a small hole having a diameter of 25 microns approximately. The appropriate accelerating potential is then applied to the ions using a double grid after which the ions enter the quadrupole field. The output of the quadrupole field, viz., the mass analyzed ions are then focused, using a simple electrostatic lens, into the first dynode of the ion multiplier. The focusing is required at this stage, since the effluent ions oscillate in the quadrupole field and hence have a wide exit angle. The signal current output from the ion multiplier could either be displayed on an oscilloscope or be integrated through a vibrating reed electrometer and the mass peaks recorded on a strip chart recorder.

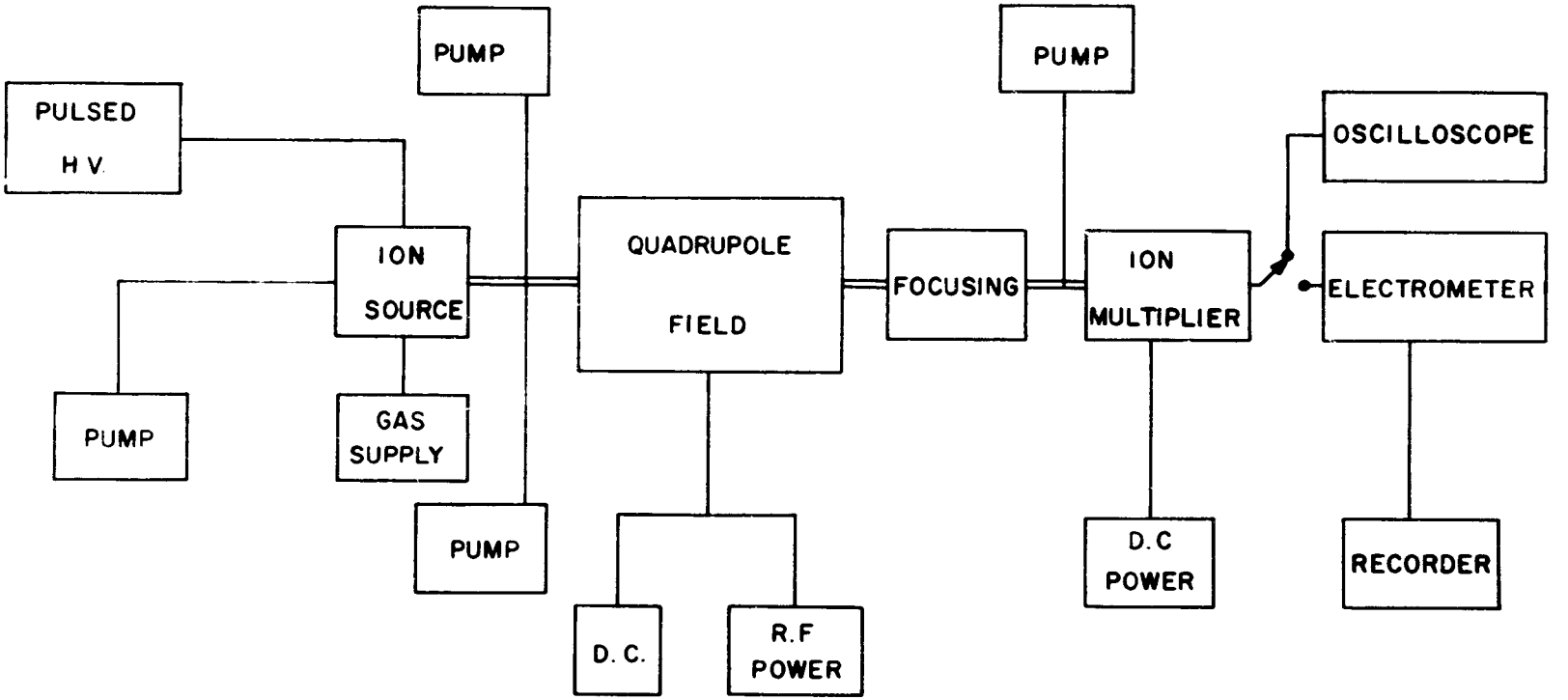

FIG 4.1
QUADRUPOLE MASS SPECTROMETER BLOCK DIAGRAM

Chapter 5

The Ion Source

It was previously mentioned that the mass-spectrometer will be used in a careful study of the basic collision processes occurring in active, as well as in decaying plasmas.

The ion source, and the associated gas handling system are shown in Fig. 5.1 (a,b) consists primarily of a gaseous discharge tube (A), about one inch in diameter, filled to a well-defined pressure with the gas (or mixture of gases) to be studied. The high voltage applied to the tube produces a discharge thus ionising the gas. A small hole (B), approximately 25 microns in diameter permits the ions to diffuse out of the tube; these ions are then required to be mass analysed by the spectrometer. The gaseous discharge tube is enclosed by a stainless steel cylinder which is sealed to the fore end of the spectrometer via a gold ring-flange vacuum seal. The two ends of the gaseous discharge tube extend out of the cylinder via glass-kovar metal seals. One end is sealed off and the other connects via a "Granville-Philips" Type C ultra-high vacuum metal valve to the pump and gas handling system. This system consists of a "Consolidated" three stage oil diffusion pump which is air cooled and backed by a "Cenco" high vacuum rotary mechanical pump. The diffusion pump employs Octoil-S fluid.

The system is baked out at 350°C for approximately 12 hours and pumped down to a pressure of the order of 10^{-9} mm Hg in order to ensure that the discharge tube is sufficiently clean before admitting any gas. The valve is then closed and the gas to be studied is introduced from the gas bottles into the discharge tube via a leak valve (C) which is

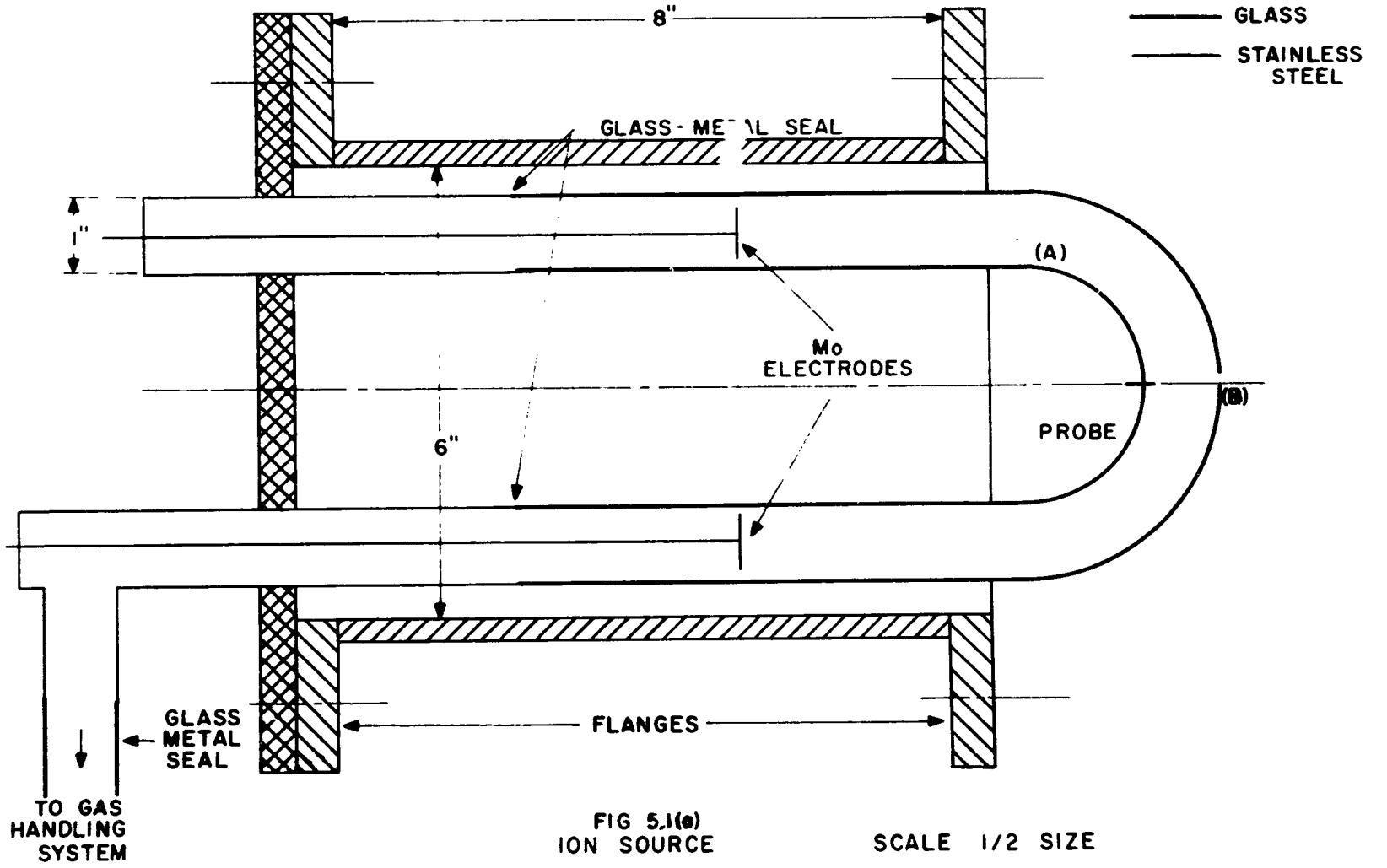

FIG 5.1(a)
ION SOURCE

SCALE 1/2 SIZE

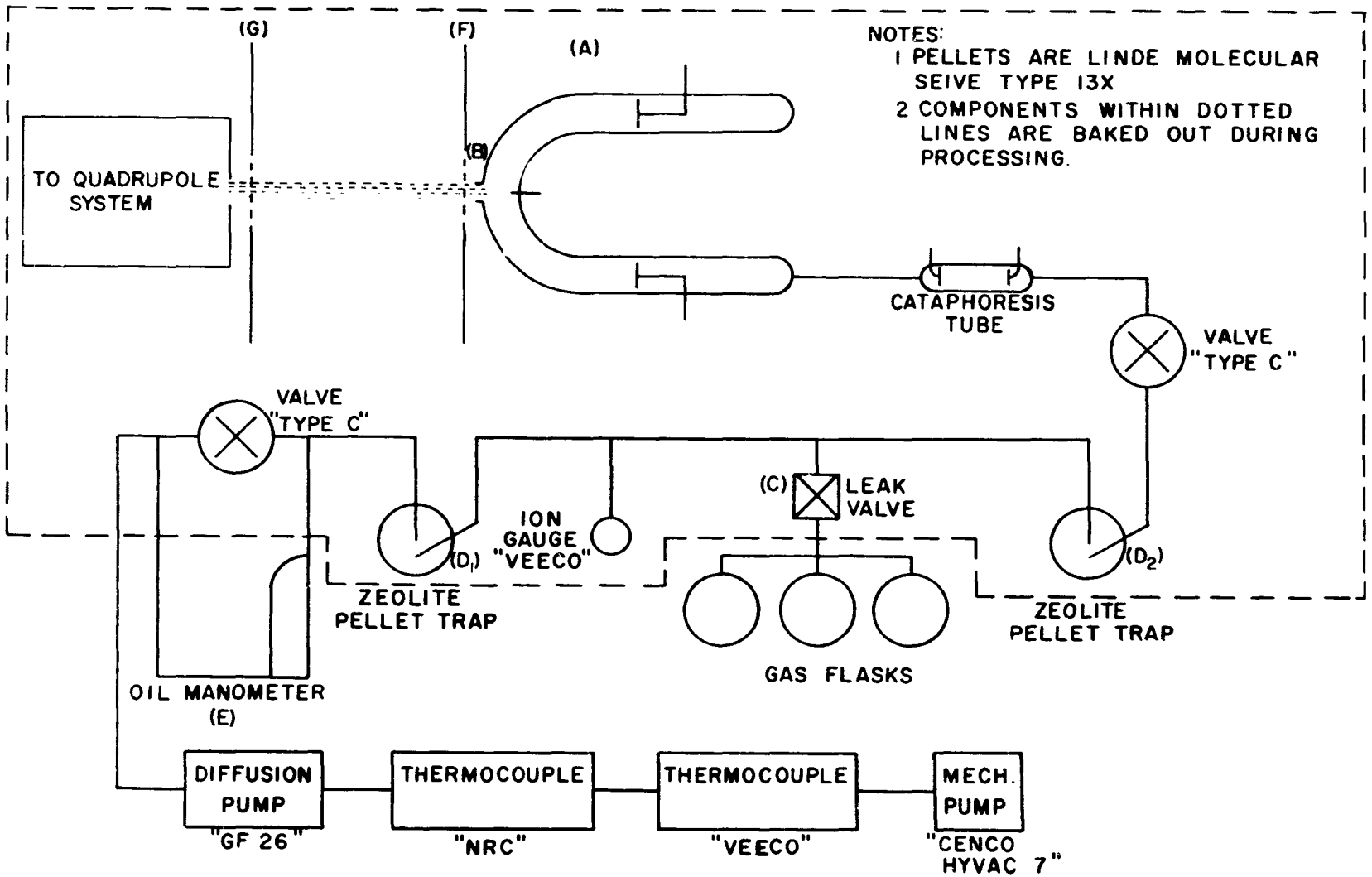
(G)
(F)
(A)
(B)
NOTES:
1 PELLETS ARE LINDE MOLECULAR SEIVE TYPE 13X
2 COMPONENTS WITHIN DOTTED LINES ARE BAKED OUT DURING PROCESSING.
TO QUADRUPOLE SYSTEM
CATAPHORESIS TUBE
VALVE "TYPE C"
VALVE "TYPE C"
(C) LEAK VALVE
ION GAUGE "VEECO"
(D1)
(D2)
ZEOLITE PELLET TRAP
ZEOLITE PELLET TRAP
GAS FLASKS
OIL MANOMETER (E)
DIFFUSION PUMP "GF 26"
THERMOCOUPLE "NRC"
THERMOCOUPLE "VEECO"
MECH. PUMP "CENCO HYVAC 7"

FIG 5.4(b)

adjusted so as to maintain a constant gas pressure inside the discharge tube. Two Zeolite traps, (D_1 and D_2) are placed between the diffusion pump and the discharge tube which serve to absorb the oil molecules which are streaming back from the diffusion pump. A special type of oil manometer (E), designed by Biondi,[1] is used for measuring the pressure of the gas in the discharge tube. This manometer is obviously not bakeable, but a small heating wire is immersed in the oil reservoir to degas the oil during bakeout.

The two tungsten grids (F) and (G) are utilized for accelerating the diffusing ions to the appropriate energy required for efficiently traversing the quadrupole field.

Grid (G) is maintained at ground potential and the positive or negative accelerating potential for positive or negative ion analysis respectively is applied to grid (F). This arrangement is made to obtain a zero potential difference between the axis of the quadrupole field and the axis of the ion beam. This condition is very important for maximum efficiency requirements because if the incoming "stable" ion sees a potential difference, it will acquire a radial energy which might be larger than the allowable radial energy, and hence will result in the loss of this "stable" ion to the electrodes of the quadrupole field. To fulfill this condition, the accelerating field is made as homogeneous as possible by decreasing the distance between the two grids.

Figure 5.2 shows an enlarged view of the gaseous discharge tube tip containing the hole. The choice of the size of the hole (about 25 microns) is based on the requirement that it should be very much smaller than the thickness of the plasma sheath in order not to disturb the sheath configuration. The hole is made by first sealing a

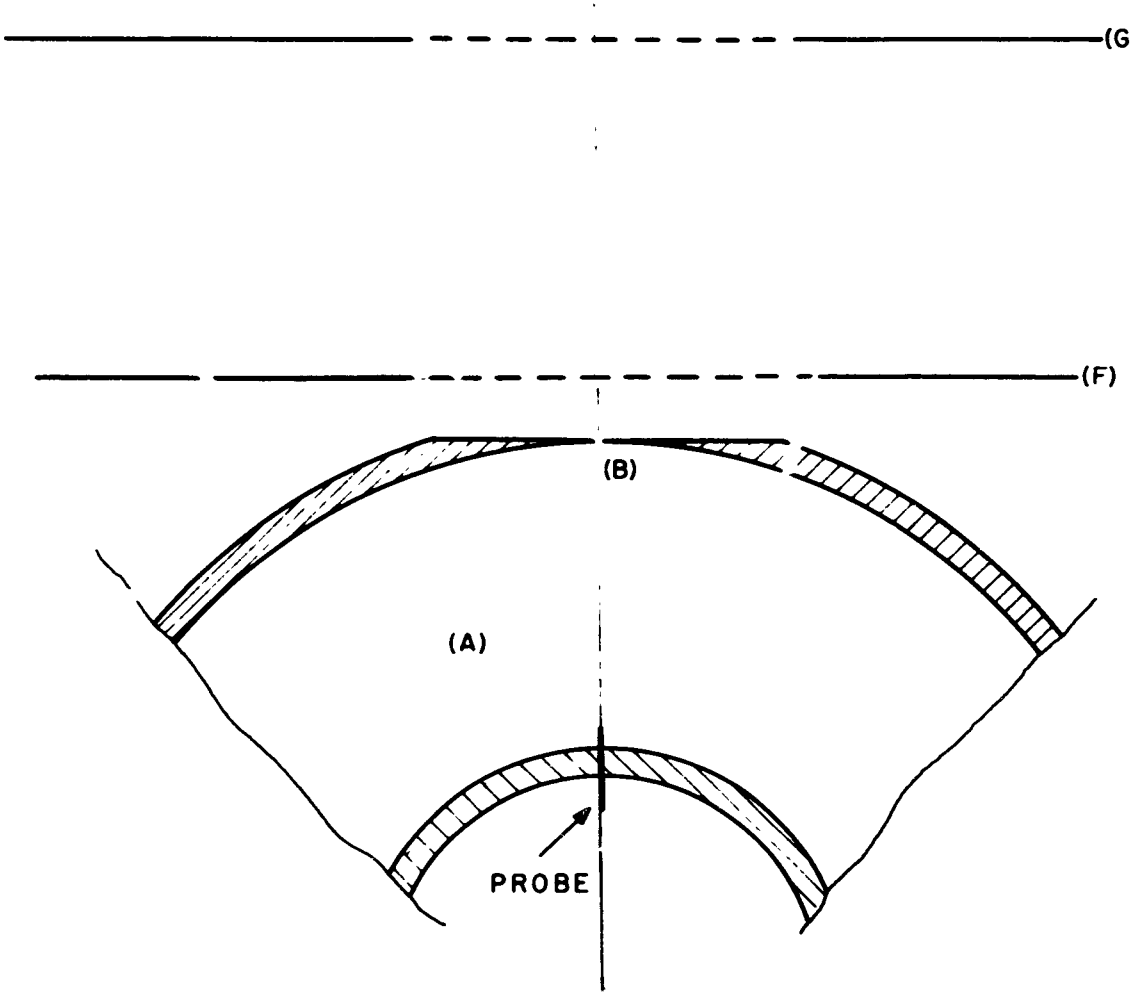

FIG 5.2

tungsten wire with a diameter equal to the required hole size into the glass tube. The tube wall, at the face of the hole, is then ground and the wire is subsequently etched away. The electrodes of the discharge tube are made out of Molybdenum sheet; the diameter of the electrodes is one inch or less.

A thermocouple pressure gauge measures the fore-pressure of the mechanical pump and thus serves as a high pressure control. If during bakeout, for example, the pressure rises above a certain preset value, the thermocouple potential (proportional to the pressure) rises and trips a relay so as to switch off the power to the ovens and the diffusion pump. Figure 5.3 shows the wiring diagram for the ion-source vacuum system.

Reference

1. Biondi, M. A., "Oil manometer for ultra-high vacuum systems", Rev. of Sc. Inst. 24, 989 (1953).

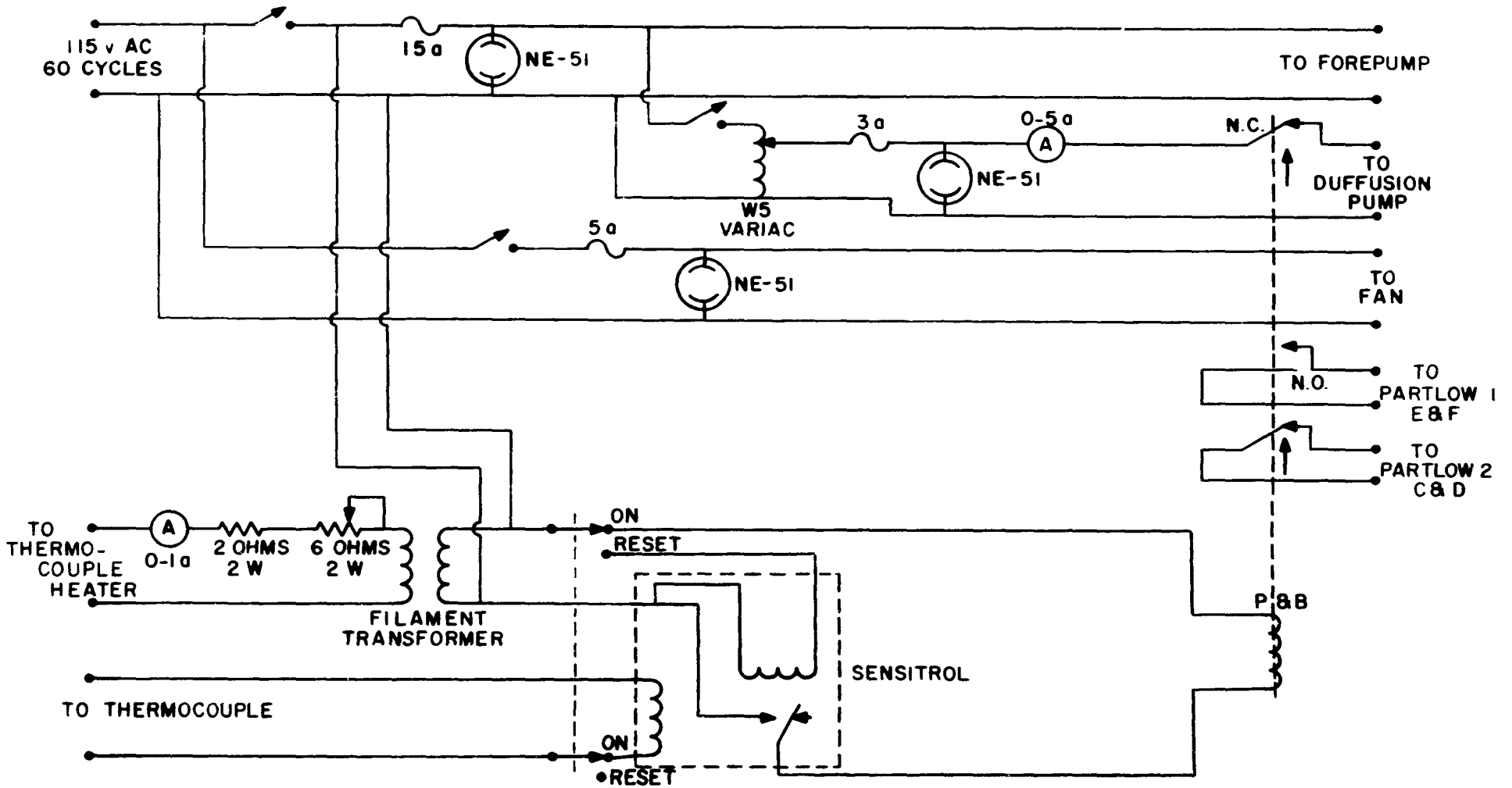

FIG 5.3 ION SOURCE CONTROL PANEL

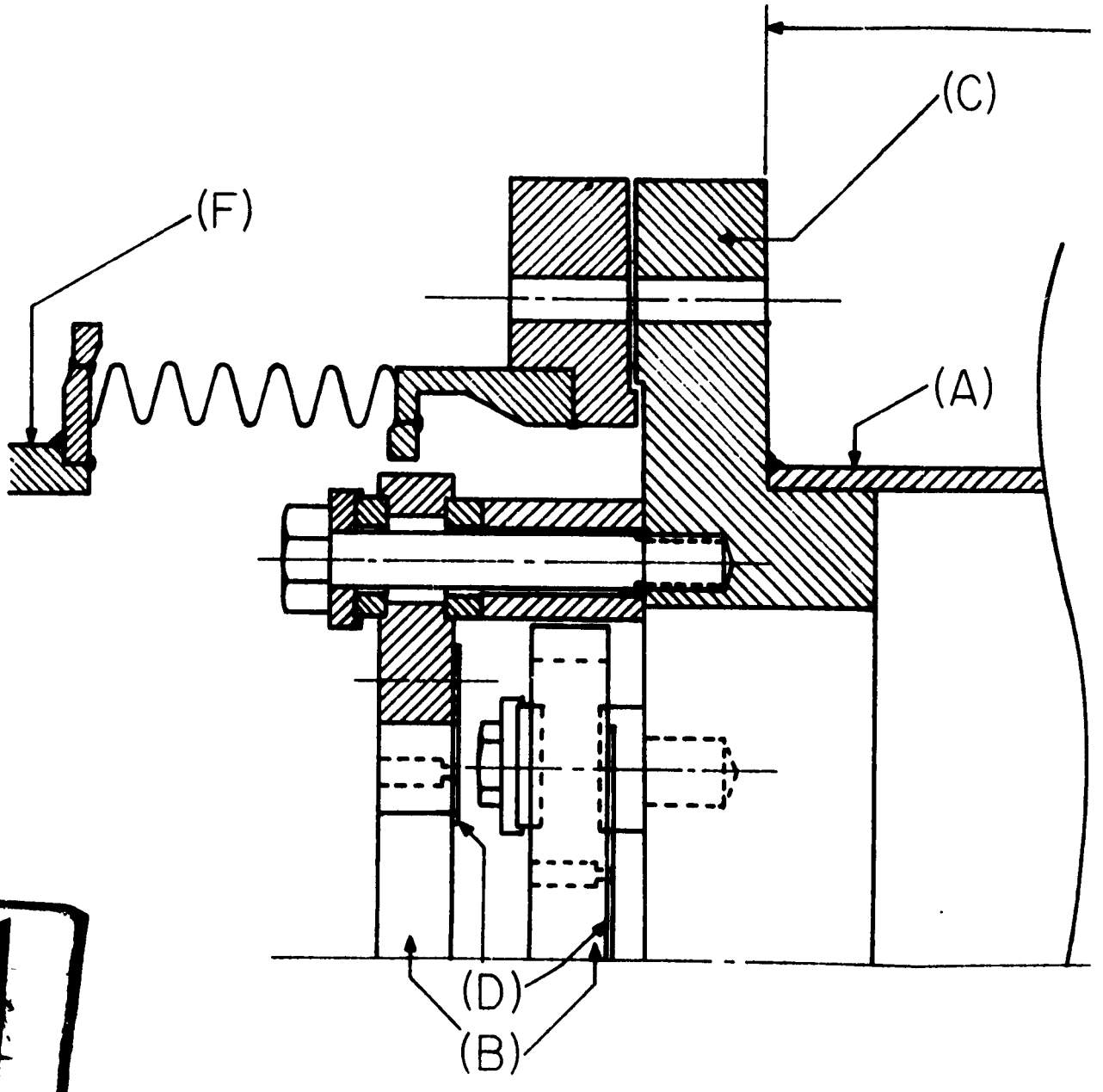

1

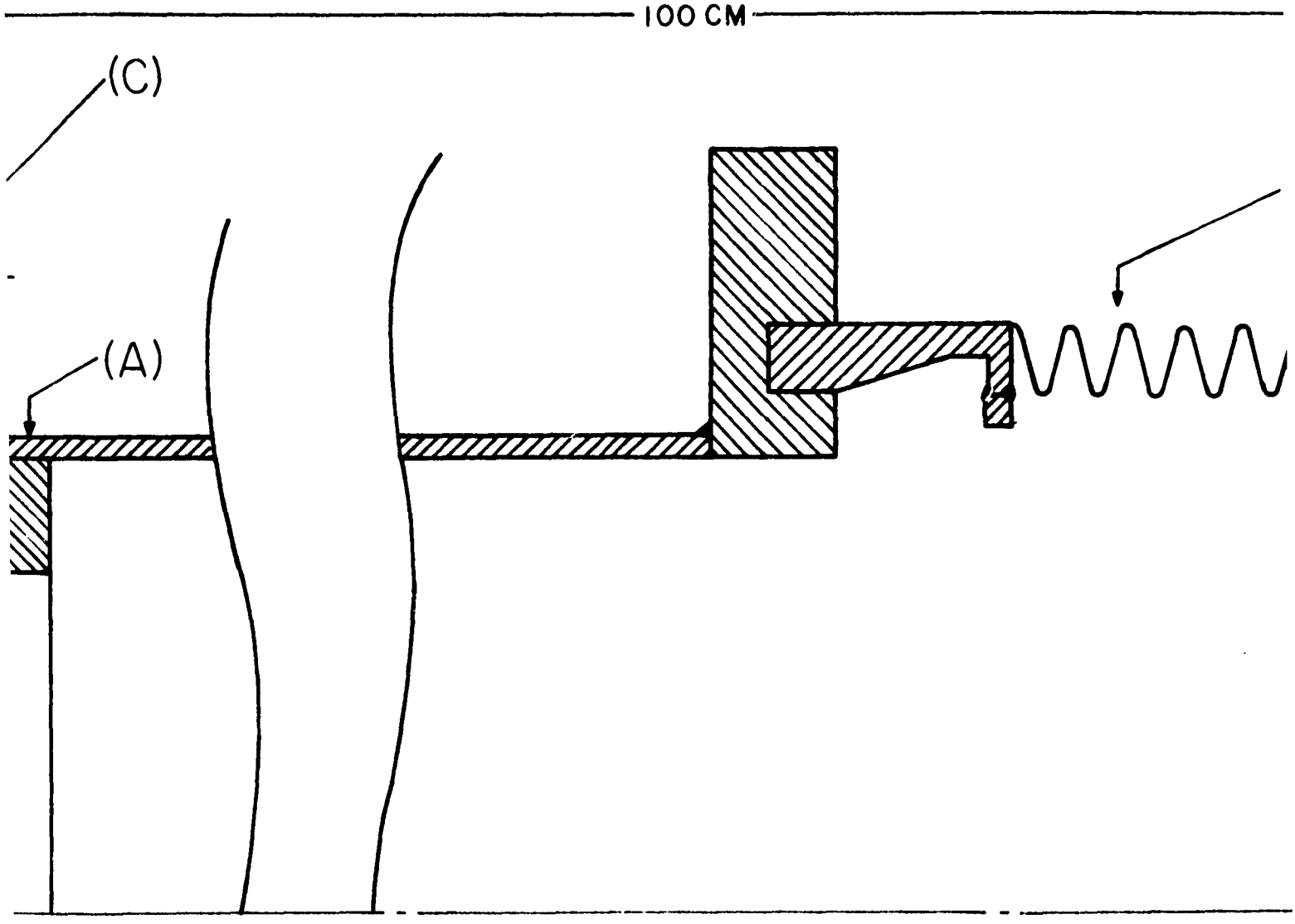

SCALE FULL

FIG 6.1

2

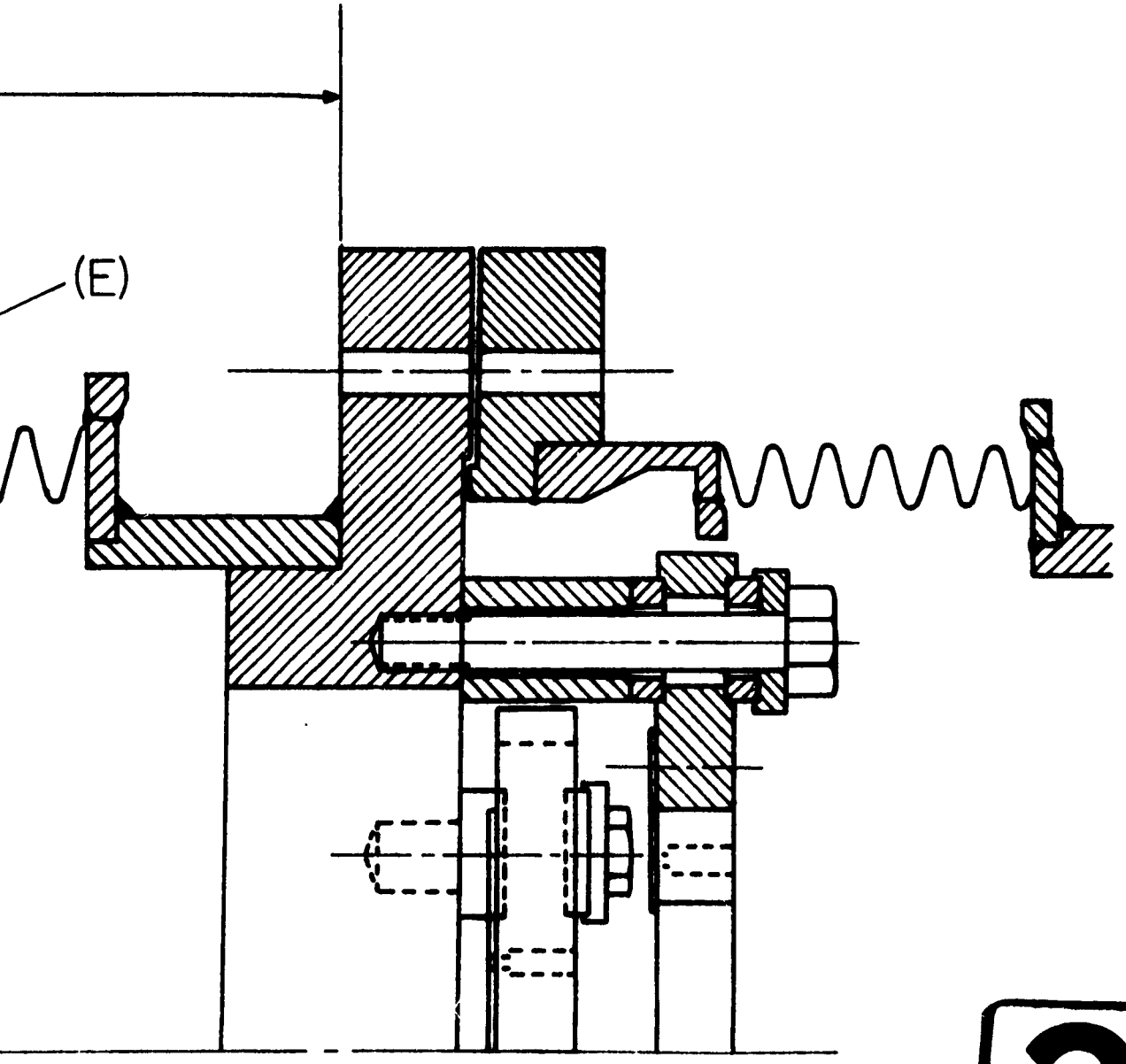

FULL SIZE

3

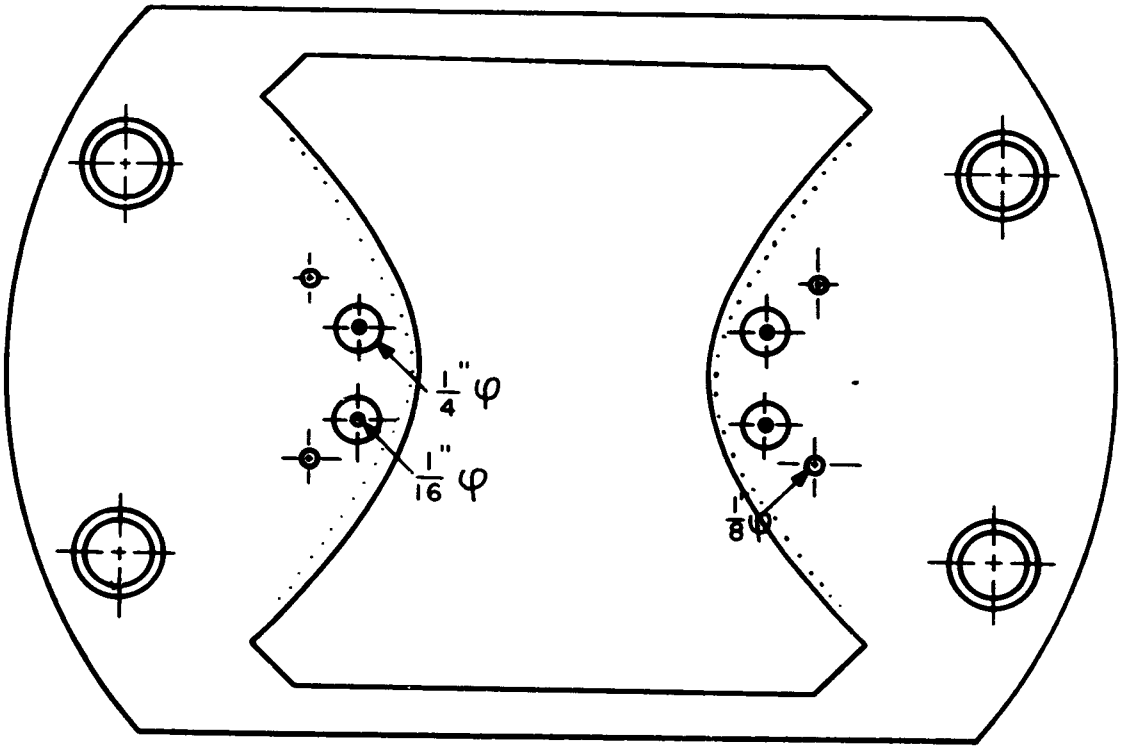

SCALE FULL SIZE

FIG 6.2

Chapter 6

Mechanical Design Considerations

6.1 The quadrupole system

The quadrupole field is obtained by four electrodes shaped to form an equilateral hyperbola having $a = b = r_o = 2$ cm. An assembly of the electrode system is shown in Fig. 6.1.

The outer casing (A) is a stainless steel Type 304 pipe, 6 inches internal diameter and 0.128" wall thickness; the tube is 100 cm long. Each of the four hyperbolic electrodes is formed by stretching 31 Molybdenum wires of 0.508 mm in diameter along the length of the tube; the cross section of each set of wires thereby lying on an arc of the equilateral hyperbola. The wires are fastened on each end by small stainless steel screws to two stainless steel Type 303 plates (B) of the shape shown in Fig. 6.2. It is to be noted that each set of diagonally opposite electrodes (wires) are fastened to the same plate since they carry the same polarity of potential. This is done in order to reduce the alignment problem which will be discussed later. It is interesting to mention that the hyperbolae were accurately cut in plates (B) by determining first the length of the hyperbolic arc (which involved the evaluation of an elliptic integral*), thus accurately determining the exact position of each wire with respect to a chosen reference point. The metal was thereafter removed with the aid of a precise milling machine. Plates (B) are held in place by four studs each to the specially shaped set of flanges (C). A total of

---

*For the method of calculation, the reader is referred to the appendix.

eight stainless steel plates (D) $\frac{1}{16}$" thick are fastened each under a hyperbolic arc as shown in Fig. 6.1. Each plate has a set of holes 0.508 mm in diameter very accurately drilled along an identical hyperbolic arc through which the set of wires pass. Plates(D), therefore, act as guides to the wires and are utilised for very fine adjustments during the alignment procedure.

Insulation is achieved using small bushings made of "AlSiMag" material and were kindly supplied by the Power Tube Division of General Electric Company, Schenectady, New York. This material has the advantage of possessing a high compression strength combined with the ability to withstand high bakeout temperatures while maintaining good dimensional stability.

6.2 Admissible over-all machining and alignment tolerances

It is understood that the behaviour of the mass-spectrometer is largely determined by the position of the operating point in the stability diagram, i.e., by the parameters "a" and q (compare section 2.9). It follows that these parameters must be stabilised to approximately (1: $2m/\Delta m$) of their value.[1] Hence, the field radius r_o must be constant to better than (1: $4m/\Delta m$). This sets the upper limits to the tolerances in machining, which, in our specific case were kept within $\pm$ 0.001 inch; this permits, therefore, a maximum resolution of 320.

The performance of the spectrometer is also determined by the degree of symmetry of the quadrupole field and especially its symmetry about the tube axis. In other words, it is required, as previously mentioned in chapter 5, that the axis of the spectrometer tube be at ground potential. This condition is approached at high degrees of symmetry of the quadrupole field. In practice, this is achieved by

stretching a fine conducting wire along the tube axis, switching on the dc and rf potentials and adjusting the position of the wires so as to obtain a minimum potential on the wire with respect to ground.

6.3 Wire tension

The molybdenum wires are required to be under a tension equal to approximately 40% of its breaking load. This explains the reason for choosing molybdenum as a material for the wires since it possesses the required tensile strength. There are two reasons for applying this large amount of tension, namely,

1. to keep the deflection due to the attractive forces between two sets of adjacent wires, especially those at the end of the hyperbolic arcs which are closest to each other, within the set tolerances. When calculating the force of attraction in this region of very high field strength, it is found that the required tensile force is quite large, exceeding, in effect, the yield strength of some of the known conducting materials; hence, the choice of molybdenum.

2. to minimize sagging of the wires.

6.4 The differential expansion problem

One of the basic requirements, which had to be taken into account in the design of the spectrometer, is the ability to bake out the whole system under vacuum at 450°C for a period of at least 12 hours. This is done to ensure having a clean vacuum system which is essential for reliable interpretation of experimental data. Bakeout presents a problem only in the quadrupole system. Here, the difference in the thermal coefficient of expansion between the stainless steel outer tube and the molybdenum wires becomes quite serious. If the wires are installed and the system heated, the tension on the wires will gradually

increase due to the larger coefficient of expansion of stainless steel. A simple calculation showed that at a temperature as low as 300°C, the tension becomes so large that it will exceed the yield strength of molybdenum resulting in a permanent deformation of the wires. Consequently, when the system cools after bakeout, the tension on the wires will be lost and they will therefore sag. This problem was studied very carefully and it was found, unfortunately, that it could not be solved by changing the material of the wires because, a material having a higher tensile strength like tungsten, say, has also a smaller thermal coefficient of expansion. Stainless steel wires, on the other hand, could not be used since they possess a high creep rate, especially at higher temperatures. Thus, while it eliminates the differential expansion problem altogether, after a few bakeouts we will end right where we started from.

The problem was solved, therefore, by deliberately sagging the wires, baking out the system with the wires sagged, cooling to room temperature and then pulling the wires back to the required amount of tension. This was achieved through the use of an extra flange and bellow (E), fastened to the tube at the far end of the spectrometer (Fig. 6.1). The bellow is first rigidly fixed in its neutral state (neither expanded or compressed). The wires are then installed and pulled to the required amount of tension. Before bakeout, the bellow is allowed to contract, thereby sagging the wires, and is then pulled back after bakeout. A hydraulic jack system will probably be used to measure the force on the flange thereby making it possible to adjust the tension on the wires after bakeout. This method adds the advantage of easily adjusting the tension on the wires since it might change due to electrical heating effects or otherwise.

The quadrupole system is connected to the ion source via a short section (F) of stainless steel 6" tubing with gold-ring sealed flanges as shown in Fig. 6.1. To ensure maximum sealing efficiency of the flanges, a bellow must be inserted wherever a set of two flanges connects together. This bellow relieves the stresses which might occur in the flanges if all connections were rigid. These stresses are the main cause for leakage around the gold ring.

Three sections of 3" diameter tubing are connected to the main section (F), thereby providing access to the system. One tube connects to the mass-spectrometer pumping system. The second tube is utilised for electrical wire inputs and fastening of grids. The third tube is preserved for further development of the studies and may be combined with a quartz window for optical viewing of the gaseous discharge in the ion source.

At the far end of the spectrometer, a similar section of tubing connects the output of the quadrupole system to the ion multiplier detection system. The ports at this end are again utilised for pumping and focusing of the effluent ions.

6.5 Mounting of the mass-spectrometer system

A desired feature, which was taken into account in the design of the system, was equipment "mobility". The entire mass-spectrometer system is constructed to be a mobile system. It was both plausible and desirable to design it in this manner when taking into consideration the future developments in our research program which will require the combination of the mass-spectrometer with other research equipment for simultaneous measurements.

The entire system is placed on a table 93" x 38" x 30" high, which is made of "Dexion" slotted angle iron. The table has a 3/4" plywood and formica top and is supplied with heavy-duty casters. Mounted on the table is an angle iron frame on top of which are placed a number of heat insulating blocks made of aluminum filled with glass wool and covered with Transite material. These blocks cover the whole area of the table and act to insulate the heat of the ovens from the bottom part of the table.

The mass spectrometer, excluding the ion source vacuum and gas handling system, is held above the Transite top with three heavy U-shaped stainless steel cups because of the low bending stress of the Transite. The cups holding the spectrometer are fastened very rigidly to two channel-beam sections running lengthwise under the table top and are in turn rigidly fastened to the frame of the table.

By clamping the mass-spectrometer tube rigidly at the ion source end, it is, therefore, possible to allow thermal expansion of the tube during bakeout to take place in one direction only, namely, down the tube toward the detection system. This is done in order to preserve the critical alignment of the quadrupole system with the ion source.

The system is heated for bakeout purposes through the use of six inverted U-shaped oven sections which are placed over the entire area of the table. The ovens use ten kilowatts of electric power to heat the mass-spectrometer system. The ovens are divided into two parts, the ion source oven and the mass-spectrometer oven. Each of the two ovens is separately controlled by a "Partlow Temperature Control" and in addition, each is supplied with a cutoff relay system for switching off the oven supplies in case of serious pressure rise in the system. The

circuit diagram for the oven control systems is shown in Fig. 6.3.

Reference

1. Paul, W., Reinhard, H. P., and von Zahn, U., "Das elektrische Massenfilter als Massenspektrometer und Isotopentrenner", Z. Phys. 152(2), 143 (1958).

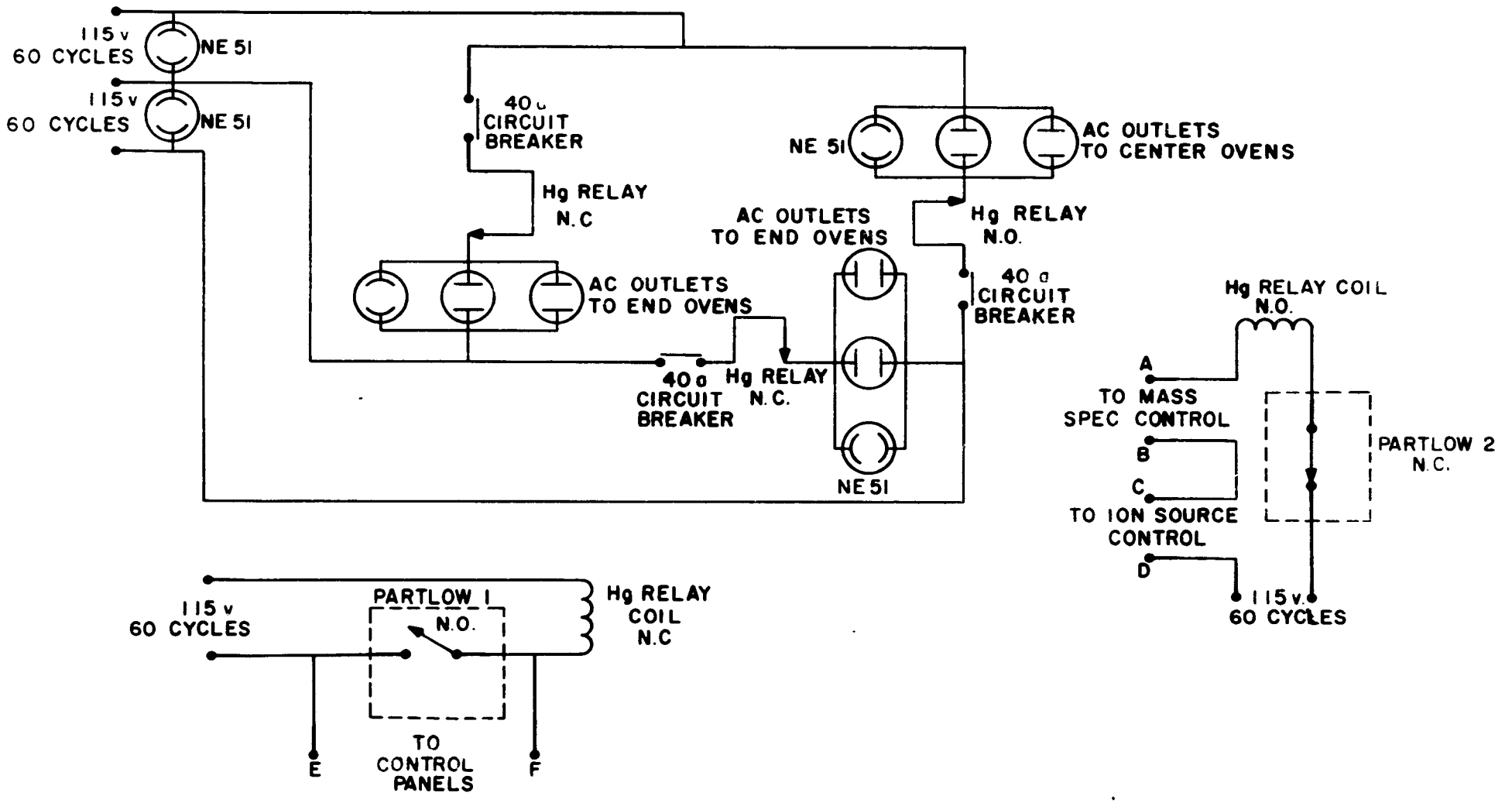

FIG 6.3 OVEN CONTROL (3 PANELS)

Chapter 7

The Mass-Spectrometer Vacuum System

7.1 Pumping speed considerations

In the practical and experimental fields of the science of high vacuum in general, it is quite essential to determine the "conductivity" of the channels through which the gases flow. The conductivity is defined as the rate of flow of gas in cubic centimeters per second per unit pressure difference.

Since the conductivity is a function of the dimensions of the tube, as expected, it will certainly be influenced by a sudden change in the cross-sectional area of the tube.

An expression for the conductivity could be defined as

$$F = \frac{1}{W_r \rho_1^{1/2}} = \frac{1}{p_1 - p_2} \qquad (7.1)$$

where

Q is the quantity of gas flowing, at a pressure of 1 dyne/cm^2, through the tube.

F is the conductivity.

$W_r\rho_1^{1/2}$ is the total resistance of the tube together with the influence of the end opening.

ρ_1 is the density of the gas at normal temperature and a pressure of 1 dyne/cm^2 = 7.5006 x 10^{-4} mm Hg.

Hence, $W_r\rho_1^{1/2}$ represents the combined "resistance" of the tube to molecular streaming at a pressure of 1 dyne/cm^2.

It has been shown by Jnanananda[1] that the "resistance" of a tube of cylindrical configuration to the flow of the gas may be expressed as

$$\rho_1^{1/2} W = \frac{6}{(2\pi)^{1/2}} \frac{L}{D^3} \rho_1^{1/2} ,$$

where

L is the length of the tube in cm

D is the diameter of the tube in cm.

If one end of the tube be circular with diameter D′ cm, the total resistance $W_r\rho_1^{1/2}$ of the tube, together with the influence of the end opening, is given by[1]

$$\rho_1^{1/2} W_r = (W + W')\rho_1^{1/2} = \left(\frac{6L}{(2\pi)^{1/2}D^3} + \frac{3.192}{D'^2}\right)\rho_1^{1/2} . \tag{7.2}$$

Hence

$$F = \left(\frac{2.394L}{D^3} + \frac{3.192}{D'^2}\right)^{-1} \frac{1}{\rho_1^{1/2}} . \tag{7.3}$$

It follows from the gas laws that the density ρ_1 at a pressure of 1 dyne/cm^2 is

$$\rho_1 = \frac{M}{RT} ,$$

where

M is the molecular weight.

R is the universal gas constant.

T is the temperature in degrees Kelvin.

Therefore,

$$F = \left(\frac{2.394L}{D^3} + \frac{3.192}{D'^2}\right)^{-1} \left(\frac{RT}{M}\right)^{1/2} . \tag{7.4}$$

It is to be noted that equation (7.3) and (7.4) hold only when the ratio of the diameter of the tube D to the mean free path of the gas

molecules is very small (Knudsen flow).

We will now proceed to obtain an estimate of the resistance of the tubing connecting the mass-spectrometer to the diffusion pumps using equation (7.2).

Resistance of tube connecting the mass-spectrometer to the high vacuum valve.

The diameter of the tube is taken to be 3 inches = 7.5 cm. The inlet diameter of the valve is 2 inches = 5 cm. The length of the tube is estimated to be 30 cms, so that

$$\rho_1^{1/2} W_{r_1} = \frac{6 \times 30}{(2\pi)^{1/2} \times (7.5)^3} + \frac{3.192}{(5.0)^2} = 0.183 \rho_1^{1/2} \text{cm}^{-3} \text{ sec.}$$

Resistance of tubing connecting high vacuum valve to diffusion pump

It is assumed that the resistance of the valve when fully open is negligible.

Taking an estimated tube length of 75 cms, we find

$$\rho_1^{1/2} W_{r_2} = 0.438 \, \rho_1^{1/2} \text{ cm}^{-3} \text{ sec.}$$

Hence, the total tube resistance is

$$\rho_1^{1/2} W_{r_{\text{total}}} = (0.438 + 0.183)\rho_1^{1/2} = 0.621 \rho_1^{1/2} \text{cm}^{-3} \text{ sec.}$$

For air at room temperature

$$\left(\frac{RT}{M}\right)^{1/2} \simeq 29 \times 10^3 \text{ dyne cm} .$$

Hence

$$F = \frac{29 \times 10^3}{0.621} = 46.7 \times 10^3 = 46.7 \text{ liters/sec.}$$

Calculation of pumping speed

The pumping speed is one of the characteristics of a vacuum pump. It is defined as follows:

The pumping speed at any given pressure is the volume of gas abstracted per unit time, measured at that pressure, from an enclosure containing gas at the same mean pressure. This definition, which is due to Gaede, thus confines itself to the speed at a given pressure instead of the pump speed in general for all pressures. This restriction is proper, for in most of the pumps the pumping speed varies with the variation of pressure.

In accordance with the above definition, the pump speed S may be given the precise expression

$$S = \left(\frac{dV}{dt}\right)_p . \tag{7.5}$$

Influence of connecting tube system upon the pumping speed

As a result of "resistance" of the tube system encountered by the gaseous flow, the actual pumping speed E depends not only upon the intrinsic pump speed S of the pump but also upon the "conductivity" F. The pressure p at the lower pressure terminus of the pump therefore differs from the pressure p_1 in the vacuum enclosure.

An equation, expressing the relation between the intrinsic pump speed S, the "conductivity" F, and the actual pumping speed E can easily be obtained. This is found to be

$$E = \frac{SF}{S + F} . \tag{7.6}$$

Upon close observance of this expression, one can readily see that it is important for an efficient utilization of the maximum speed of a pump that the dimensions of the connecting tube be so chosen that F

is made as large as practicable. If the dimensions of the tube system were, however, to be determined by other consi lerations, so that F is not of sufficiently large magnitude, it would be futile to make use of a pump of high intrinsic speed.

Three air-cooled three stage glass oil diffusion pumps are used to pump down the mass-spectrometer system. The pumps, employing Octoil-S pumping fluid are manufactured by Consolidated Electro-dynamics, Type No. GF26. Each pump is connected separately to the system by similar tube and valve arrangements. Each pump has a specified intrinsic speed of 25 liters/second. Hence, using the estimated conductivity F of tubing for each pump, we obtain the actual pumping speed as

$$E = \frac{25 \times 46.7}{25 + 46.7} = 16.28 \text{ liters/sec.}$$

Hence, the total pumping speed of the system is

$$E_{total} = 3 \times 16.28 \simeq 49 \text{ liters/sec.}$$

This pumping speed proves to be quite adequate since the approximate total volume of the mass-spectrometer system is 42 liters.

7.2 Description of the vacuum system

The vacuum system layout is shown schematically in Fig. 7.1. The diffusion pumps are backed by a "Cenco Hypervac 25", 264 liters/minute two stage rotary mechanical pump which produces a forepressure of about 10^{-4} mm Hg. The vacuum system connections are very similar to that of the ion source system which has been described in chapter 5, except for the following points which should be mentioned:

1. The valves shown, which are used for the connections between the mass-spectrometer and the diffusion pumps are 2" in diameter to

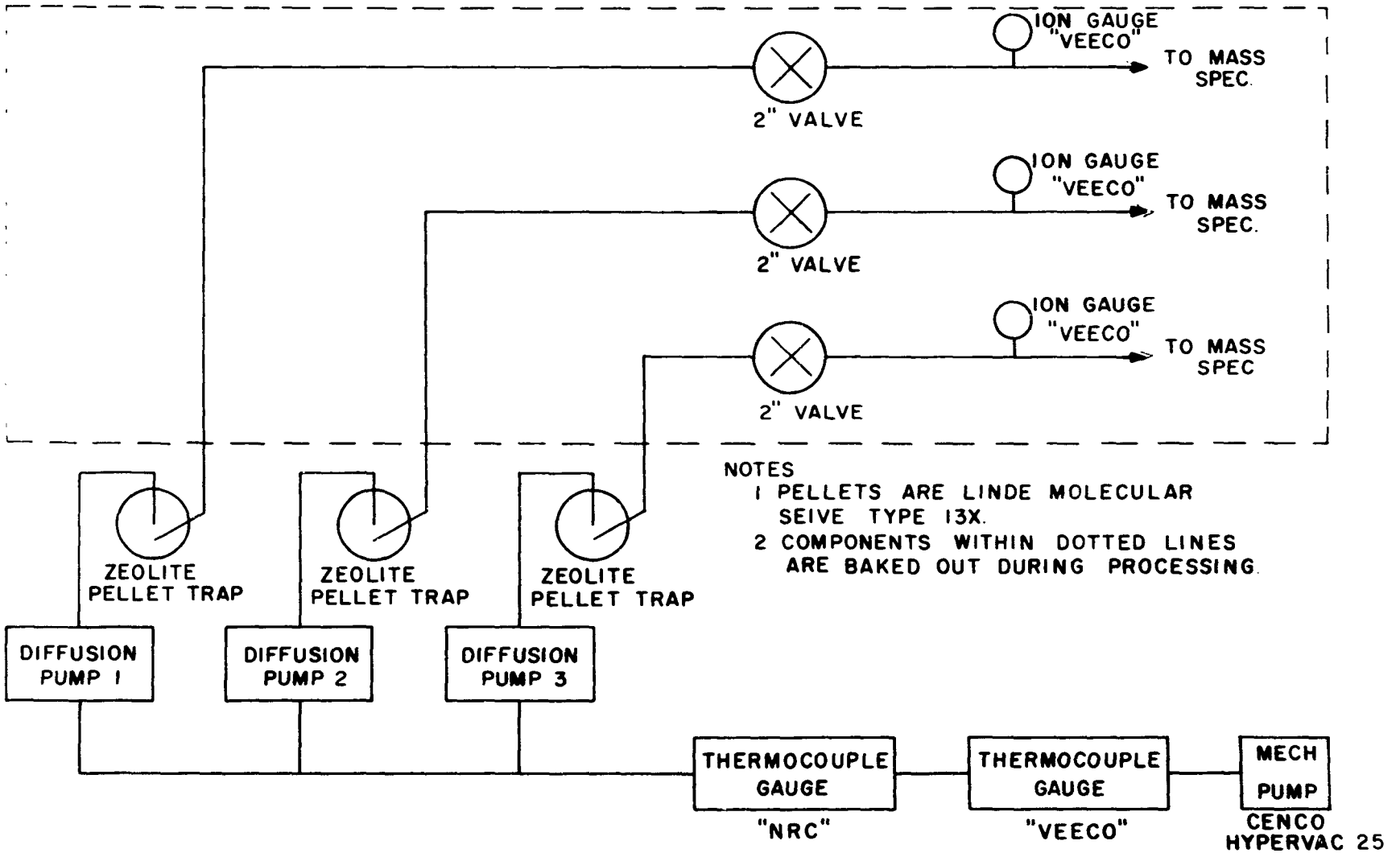
ION GAUGE "VEECO"
TO MASS SPEC.
2" VALVE
ION GAUGE "VEECO"
TO MASS SPEC.
2" VALVE
ION GAUGE "VEECO"
TO MASS SPEC
2" VALVE
NOTES
1 PELLETS ARE LINDE MOLECULAR SEIVE TYPE 13X.
2 COMPONENTS WITHIN DOTTED LINES ARE BAKED OUT DURING PROCESSING.
ZEOLITE PELLET TRAP
ZEOLITE PELLET TRAP
ZEOLITE PELLET TRAP
DIFFUSION PUMP 1
DIFFUSION PUMP 2
DIFFUSION PUMP 3
THERMOCOUPLE GAUGE
"NRC"
THERMOCOUPLE GAUGE
"VEECO"
MECH PUMP
CENCO HYPERVAC 25

FIG 71

keep the conductivity of the tubing as high as possible. These valves have been newly developed by Granville-Philips Company and are bakeable up to 450 degrees Centigrade.

2. The zeolite traps are placed on the diffusion pump side of the valve. The reason being that these traps are to be baked out separately, with the valve closed for isolating the ion multiplier detector from any oil vapors which, apparently, are quite harmful.

3. The three ion gauges shown are operated by one "Veeco Type RG3-A vacuum gauge control panel" using a relay switching mechanism for measuring the pressure at each ion gauge separately. The same "Veeco" measures the forepressure of both mechanical pumps through the use of two thermocouple gauges.

4. High pressure cut-off relays are also inserted and are installed in a manner similar to that described in the ion-source vacuum system. The circuit diagram of the mass-spectrometer vacuum control panel is shown in Fig. 7.2.

Reference

1. Jnanananda, S., "High Vacua", D. van Nostrand Company, (1947).

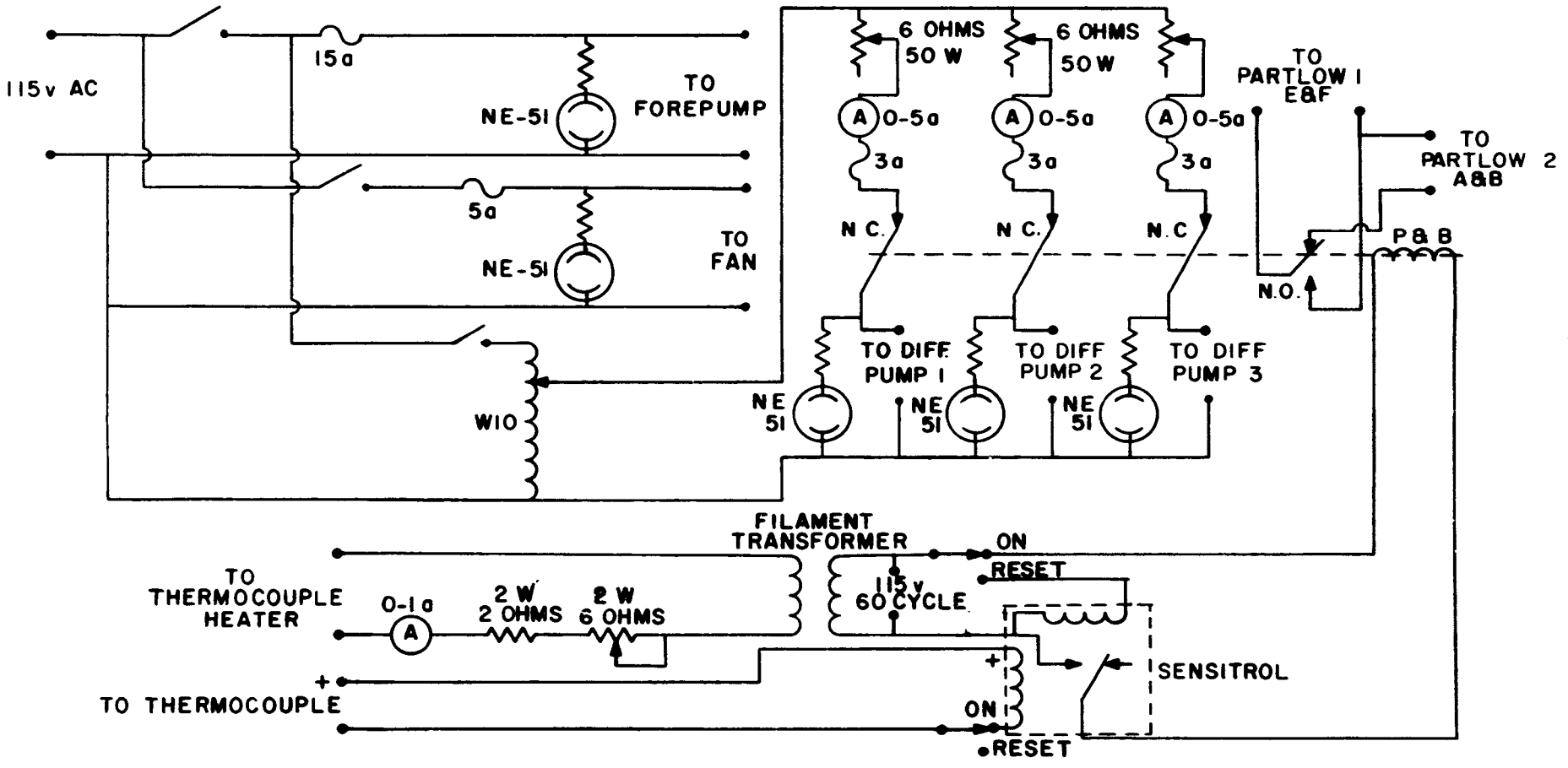

FIG 7.2 MASS SPECTROMETER CONTROL PANEL

Chapter 8

Design of Electronic Apparatus

8.1 Electric power requirements for the quadrupole system

With reference to chapter 3 which dealt with the design parameters of the spectrometer, the following electric power requirements were obtained:

RF Power: Frequency: 0.5 Mc/s, 1.0 Mc/s, 2.0 Mc/s
Voltage range: 116 volts to 1457 volts
Range of power requirement: 0.6 watts to 50 watts
Stability and accuracy: better than $\pm$ 0.1%

DC Power: Voltage range: 20 volts to 240 volts
Stability and accuracy: better than $\pm$ 0.1%
Power requirement: nil.

A block diagram of the components used in meeting these requirements is shown in Fig. 8.1. This consists of the following units:

1. A very stable and accurate signal generator which is utilized for generating the required radio frequencies. The generator is a "Siemens Type Rel 3W 518/c2a level oscillator" having the following specifications:

Frequency range: 30 kc/s to 15 Mc/s, with frequency lock-in in 100 kc/s steps.
Additional incremental frequency control, continuously adjustable from 0 to 100 kc/s.
Maximum frequency error $\pm$ 2 x 10^{-5} $\pm$ 300 c/s.
Maximum frequency variation with 10% line voltage variation: $\pm$ 1 x 10^{-6} $\pm$ 30 c/s.

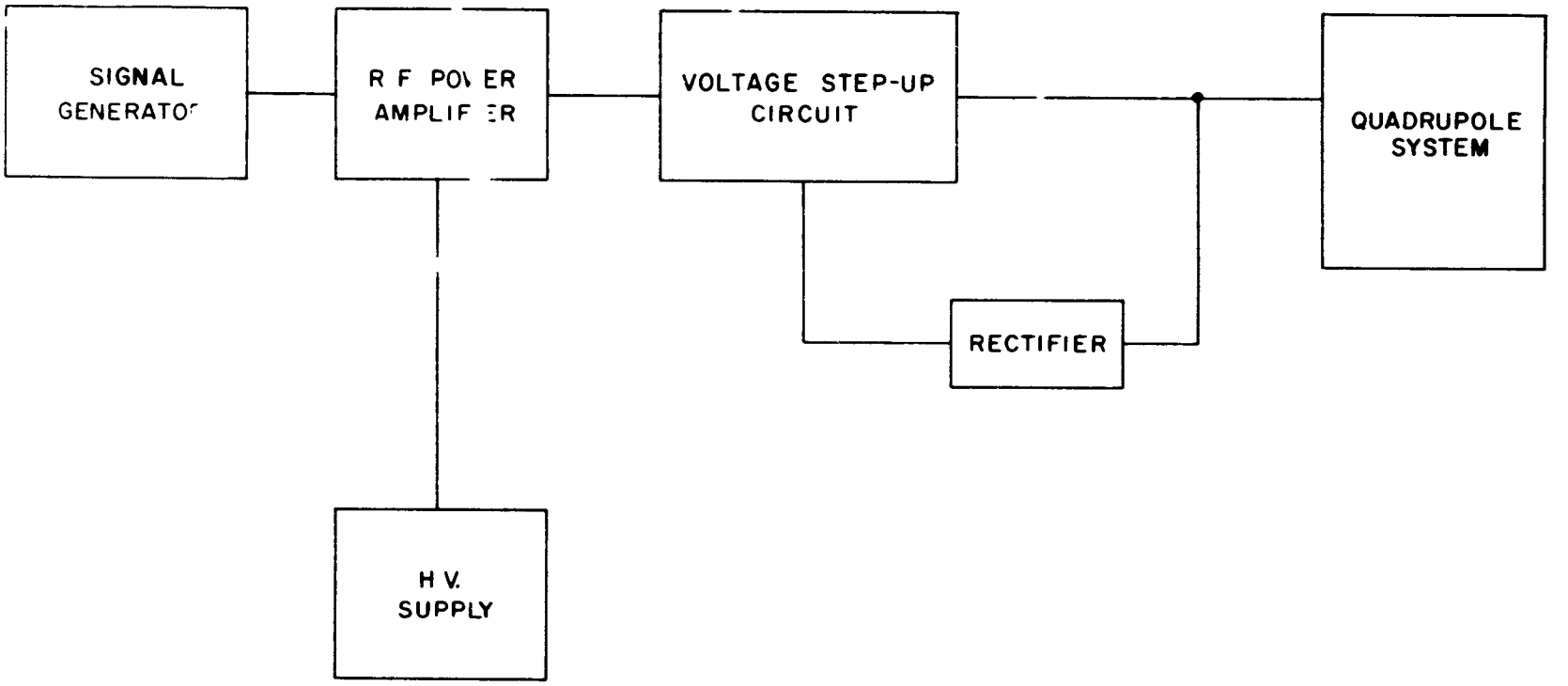
SIGNAL
GENERATOR
R F POWER
AMPLIFIER
VOLTAGE STEP-UP
CIRCUIT
QUADRUPOLE
SYSTEM
RECTIFIER
H V.
SUPPLY

FIG 8.1

Output level (full scale deflection) -60 db to +10 db.

Source impedance can be switched: 0 to 150 ohms in steps.

Automatic synchro-tuning system.

Frequency sweep facility when used in conjunction with a sweep generator.

2. RF Linear amplifier

The output sinusoidal radio frequency signal is fed into a linear push-pull amplifier which is capable of delivering up to 170 watts of radio frequency power to the load. A linear amplifier was used in order to eliminate the need for an intermediate driving stage between the signal generator and the amplifier.

3. Voltage step-up unit

In order to meet the high rf voltage requirement while maintaining a good degree of stability, the amplifier is loosely coupled to the load (quadrupole system) through a voltage step-up unit. Loose coupling has the advantage of minimizing the effect of load impedance variation on the amplifier. This is important in our case since it has been shown that the capacity of the quadrupole system changes with the mass of the injected ions. Voltage step-up is achieved through making use of the fact that the quadrupole system presents a capacitive load to the amplifier. Therefore, two variable inductors are introduced, as shown in Fig. 8.2, which are utilized to series-tune the circuit while maintaining symmetry and thus obtaining maximum voltage across the capacitive quadrupole system.

4. Rectifier

It was seen that the resolution of the mass-spectrometer is solely determined by the ratio of the applied dc voltage to the rf voltage

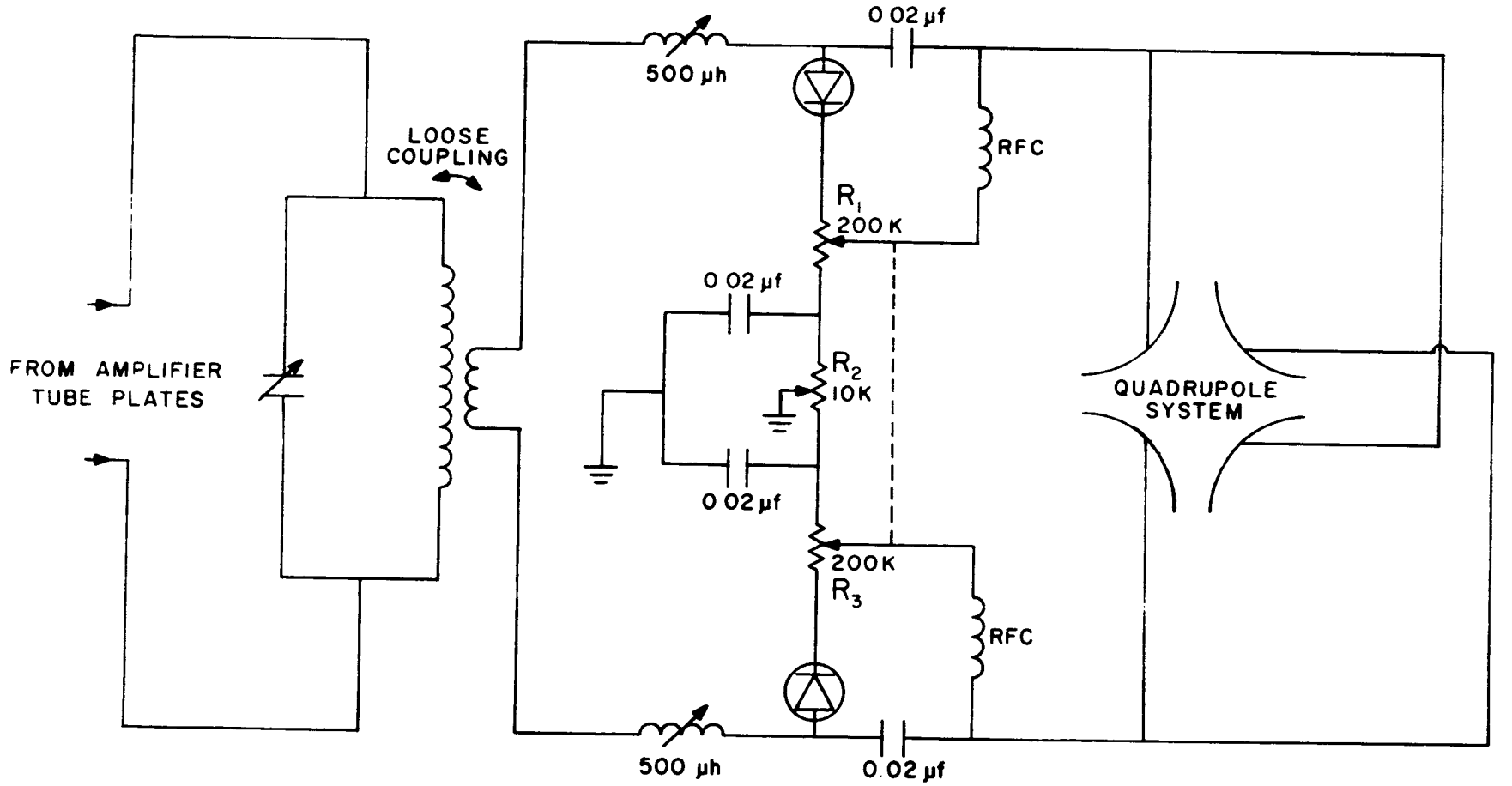

FIG 8.2

STEP-UP VOLTAGE & RECTIFIER UNITS

amplitude. It was, therefore, advantageous to generate the required dc voltage through rectification of the rf signal and using potential dividers to obtain the desired ratio as shown in Fig. 8.2. This method, therefore, makes it possible to maintain the resolution of the spectrometer constant, since any change applied to the rf voltage V will produce a proportional change in the dc voltage U, provided the potential divider settings remain unchanged.

Two high voltage silicon rectifiers were used for obtaining positive and negative dc potentials through half wave rectification. The desired portion of the rectified voltage is selected via the potential dividers R_1 and R_2 and is then superimposed on the rf signal through radio frequency chokes of the appropriate value. The combined signal is then delivered to the quadrupole system. R_3 is a 10 kilo-ohm potentiometer which is adjusted to obtain the desired symmetry of the field. R_1 and R_2 are mechanically coupled in order to ensure that symmetry is maintained while changing the resolution of the mass-spectrometer.

8.2 Design of the rf linear power amplifier

The push-pull linear amplifier was designed using the following vacuum tubes:

Type: EIMAC 4CX300A compact ceramic integral-finned power tetrode.

Maximum plate dissipation: 300 watts each.

Cooling: Forced air.

Maximum operating frequency: 500 megacycles per second.

The most important characteristic of a linear amplifier is the relationship between output voltage and exciting voltage, since this shows the extent to which the amplifier is actually linear. In a

typical characteristic, the relation between the two is quite linear up to a certain critical exciting voltage, after which the output levels off or saturates. The linearity of the amplifier characteristic below saturation is greatest when the amplifier tube is biased to projected cutoff exactly.[1]

We will now proceed to determine the operating voltages and currents of the amplifier on a one tube basis, since in push-pull amplifiers both tubes are operating under identical conditions.

From the available data of the 4CX300A tube, we obtain the following values:

Amplification factor (grid to screen) $\mu_{sg} = 4.8$.

Typical dc plate operating voltage $E_b = 2000$ volts.

Maximum allowable plate dissipation = 300 watts.

DC screen voltage $E_s = 350$ volts.

Peak space current $I_{max} = 500$ ma.

Since the amplifier is to operate at projected cutoff, the angle of plate current flow 2ϕ, shown in the instantaneous diagrams in Fig. 8.3, is equal to 180°. Therefore, the required dc bias voltage

$$E_c = \frac{E_s}{\mu_{sg}} = \frac{350}{4.8} = 73 \text{ volts.}$$

The grid driving voltage E_g can now be taken to be 70 volts. From the existing curves, which give the relation between the direct current I_{av} and the fundamental frequency component of the space current amplitude I_1 to the peak amplitude I_{max} as a function of angle flow, we obtain for $\phi = 90^\circ$

$$\frac{I_{max}}{I_{av}} = \pi \quad \text{and} \quad \frac{I_{max}}{I_1} = 2 \quad ,$$

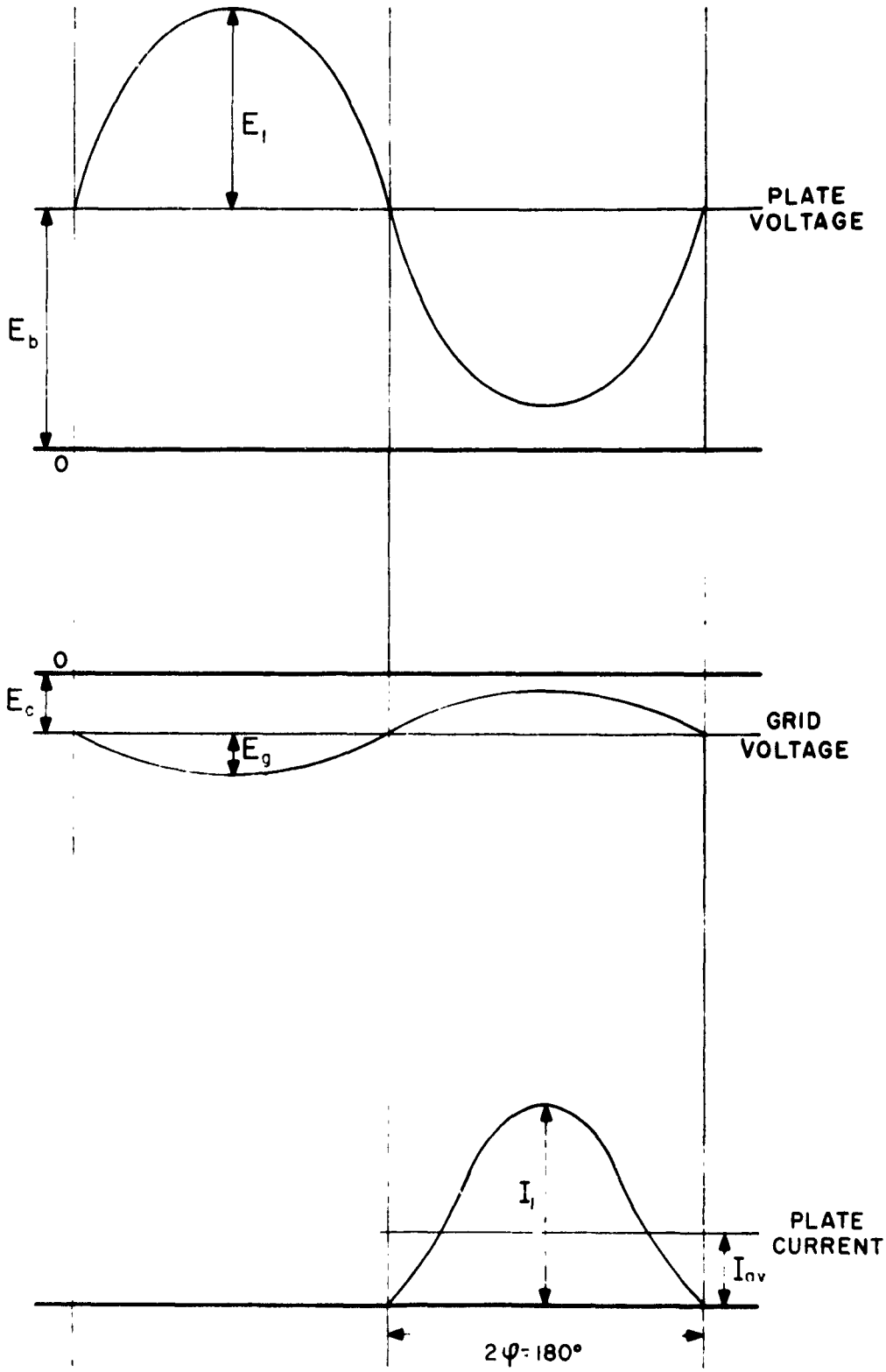

FIG 8 3

INSTANTANEOUS VOLTAGE & CURRENT RELATIONS IN A LINEAR AMPLIFIER

so that

$$I_1 = 0.5 \times 500 \times 10^{-3} = 250 \text{ ma}$$

and

$$I_{av} = 0.318 \times 500 \times 10^{-3} = 160 \text{ ma} .$$

It is known that the choice of a low load impedance in a linear amplifier extends its linearity, but will, unfortunately, also lower the output power and efficiency. The load impedance Z_ℓ is chosen to be 2.0 kilo-ohms.

$$Z_\ell = \frac{E_1}{I_1} ,$$

where E_1 is the rf plate voltage amplitude. Therefore,

$$E_1 = I_1 Z_\ell = 250 \times 10^{-3} \times 2.0 \times 10^3 = 500 \text{ volts}$$

$$\text{Output power/tube} = \frac{E_1 I_1}{2} = \frac{500 \times 250 \times 10^{-3}}{2}$$

$$= 62.5 \text{ watts.}$$

Thus, the total available power output from the amplifier is equal to 125 watts. This value is quite adequate since the theoretical power requirements, as calculated in chapter 3, yielded a maximum of 50 watts. This output power does, by no means represent the maximum capacity of the amplifier, since much larger powers could be easily obtained if desired as previously mentioned.

Input power = $E_b I_{av} = 2000 \times 160 \times 10^{-3} = 320$ watts.

Plate dissipation = 320 - 62.5 = 257.5 watts.

Thus, the design is safe.

Tank circuit design.

Load impedance = $2 \times 10^3 = \omega LQ$.

Assuming an effective Q to be 10,

we have

$$\omega L = \frac{2 \times 10^3}{10} = 2 \times 10^2 = 200 \text{ ohms} = \frac{1}{\omega C} .$$

For a frequency of 0.5 Mc/s

$$L = \frac{200}{\pi \times 10^6} = 63.5\mu h$$

and,

$$C = \frac{1}{200\ \pi\ 10^6} = 1590 \text{ pf}$$

For 1 Mc/s:

$$L = 32\mu h \quad \text{and} \quad C = 800 \text{ pf}$$

For 2 Mc/s:

$$L = 16\mu h \quad \text{and} \quad C = 400 \text{ pf},$$

The actual circuit diagram of the amplifier is shown in Fig. 8.4.

The required control grid bias voltage was supplied from a very stable fixed "Hewlett-Packard, Type 712" regulated power supply. The screen grid power requirements are also supplied separately from the same power supply. The screen voltage is very highly regulated and is maintained constant with 1×10^{-5} of its value, thereby ensuring great stability of the amplifier.

The plate power supply, the circuit diagram of which is shown in Fig. 8.5, was designed and built in the laboratory. It is capable of supplying up to 3000 volts at 500 ma through the use of a full wave

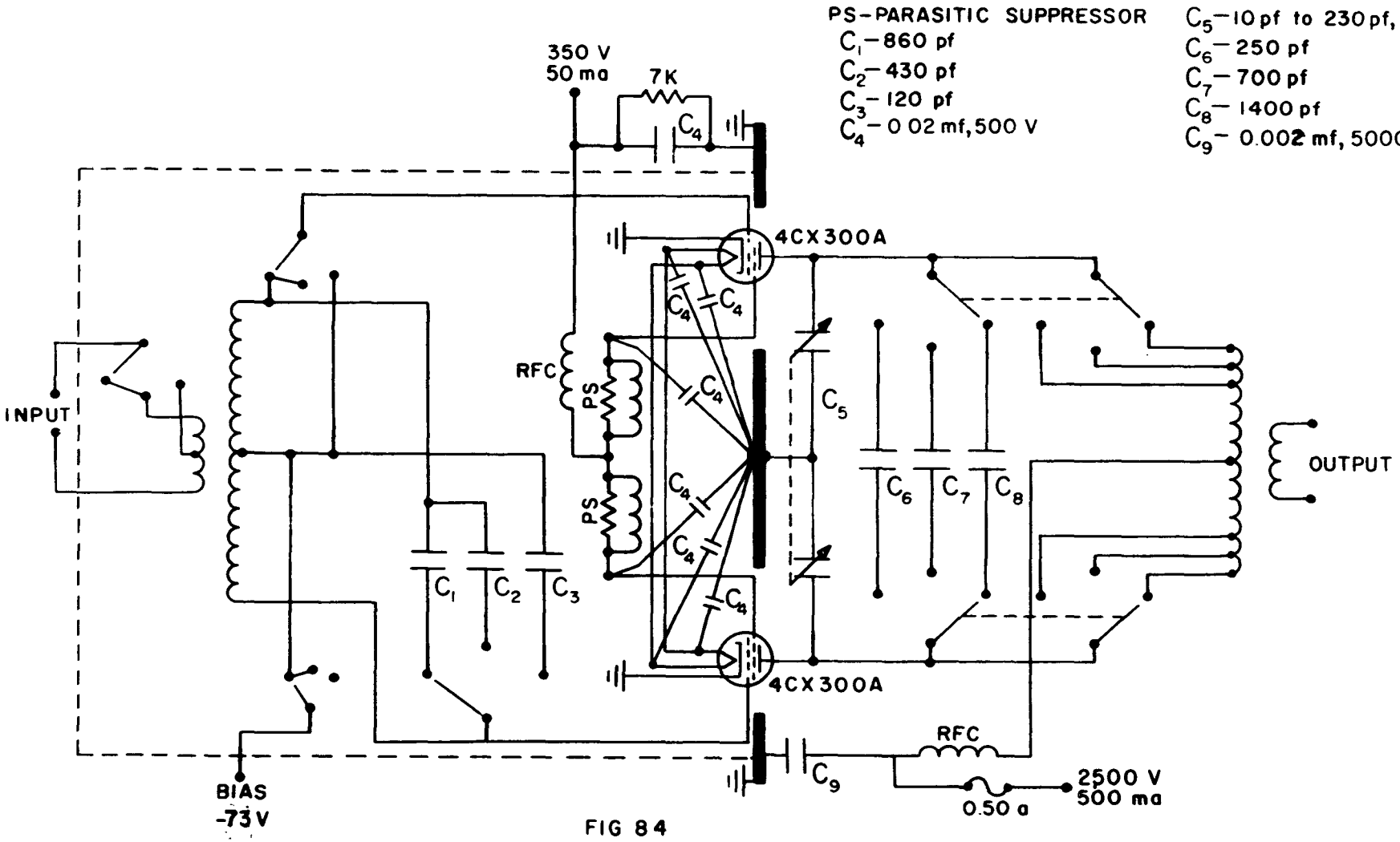

FIG 84

CIRCUIT DIAGRAM OF R F LINEAR AMPLIFIER

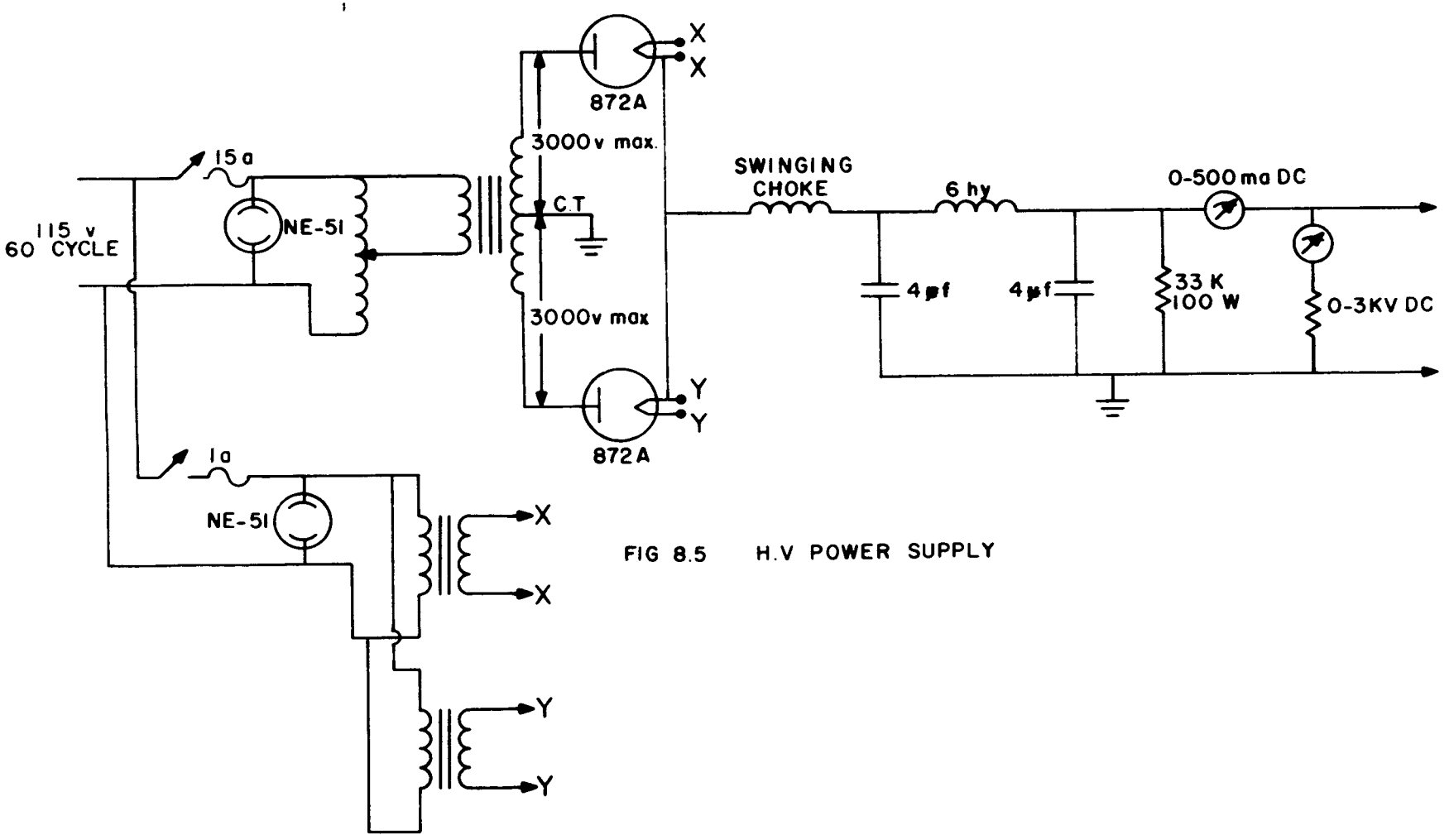

FIG 8.5 H.V POWER SUPPLY

mercury vapour rectifier. Through proper filtering, it was possible to maintain the ripple below 0.5% with adequate regulation. To achieve the required stability, the amplifier and power supplies were connected to the line voltage via a special "Sola" constant voltage transformer, which eliminates any effects due to line voltage variation.

Special precautions were taken in the construction of the amplifier for elimination of parasitic oscillations and other instability effects. Adequate forced air cooling was supplied to the tubes and shielding was adequately employed wherever it deemed necessary. Special precautions are also taken against damaging the tubes due to sudden failure of the plate or grid supply voltages by using over-current cutoff relays.

Reference

1. Mahmoud, A., "Lecture course, Cairo University", (1957).

Chapter 9

The Detection System

In this chapter, an attempt will be made to illustrate the different methods by which ions extracted from a mass-spectrometer could be detected. The method suited to our applications is thence chosen and applied to the quadrupole spectrometer. An evaluation of the problems arising with the method will be attempted, together with suggestions as to the methods of solving them. Unfortunately, at the time of writing this manuscript, it was not possible to varify the solution experimentally but it is hoped that clear apprehension of the problem would, at least, be achieved.

9.1 Brief outline of methods of detection

Several methods have been developed to detect the motion of a beam of ions flowing out of an analytical instrument. The following are a few of the more common and interesting methods:

a. Detection by the use of a Faraday Cage

This method has the advantage of possessing a high collection efficiency due to the large coverage space of the collector, but, unfortunately, is much less sensitive than some of the other methods. This method was used in some of the earlier types of quadrupole mass-spectrometers and proved to be successful for detecting currents in the range 10^{-10} amps to 10^{-12} amps combined with an electrometer.

b. The ion-multiplier oscilloscope method

This method combines the use of an ion multiplier, which amplifies the ion current through secondary electron emission gain, with an oscilloscope triggered by the ion beam. This method is very useful for fast scanning purposes.

c. Scintillation type mass-spectrometer ion detector

This is a new and relatively simple type of mass-spectrometer ion detector developed by Daly.[1] The positive ions are accelerated through 40 kV and impinge onto an aluminum surface releasing secondary electrons, and these in turn are accelerated onto an organic scintillator, viewed by a sealed-off photomultiplier. Counting methods could be used to measure the intensity of ion beams. Since the detector has a low noise level (4×10^{-20} amp) it is, therefore, quite sensitive and is easily capable of measuring currents of the order of 10^{-18} amps. Its disadvantage lies, however, in the extremely high accelerating voltage requirements.

d. The ion-multiplier electrometer-recorder method

The current output of the ion multiplier due to the impingement of the ion beam on the first dynode, is integrated using an electrometer (usually of the vibrating reed type) and the signal is thereafter recorded on a strip-chart recorder.

Considering that the normal gain of an ion multiplier is of the order of 10^6 and that an electrometer is capable of easily measuring currents of the order of 10^{-13} amps, it is evident that this method is quite sensitive also, and could be used for the measurement of very low ion currents; individual ions should, therefore, be observable.

Method (d) has been adopted in the present instrument, together with the possible use of method (b), for the basic reason that it satisfies the high sensitivity requirement together with the ease and simplicity of the circuitry involved.

9.2 The exit angle problem

It has been previously shown that the ions, while passing through the quadrupole system, undergo a two-dimensional oscillatory type of

motion. One would expect, therefore, that a "stable" ion upon reaching the end of the field will emerge at an angle to the axis depending upon its phase of injection. This is indeed the case and it constitutes a problem, especially since maximum collection efficiency is desired. This is also true when operating at very low ion currents (a few ions per second) since the individual ion now forms a measurable portion of the beam.

In order to solve this problem, two suggestions could be made:

a. Through the use of a simple electrostatic lens inserted between the end of the quadrupole system and the ion multiplier. This lens, which is constituted mainly of two diaphragms having a potential difference between them, will tend to focus the diverging beam and thus collimate it onto the first dynode of the ion multiplier.

b. Placing the ion multiplier as close as possible to the exit of the quadrupole system. In this case, however, extreme care has to be taken in shielding the ion multiplier from the end effects of the rf field which might modulate the secondary electron beam and heat the multiplier by induction. A suggested method to accomplish this is to wrap the ion multiplier in a slitted metal cylinder thus achieving shielding and prevention from induction heating simultaneously.

Reference

1. Daly, J. R., "Scintillation type mass-spectrometer ion detector", Rev. of Sc. Inst. 31, #3, 264 (1960).

Chapter 10

Planned Applications of the Mass-Spectrometer

As mentioned in the introduction of this manuscript, the identification of ions is of prime importance for a reliable interpretation of gaseous plasma phenomena.

Beside the more common usefulness of a mass-spectrometer in the study of ionization probabilities, appearance potentials, etc., the mass-spectrometer described is constructed specifically for linking results obtained with other measuring techniques established within the research group at the Department of Electrical Engineering of the University of Minnesota. The main effort of this group is directed towards the study of the physics of disintegrating plasmas. Consequently, a full apprehension of the phenomena involved requires completion of the following planned studies.

1. Afterglow studies

The types of ions present during the afterglow period will be identified and their time rate of change measured.

2. Mass-mobility relationships

The mass-spectrometer will be combined with the available drift tube "spectrometer" for a conclusive determination of the relationships between the mass of ion and its mobility in various gases. This combination makes it also possible to study ion-conversion phenomena. For instance, an accurate determination of the conversion frequency for processes of the type

$$X^+ + X + Y \rightarrow X_2^+ + Y$$

$$\rightarrow (XY)^+ + X$$

is of prime importance.

The gases which are planned to be studied are

a. Rare gases and their mixtures

We hope to obtain more conclusive information about the properties and production mechanisms of molecular ions, such as He_2^+, Ne_2^+, $(HeNe)^+$, etc.

b. Hydrogen and rare gas-hydrogen mixtures

When studying plasma phenomena in hydrogen the identification of the type of ion involved is especially significant, since at least three types of hydrogen ions exist, namely, H^+, H_2^+, H_3^+. Moreover, very little information is available about the properties and production mechanisms of the composite ions, such as $(HeH)^+$, $(NeH)^+$, etc.

3. Further developments of the mass-spectrometer

A study will be made of the possibilities which might exist in the improvement of certain components of the mass-spectrometer; in particular, the ion source design and the detection system. A possibility exists to improve the latter through the use of the induced currents at the electrodes due to the vibration of the ions as a method of detection.

APPENDIX

Calculation of the Arc-Length of an Equilateral Hyperbola

The equation of an equilateral hyperbola can be reduced to the simple form:

$$x^2 - y^2 = a^2 .$$

Hence,

$$\frac{dy}{dx} = \frac{x}{y} = \frac{x}{(x^2 + a^2)^{1/2}} .$$

The length of one arc of the hyperbola from $x = a$ to $x = x_o$ is equal to

$$L = \int_a^{x_o} (1 + (dy/dx)^2)^{1/2} \, dx = \int_o^{x_o} (1 + (dy/dx)^2)^{1/2} \, dx$$

since the hyperbola does not exist for $x < a$,

Thus,

$$L = \int_o^{x_o} (1 + (x^2/x^2+a^2))^{1/2} \, dx = 2^{1/2} \int_o^{x_o} (x^2 + a^2/2)/(x^2+a^2)^{1/2} dx .$$

Let

$$x = b \tan \phi$$

$$b = (a^2/2)^{1/2} .$$

Hence,

$$x_0 = b \tan \phi_o \quad \text{or} \quad \phi_o = \tan^{-1} x_o/b$$

also, $dx = b \sec^2 \phi \, d\phi$.

Substituting in the expression for L, we get

$$L = 2^{1/2} \int_0^{\phi_o} \frac{b^2 \sec^3\phi \, d\phi}{\left(\frac{a^2}{2}\tan^2\phi + a^2\right)^{1/2}}$$

$$= 2^{1/2} b \int_0^{\phi_o} \frac{\sec^3\phi \, d\phi}{(\tan^2\phi + 1 + 1)^{1/2}}$$

$$= 2^{1/2} b \int_0^{\phi_o} \frac{\sec^3\phi \, d\phi}{\sec\phi \, (1 + \cos^2\phi)^{1/2}}$$

$$= b \int_0^{\phi_o} \frac{d\phi}{\cos^2\phi \, (1 - k^2\sin^2\phi)^{1/2}} \quad \text{where } k^2 = 1/2 \text{ .}$$

This is a standard elliptic integral, the solution of which is tabulated as

$$L = \frac{\Delta \tan\phi_o + k^2 (D - F)}{k'^2}$$

where

$$\Delta = (1 - k^2 \sin^2\phi_o)^{1/2}$$

$$k^2 = 1/2$$

$$k'^2 = 1 - k^2 = 1/2$$

$$D = \int_0^{\phi_o} \frac{\sin^2 x \, dx}{(1 - k^2\sin^2 x)^{1/2}} = \frac{F - E}{k^2}$$

in which

F = elliptic integral of argument k of the first kind

E = elliptic integral of argument k of the second kind.

Hence, the length of the arc can be computed.

In the case of the spectrometer electrode, it was found to be 4.6028 cm.